CHEMICAL REVIEWS

pubs.acs.org/CR

Review

Relativistic Heavy-Neighbor-Atom Effects on NMR Shifts: Concepts and Trends Across the Periodic Table

Jan Vícha, Jan Novotný, Stanislav Komorovsky, Michal Straka,* Martin Kaupp,* and Radek Marek*

Cite This: *Chem. Rev.* 2020, 120, 7065−7103

Read Online

ACCESS | Metrics & More | Article Recommendations

ABSTRACT: Chemical shifts present crucial information about an NMR spectrum. They show the influence of the chemical environment on the nuclei being probed. Relativistic effects caused by the presence of an atom of a heavy element in a compound can appreciably, even drastically, alter the NMR shifts of the nearby nuclei. A fundamental understanding of such relativistic effects on NMR shifts is important in many branches of chemical and physical science. This review provides a comprehensive overview of the tools, concepts, and periodic trends pertaining to the shielding effects by a neighboring heavy atom in diamagnetic systems, with particular emphasis on the "spin-orbit heavy-atom effect on the light-atom" NMR shift (SO-HALA effect). The analyses and tools described in this review provide guidelines to help NMR spectroscopists and computational chemists estimate the ranges of the NMR shifts for an unknown compound, identify intermediates in catalytic and other processes, analyze conformational aspects and intermolecular interactions, and predict trends in series of compounds throughout the Periodic Table. The present review provides a current snapshot of this important subfield of NMR spectroscopy and a basis and framework for including future findings in the field.

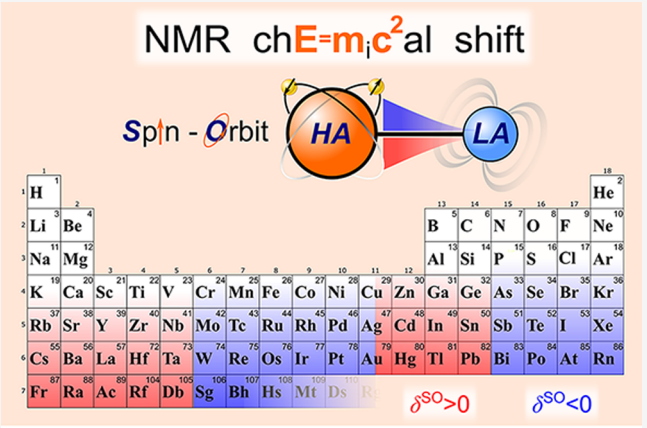

CONTENTS

Received: December 6, 2019
Published: June 23, 2020

https://dx.doi.org/10.1021/acs.chemrev.9b00785
Chem. Rev. 2020, 120, 7065−7103

1. INTRODUCTION AND HISTORICAL OVERVIEW

The NMR chemical shift, the resonant frequency of a particular nucleus relative to a standard in an NMR spectrum, provides crucial information about the molecular and electronic structure of the given system. In order to optimize the information obtainable from an NMR spectrum, a qualitative and quantitative understanding of the shift values expected for a given substance is fundamentally important. In this review we will lay out the current level of understanding of the relativistic effects of one or more heavy atoms (HAs) on the NMR shifts of its neighboring atoms. The term "heavy-atom effect", coined by Pyykkö,[1] initially referred to the nuclear shielding of the heavy atom itself, i.e., the "heavy-atom effect on the heavy-atom shielding" (HAHA effect).[2] The effect of a heavy atom on a neighboring light atom was subsequently termed "heavy-atom effect on the light-atom shielding" (HALA effect), even though we now know that this effect also applies when the NMR nucleus probed is itself a heavy atom. Keeping this fact in mind, we will use the established HALA label throughout this review. Many HALA effects are due to spin−orbit (SO) coupling, but there are also scalar relativistic (SR, also known as spin-free relativistic, SFR) HALA effects.[3] Because it is far more difficult to derive useful qualitative chemical concepts for the relativistic effects of a heavy atom on its own shielding,[4] we will not cover the HAHA effects in any detail here, but will mention the relevant literature toward the end of this section. Moreover, while crucial for the absolute shielding of the heavy atom, HAHA effects mostly cancel out in the relative shifts that NMR spectroscopy typically focuses on (with some exceptions, see refs 2−16). We also restrict our coverage to formally diamagnetic systems.

As this review will largely focus on the progress in understanding achieved since the last extensive reviews in 2004[3,13] (reviews including the topic as part of a wider discussion have appeared occasionally in the meantime[15−18]), it seems appropriate to start with a brief overview of the state of the field prior to 2004. Much of what is summarized in this section is explained in much more detail in ref 3.

The potential importance of the effects of special relativity in describing the magnetic-resonance parameters, including NMR chemical shifts, was recognized early on. The inner core−shells of the atoms are often crucially involved and, in many instances, the important role of the electronic spin introduces spin−orbit coupling contributions. Because this applies to NMR shifts, the effects of SO coupling will be the central focus of this work, but we will also discuss the influence of SR effects on the NMR shifts of neighboring atoms.

The first attempts by Nakagawa and co-workers to use perturbation theory (PT) to extend the theory of nuclear shielding in diamagnetic systems beyond the nonrelativistic (NR) Ramsey equation (see also section 2) were published in an organic chemistry journal[19] (and in the proceedings of a domestic Japanese NMR conference).[20] Note also that these ideas were preceded by the first theories of pseudocontact shifts in paramagnetic systems,[21−25] which are also known to have an SO origin. Nakagawa et al. laid out the third-order perturbation-theory (PT3) framework that resulted from including SO coupling as an additional perturbation in Ramsey's theory and pointed out the important analogy of the SO-induced HALA effects with the Fermi-contact mechanism of indirect spin−spin coupling constants, which was further exploited based on quantitative computations almost 30 years later.[26,27] The first explicit computations within such a third-order perturbation scheme in the 1970s and 1980s relied on semiempirical approximate molecular-orbital (MO) theory.[28−32] The perturbational treatment has been extended to accurate post-Hartree−Fock wave functions as well as to Kohn−Sham DFT, and it has been used for various applications and for detailed analyses.[3] We will present the PT framework in section 2 and exploit it extensively in section 3.

The extension of the second-order perturbation theory (PT2) Ramsey equations to a variational treatment of SO coupling in a four-component framework (see section 2) dates from 1983, when three independent research groups published proposals.[33−35] The limited computational resources available at the time forced initial implementations of such relativistic PT2 theories to use even more qualitative MO schemes (of the extended-Hückel type) than those used for PT3. Some crucial understanding of the HALA effect on, e.g., the ^{1}H shielding in HI in terms of the spin and spatial symmetry of four-component spinors was extracted even at this early stage, many years before

https://dx.doi.org/10.1021/acs.chemrev.9b00785
Chem. Rev. 2020, 120, 7065−7103

more quantitative ab initio or DFT four- or two-component relativistic schemes were introduced to compute NMR shieldings.[1] We note in passing that the first studies of the SR neighbor-atom effects in the 1990s used effective-core potentials (ECPs) on the heavy atom, typically at DFT levels, to efficiently incorporate the SR effects of the heavy atom on the overall electronic structure and thus on the NMR shielding of the neighboring atoms (e.g., ligand atoms in a heavy-metal complex).[36−39] While comparison of relativistic and nonrelativistic ECP computations is still an efficient way to study the SR effects on the neighbor-atom NMR shieldings, in the years since the 2004 review, relativistic all-electron methods of one-, two-, or four-component types (see section 2) have evolved to offer easy access to similar information.

Methodological aspects will be described in detail in section 2. Here we summarize the qualitative understanding of HALA effects on nuclear shieldings as of 2004. The analogy between SO-HALA effects and the Fermi-contact (FC) mechanism of indirect spin−spin coupling, implied qualitatively by Nakagawa et al.,[20] was computationally tested in detail in a 1998 paper.[26] DFT calculations on a series of organoiodine complexes showed closely parallel behavior of the SO-HALA contributions to ^{13}C and ^{1}H NMR shieldings for different positions in iodobenzene and the corresponding I−C and I−H reduced spin−spin coupling constants, an enhancement of both quantities with carbon s-character in the C−I bond in iodoethane, iodoethene, and iodoethyne, as well as the Karplus-type dependence of the three-bond SO-HALA effects on the ^{1}H NMR shieldings on the I−C−C−H dihedral angle in iodoethane. These findings clearly established the validity and usefulness of Nakagawa's analogy and have been confirmed by subsequent studies (see section 3). The dominance of an FC-type mechanism for the SO-HALA effects can best be understood and appreciated using the third-order-perturbation framework (PT3) presented in section 2; therefore, detailed explanations will be presented in section 3.

The dependence of the FC-mechanism on the s-character of the bonding at the spectator NMR atom[26] is shown by the fact that (a) ^{1}H NMR shieldings are most sensitive to SO-HALA effects because the hydrogen 1s-orbital predominates in bonding, (b) ^{13}C SO-HALA effects increase, e.g., from sp^3 to sp^2 to sp hybridization of carbon atoms, (c) for p-block elements as LA, SO-HALA effects on the shifts tend to be largest for their highest oxidation state, where the participation of the s-orbital in bonding is maximized,[3,13,40] (d) SO-HALA effects thus tend to be small for fluorine and oxygen, where p-orbitals dominate the bonding,[41] (e) SO-HALA effects are also small for the early transition-metal elements Ti, Zr, Hf, V, Nb, Ta, Cr, Mo, and W as LA in d^0 halide complexes because the metal−halogen bonds in such systems are dominated by the metal d-orbitals,[3] but (f) SO-HALA effects increase for the NMR shieldings of the metal in late transition-metal halide complexes where the metal s-character is again more significant in the bonding.[3] These considerations explain the predominance of the normal halogen dependence (NHD) of shifts for p-block nuclei (in particular those in their maximum oxidation state), the inverse halogen dependence (IHD) for early d^0 systems (and the closely related lanthanum[42]), and a return to NHD for the late transition metals. NHD shows a decrease in the shifts (increased shielding) from chloride to bromide to iodide substituent(s), whereas IHD indicates the opposite behavior. NHD is most often, but not always, caused by shielding SO-HALA effects, whereas IHD tends to arise from the trend of the paramagnetic shielding contributions when the SO-HALA effects are small. Many examples of NHD induced by SO-HALA effects have been studied (see section 4), and some mistakes in the interpretations of NHD have been exposed, for example, for the ^{13}C NMR shifts in trihalomethyl cations (CX_3; X = Cl, Br, I).[43] Other observations related to the s-character in bonding such as the enhancement of hybridization defects[44,45] (caused by the size mismatch between the valence s- and p-orbitals)[46] and thus of s-character and SO-HALA effects, whereby more electronegative substituents withdraw charge from the spectator NMR atom, have been discussed in the 2004 review.[3] This last aspect explains why the halomethanes $CH_{4-n}X_n$ (X = Br, I) exhibit a "nonlinear NHD" with increasing n, whereas the corresponding mixed complexes $CY_{4-n}X_n$ (e.g., Y = Br, X = I) show an essentially linear decrease.[3] We note in passing that two computational studies have shown that the dependence of SO-HALA effects on the bond length in systems like HX (X = halogen) differs from that of nonrelativistic shifts. As a consequence, SO-HALA effects may alter the ro-vibrational corrections to these shifts and give rise to unusual isotope effects and temperature dependencies.[47,48]

The importance of π-type lone electron pairs (LPs, or nonbonding pairs, n) for shielding SO-HALA effects (see sections 2 and 3) had received substantial attention by 2004: MO analyses showed that such π-LPs are important for shielding SO-HALA effects. A comparative study of the ^{13}C shifts in the series CF_3IF_n (n = 0, 2, 4) demonstrated that the two iodine LPs in CF_3I dominate the ^{13}C SO-shifts. The latter are about halved with one LP in CF_3IF_2 and essentially vanish in the absence of π-LPs in CF_3IF_4.[49] Similarly, chalcogenide substituents, which tend to feature only one π-type LP, give rise to only about half of the SO-HALA effects provided by halides.[3,50−52] Shielding SO-HALA effects have also been identified for the ^{13}C NMR shifts in transition-metal carbonyl complexes and related systems.[39,53,54] In contrast, high-lying σ-bonding MOs in systems like $XHgCH_3$ or $InCH_3$ have been found to cause deshielding SO effects on the ^{13}C NMR shifts.[38,39,55] The overall observations as of 2004 are summarized as follows: high-lying occupied nonbonding orbitals with π-symmetry relative to the bond between the NMR-active LA and the HA substituent(s) provide shielding SO-HALA effects, while high-lying σ-bonding orbitals have deshielding SO-HALA effects. Already in 1987, the 4-component extended-Hückel computations on HI showed that π-type iodine LPs make a shielding ^{1}H HALA contribution while a σ-bond causes deshielding.[1] We will discuss in section 3 how a consistent interpretation within a third-order-perturbation theory framework allows us to place these observations, and particularly the sign of SO-HALA effects, into a more general picture.

SR-HALA effects are easily evaluated computationally using an ECP or all-electron approach, but their interpretation is not as direct as that for the SO-HALA effects discussed above. They are not governed by one dominant and distinct mechanism[56,57] like the SO/FC mechanism for SO-HALA effects that we will describe in detail in section 2. The SR effects also originate in the core−shells of the HA(s), but it is their effect on the overall electronic structure of the valence shell that matters for the NMR shifts of neighboring atoms. This may happen via relativistic changes in the shapes of MOs that involve both the relativistically modified AOs of the HA and those near the LA. The paramagnetic shielding contributions may also be affected by relativistically modified energy denominators. These SR effects tend to become important somewhat lower in the Periodic Table than SO-HALA effects, typically in the sixth

https://dx.doi.org/10.1021/acs.chemrev.9b00785
Chem. Rev. 2020, 120, 7065−7103

period and beyond. They also tend to obey shell-structure effects known for SR effects on other properties, such as structures or energetics. Thus, we expect to see a "coinage-metal maximum" around group 11, related to the famous "gold maximum".[58] Initial studies carried out in the 1990s and early 2000s included the ^{17}O NMR shieldings of oxo complexes,[36,39] ^{13}C and ^{17}O NMR shieldings of carbonyl complexes,[39,53,54] as well as ^{13}C and ^{1}H NMR shieldings of organomercury complexes and mercury hydrides.[38,39] Both indirect SR effects due to relativistic structure changes and direct effects were analyzed. The relativistic contraction of the bond length and the direct SR effects at a given structure increased the ^{17}O NMR shielding in oxo complexes. However, for organomercury complexes the ^{13}C NMR shieldings were still increased by the relativistic bond-length contraction but reduced by the direct SR effects at a given structure (SO effects on structures tend to be smaller and have not been studied as much[59]). These differences were attributed to the difference in bonding character at the metal center, a dominant 5d-expansion in the oxo complexes vs a dominant 6s contraction in the mercury species. Further examples studied included the ^{19}F NMR shifts of mixed uranium halide complexes.[9,10,41] In this case the SO-HALA effects were rather small because of an inefficient SO/FC mechanism, whereas the SR effects were sizable. We should also mention that SR- and SO-HALA-effects are not additive. SR-induced changes in the electronic structure (e.g., contraction/expansion of MOs, modification of the radial nodal structure, or changes in the energy spectrum) may alter the SO effects.[60−62]

Finally, we mention in passing the so-called HAHA effects. These relate largely but not exclusively to the core−shells of the relativistic HA.[2,3,5−16] Made up of both scalar and spin−orbit contributions, they are generally included in full four-component treatments but are less well described in some quasi-relativistic treatments like the ZORA (zeroth-order regular approximation) approach.[63] While analyses based on Breit-Pauli (BP) perturbation theory yield a number of terms, it often appears that a cross term between the Fermi-contact operator and the kinetic spin-Zeeman term dominates the HAHA effects.[14] Such contributions seem not to occur for spin-rotation constants, and a historical approach frequently used to extract the paramagnetic contributions to NMR shifts from spin-rotation constants (see section 2) breaks down for heavier atoms.[64−69]

In the following, we will first summarize the theoretical and computational background of relativistic effects on NMR shifts (section 2) and then provide a general conceptual framework for analyzing the SO-HALA effects (section 3) before embarking on a journey of the SO-HALA effects through the Periodic Table, concentrating on work published since the 2004 review[3] (section 4).

2. THEORETICAL BACKGROUND FOR THE ANALYSIS OF SO-HALA SHIFTS

As a basis to better understand our analyses in the following sections, we need to introduce some theoretical formalism based on relativistic quantum chemistry and perturbation theory. While we strive to keep matters simple, some key equations are required. Relativistic effects in computational quantum chemistry are defined as the difference between results obtained by relativistic and nonrelativistic levels of theory.[1] As such, the relativistic contribution to a particular molecular property is a purely theoretical concept that we can probe only by computations. However, the study of relativistic effects is crucial for our understanding of the molecular properties of systems containing heavy atoms and for relating these properties to electronic structure or chemical bonding. The inclusion of relativistic effects in computations always entails a compromise between accuracy and efficiency. A more accurate description of the relativistic effects usually requires a more demanding computational methodology. Potentially relevant aspects of quantum electrodynamics notwithstanding, relativistic four-component (4c) theory based on the Dirac-Coulomb-Breit Hamiltonian is considered[70,71] the gold standard for calculating molecular properties, but because of its large computational demands, more approximate quasi-relativistic two-component (2c) theories have been developed. These theories include both scalar and spin−orbit (SO) relativistic effects variationally, i.e., up to an infinite order of Taylor expansion. Further down the ladder are so-called one-component (1c) theories that neglect spin−orbit effects, significantly reducing the computational demand. In areas where the spin−orbit effects are negligible, such more expedient one-component treatments (SR or NR) are the obvious choice. One-component approaches may contain, to various degrees of accuracy, scalar-relativistic (SR) effects or no relativistic effects at all. In the latter case, a nonrelativistic (NR) theory featuring the well-known Schrödinger Hamiltonian is obtained. Finally, at any level of Hamiltonian (1c-NR, 1c-SR, 2c, or 4c), various corrections can be added perturbatively, including, for example, SO effects on top of 1c (NR or SR) computations.

From the computational point of view, all of the above relativistic methods can be formulated at the all-electron or ECP (effective core potential) level of theory, provided the core−shells of the spectator NMR-active atom are covered, and the full core nodal structure of its valence orbitals is thus treated correctly. Of course, all-electron calculations are more computationally demanding because they take into consideration all of the degrees of freedom for every electron variable. On the other hand, ECP theory excludes core electron variables from the computation. This approximation is based on the observation that core electrons are not involved in chemical bonding and therefore can be included in the calculation as an effective potential. This technique leads to computationally efficient approaches, but because the number of electrons treated by the ECP influences the final accuracy of the results, it requires additional validation.[41] Moreover, any relativistic effects can be included in the ECP as well. For example, it is popular to include SR effects in the ECP but to treat the remaining valence electrons at the NR level of theory. In this way the relativistic effects are also included for the valence shell through the action of the ECP. As relativistic all-electron approaches have become more efficient over the years, the need to use ECPs has diminished to some extent.

2.1. Nuclear Magnetic Shielding and NMR Shift

With some exceptions (see below), an analysis of the effects of the electronic structure on relative isotropic NMR chemical shifts for diamagnetic species containing only light elements typically requires consideration of only the paramagnetic contribution. In the following, we will rationalize this statement in a nonrelativistic framework using a relation suggested by Flygare and Goodisman[72] and discuss why it cannot be transferred to relativistic theory.

The isotropic NMR chemical shift of the "light atom" of interest (herein labeled LA) is defined as the difference between

https://dx.doi.org/10.1021/acs.chemrev.9b00785
Chem. Rev. 2020, 120, 7065−7103

the isotropic nuclear shielding of a reference system and the shielding of the system of interest

$$\delta(\mathrm{LA}) = \sigma_{\mathrm{ref}}(\mathrm{LA}) - \sigma(\mathrm{LA}) \tag{1}$$

The shielding constant and, thus, the chemical shift can be broken down into diamagnetic and paramagnetic contributions

$$\sigma(\mathrm{LA}) = \sigma^{d}(\mathrm{LA}) + \sigma^{p}(\mathrm{LA}) \tag{2}$$

$$\delta(\mathrm{LA}) = \delta^{\mathrm{d}}(\mathrm{LA}) + \delta^{\mathrm{p}}(\mathrm{LA}) \tag{3}$$

Flygare and Goodisman[72] pointed out an important relation for the diamagnetic shielding

$$\sigma^{\mathrm{d}}(\mathrm{LA}) \approx \sigma^{\mathrm{FA}}(\mathrm{LA}) + C^{\mathrm{nuc}}(\mathrm{LA}) \tag{4}$$

where $\sigma^{\mathrm{FA}}(\mathrm{LA})$ is the diamagnetic shielding of the free LA and $C^{\mathrm{nuc}}(\mathrm{LA})$ represents the nuclear contribution to the nuclear spin-rotation constant (in ppm). When the results from eqs 1−4 are combined, $\sigma^{\mathrm{FA}}(\mathrm{LA})$ cancels out, which gives us the following simple expression:

$$\delta(\mathrm{LA}) \approx C^{\mathrm{nuc}}_{\mathrm{ref}}(\mathrm{LA}) - C^{\mathrm{nuc}}(\mathrm{LA}) + \delta^{\mathrm{p}}(\mathrm{LA}) \tag{5}$$

As C^{nuc} depends only on the structure of the molecule, it is clear that the electronic structure influences isotropic NMR chemical shifts solely via the paramagnetic contribution.

Unfortunately, this result is not transferable to the calculation of SO-HALA shifts. There is some indication that relation 4 (and by extension relation 5) is applicable in the relativistic domain when the gauge origin is placed on the spectator atom LA. However, in the presence of one or more HAs, this leads to inaccurate results for any practical finite basis set.[73] Fortunately, the diamagnetic contribution to NMR shifts depends only weakly on the electronic structure (usually by up to 2 ppm); therefore, it is often sufficient to analyze only the paramagnetic contribution to understand trends in NMR shifts. ^{1}H NMR shifts are an exception, due to their small shielding range (i.e., 2 ppm is a large effect in this case) and the absence of a core−shell in hydrogen. A small shift range may cause lithium shifts to be borderline cases, where one should not a priori disregard changes in the diamagnetic terms.

In the above discussion we assumed the use of common gauge origin (CGO) methodology for calculation of the NMR shielding. While the CGO is typically not used for practical calculations, due to poor convergence of the basis set, the analysis within a CGO picture is more transparent than, e.g., with the frequently used London orbitals (gauge-including atomic orbitals, GIAOs).[74,75] This is mostly because GIAO expressions are more complicated than those for CGO, while the dependence of the GIAO and CGO diamagnetic contributions on the electronic structure remains approximately the same. Nevertheless, GIAO-based analyses can be found in the literature,[76,77] usually in cases where the higher precision of the GIAO methodology is mandatory and in-depth MO analysis is less crucial.

2.2. MO Analysis in the Nonrelativistic Domain

In view of the above description, we will focus further on the analysis of the isotropic paramagnetic shielding contribution, $\sigma^{\mathrm{p}}(\mathrm{LA})$, or shift, $\delta^{\mathrm{p}}(\mathrm{LA})$. In the nonrelativistic (NR) domain within Hartree−Fock or density functional theory, the $\sigma^{\mathrm{p}}(\mathrm{LA})$ contribution has a Ramsey-like form[78] (we will use Hartree atomic units throughout section 2)

$$\sigma^{\mathrm{NR,p}}(\mathrm{LA}) = \frac{2}{3c^2}\sum_{u=1}^{3}\sum_{i=1}^{\mathrm{occ}}\sum_{a=1}^{\mathrm{vac}}\frac{\langle\varphi_i|\hat{l}^{\mathrm{G}}_u|\varphi_a\rangle\langle\varphi_a|r^{-3}_{\mathrm{LA}}\hat{l}^{\mathrm{LA}}_u|\varphi_i\rangle}{\varepsilon_i - \varepsilon_a} \tag{6}$$

where ε_i (ε_a) are occupied (vacant) one-electron energies, φ_i (φ_a) are occupied (vacant) molecular orbitals (MOs), $\boldsymbol{r}_{\mathrm{LA}}$ is the electron position operator relative to the position of the LA nucleus, $\boldsymbol{r}_{\mathrm{G}}$ is the electron position operator relative to the position of the gauge origin, c is the speed of light, and $\hat{\boldsymbol{l}}^{\mathrm{LA}} = \boldsymbol{r}_{\mathrm{LA}} \times \boldsymbol{p}$, $\hat{\boldsymbol{l}}^{\mathrm{G}} = \boldsymbol{r}_{\mathrm{G}} \times \boldsymbol{p}$ and $\boldsymbol{p}$ represent the electron momentum operator. In eq 6, the angular-momentum operator, $\hat{\boldsymbol{l}}^{\mathrm{G}}$, represents the interaction with an external magnetic field, and the paramagnetic spin−orbit (PSO), $r^{-3}_{\mathrm{LA}}\hat{l}^{\mathrm{LA}}_{\mathrm{u}}$, operator arises from the interaction with the magnetic moment of the LA nucleus. Note that PSO describes the (nuclear-)spin-(electron-)orbit interaction and should not be confused with the (electron-)spin-(electron-)orbit interaction discussed throughout this work.

In the basis-set limit, the position of the gauge vector can be chosen arbitrarily. However, for the MO analysis to be practical, the size of the basis must be within reasonable limits. If there is no HA in the system, the gauge vector is usually placed at the position of the LA nucleus. This choice simplifies the analysis considerably, and at the same time, the size of the basis set can be kept moderately large. In contrast, to keep basis requirements reasonable for systems with one HA, the gauge vector must be placed at the position of this HA, see eqs 8, 18, and 19 below.[79] Finally, if there is more than one HA in the system, it is not possible to keep the basis-set requirements sufficiently low, and methods employing GIAOs (or related approaches) must be used. In the following, we will discuss systems containing just one HA.

Equation 6 has been used for decades to successfully analyze NMR shifts of "non-relativistic cases", i.e., for systems without HA(s). Molecular-orbital analysis based on eq 6 is performed in three steps: first, identify the frontier MOs (other MOs are insignificant because they bring in larger energy denominators), then select MOs which have nonzero contributions from atomic orbitals of the LA (the function r^{-3}_{LA} enhances contributions from these MOs), and finally, find the most significant occupied-vacant MO ↔ MO* magnetic couplings using the angular-momentum operator, $\hat{l}^{\mathrm{LA}}_{\mathrm{u}}$. A textbook example of this procedure is the $n \leftrightarrow \pi^*$ coupling in nitrogen heterocycles such as pyridine, shown in Figure 1.

2.3. Theory of Relativistic NMR Chemical Shifts

Given the central role of SO-HALA effects throughout this review, we will concentrate the following discussion on

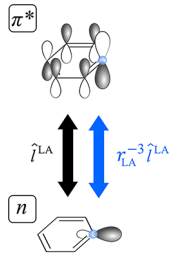

Figure 1. Schematic graphical representation of the Ramsey-type $n \leftrightarrow \pi^*$ coupling in pyridine, which dominates the isotropic ^{15}N NMR shift.[80] Angular-momentum and paramagnetic spin−orbit operators are shown in black and blue, respectively.

https://dx.doi.org/10.1021/acs.chemrev.9b00785
Chem. Rev. 2020, 120, 7065−7103

relativistic SO effects. SR effects are briefly discussed below. Each subsection starts with a brief description of the underlying methodology followed by a more detailed discussion focused on the analysis of SO-HALA NMR shifts.

There are two conceptually different approaches to considering SO effects when calculating NMR shifts: two- or four-component methods that describe SO effects variationally and methods that include leading-order SO effects by using perturbation theory.[81−85]

2.3.1. Variational Inclusion of SO Effects. Over the last two decades, the development of new theoretical and numerical techniques has allowed the practical application of relativistic methods that include both SR and SO effects variationally. Aided by growing computational power, these methods have become increasingly popular because of their accuracy and increasing efficiency. The most rigorous methods capable of treating relativistic effects on an equal footing across the Periodic Table of Elements use the four-component Dirac-Coulomb(-Breit) Hamiltonian.[86] These methods[73,87−89] were long considered to be too computationally expensive, but it has now been demonstrated that using modern computational techniques, four-component methodology can be applied on a regular basis to systems with more than 100 atoms,[90−92] or in an extreme case with more than 300 atoms,[93] when combined with Kohn−Sham density-functional theory (DFT). Two-component quasi-relativistic methods[85] introduce various approximations at different levels of theory to provide a more computationally efficient framework. Therefore, in an ideal situation, two-component methods are first validated against their more accurate four-component counterparts on a particular class of systems and are subsequently used in similar applications to provide, hopefully, an improved compromise between efficiency and accuracy (examples of such comparisons range from halogenated organic compounds[94] through transition metals[95,96] to actinide systems[97]). We can distinguish roughly approximate two-component (A2C) and exact two-component (X2C) methods. While in the former the transformation of the one-electron Dirac equation is done only approximately, in the latter it is done to machine accuracy. In both cases, the treatment of the two-electron contributions in the transformation, in particular for the SO effects, is still a matter of development and is usually neglected in practical applications. While X2C-type methods for nuclear shieldings have very recently begun receiving attention,[98] most practical 2c computations of nuclear shieldings have been done with the zeroth-order regular approximation (ZORA),[63] which is an A2C *ansatz*. Such SO-ZORA computations and related approaches are currently being applied, with reasonable approximations, to systems containing hundreds of atoms, and they have become the most popular methods for including SO effects variationally into computations of NMR shifts (note that the approximations involved in the ZORA treatment give rise to substantial errors in calculated absolute shieldings).[67]

Detailed analysis of the NMR shifts within a 2c or 4c framework is somewhat complicated, primarily by the complex structures of both the magnetic moment operators and the molecular spinors. Unlike nonrelativistic molecular orbitals, molecular spinors consist of two (four) complex functions in the case of 2c (4c) calculations. For simplicity, we will focus on 2c theory. The isotropic paramagnetic NMR shielding can be written formally as

$$\sigma^{2c,p}(\mathrm{LA}) = \frac{2}{3}\mathcal{R}\sum_{u=1}^{3}\sum_{i=1}^{occ}\sum_{a=1}^{vac}\frac{\langle\varphi_i^{2c}|\hat{m}_u^{B,2c}|\varphi_a^{2c}\rangle\langle\varphi_a^{2c}|\hat{m}_u^{\mu,2c}(\mathrm{LA})|\varphi_i^{2c}\rangle}{\varepsilon_i^{2c}-\varepsilon_a^{2c}} \tag{7}$$

Here φ_i^{2c} (φ_a^{2c}) are 2c occupied (vacant) molecular spinors (MSs), ε_i^{2c} (ε_a^{2c}) are 2c occupied (vacant) one-electron energies, $\hat{\boldsymbol{m}}^{B,2c}$ is a 2c magnetic-moment operator corresponding to the external magnetic field, $\hat{\boldsymbol{m}}^{\mu,2c}(\mathrm{LA})$ is the 2c nuclear magnetic-moment operator of the LA nucleus, and the symbol $\mathcal{R}$ specifies the real part of the following expression. To make the analysis of eq 7 feasible and tractable but still meaningful in most cases, it is best to use semilocal (nonhybrid) DFT potentials and to omit DFT kernel. For a more detailed discussion of the necessary approximations, see refs 99 and 100.

Thanks to the time-reversal symmetry of the perturbation-free Dirac-Coulomb Hamiltonian, all MSs are at least doubly degenerate. In the following, we will refer to two MSs with the same one-electron energy as a molecular spinor pair (MSP), also known as a Kramers pair.[101] Note that in addition to the complex structures of MSs and magnetic moments, their form differs significantly depending on which 2c theory is used. A pragmatic way to circumvent this problem in the analysis of eq 7 and provide a conceptual link to the PT3 approach based on the NR wave functions described further below is to focus on only the leading-order effects in a perturbation expansion, which are the same for all 2c theories. These contributions can be expressed as[100]

$$\sigma^{2c,p}(\mathrm{LA}) \cong \sigma^{NR,p}(\mathrm{LA}) + P^{AB}\frac{4\pi}{9c^2}\mathcal{R}\sum_{u=1}^{3}\sum_{i=1}^{occ}\sum_{a=1}^{vac}\left[\frac{\langle\varphi_i^{SO}|\hat{l}_u^{HA}\mathbf{1}|\varphi_a^{nr}\rangle\langle\varphi_a^{nr}|\hat{\delta}^{LA}\boldsymbol{\sigma}_u|\varphi_i^{nr}\rangle}{\varepsilon_i-\varepsilon_a} + \frac{\langle\varphi_i^{nr}|\hat{l}_u^{HA}\mathbf{1}|\varphi_a^{SO}\rangle\langle\varphi_a^{nr}|\hat{\delta}^{LA}\boldsymbol{\sigma}_u|\varphi_i^{nr}\rangle}{\varepsilon_i-\varepsilon_a}\right] \tag{8}$$

where $\hat{\delta}^{LA} = \hat{\delta}(\boldsymbol{r}_{LA})$ is the Dirac delta function centered on the LA, 1 is the two-by-two identity matrix, $\boldsymbol{\sigma}$ is a vector composed of Pauli matrices,[102] φ_i^{SO} (φ_a^{SO}) are occupied (vacant) linear-response MSs perturbed by the SO interaction

$$\varphi_p^{2c} \cong \varphi_p^{nr} + \varphi_p^{SO} = \varphi_p^{nr} + \frac{Z^{HA}}{4c^2}\sum_{\substack{q\neq p\\ q\neq p\pm 1}}^{all}\frac{\langle\varphi_q^{nr}|r_{HA}^{-3}\hat{\boldsymbol{l}}^{HA}\cdot\boldsymbol{\sigma}|\varphi_p^{nr}\rangle}{\varepsilon_p-\varepsilon_q}\varphi_q^{nr} \tag{9}$$

Z^N is the atomic number of nucleus N and φ_i^{nr}, φ_a^{nr}, and φ_p^{nr} denote occupied, vacant, and general (occupied or vacant) spin orbitals, respectively. P^{AB} is the permutation operator acting on the operators in the brackets, leading to two additional terms in brackets on the right-hand side (RHS) of eq 8 (AB+BA). The linear SO correction to the one-electron energies is zero thanks to the symmetry of the SO operator. Therefore, eqs 8 and 9 are formulated only in terms of the nonrelativistic one-electron energies, ε_p (we refrain here from trying to start from an SR wave function, as this would generate further ambiguities regarding the nature of the perturbation operators). Note that each φ^{nr} can

https://dx.doi.org/10.1021/acs.chemrev.9b00785
Chem. Rev. 2020, 120, 7065−7103

be either an alpha or a beta spin orbital with the same one-electron energy. In eq 9 we assume that the one-electron energy level ε_p is doubly degenerate and that the corresponding alpha and beta spin orbitals (φ_p^{nr} and $\varphi_{p\pm1}^{nr}$) are excluded from the summation. Furthermore, in the case of one heavy atom in the system, we approximate the SO operator in eq 9 as $\sum_{N=1}^{nuc} Z^N r_N^{-3} \hat{l}_u^N \cong Z^{HA} r_{HA}^{-3} \hat{l}_u^{HA}$. We note in passing, that in the sum-over-states theory the $\hat{\boldsymbol{l}}^{HA}\mathbf{1}$ operator couples only states with identical total spin, whereas both $\hat{\delta}^{LA}\boldsymbol{\sigma}_u$ and $r_{HA}^{-3}\hat{\boldsymbol{l}}^{HA}\cdot\boldsymbol{\sigma}$ are triplet operators and thus couple states with different total spin. Note also that after some tedious algebraic manipulations with the terms in brackets on the RHS of eq 8, we can recover the third-order perturbation theory eqs 18 and 19 given below. All necessary approximations to make the analysis at the 2c (eqs 8 and 9) or 1c (eqs 18 and 19) level of theory feasible are given below, and can be found in more detail in refs 99 and 100.

To analyze the SO corrections to the isotropic paramagnetic NMR shielding, the second term on the RHS of eq 8, we use the following guidelines:

- The energy denominator in eqs 8 and 9 restricts significant contributions to frontier molecular spinors.
- Thanks to the double degeneracy of the MSPs, each energy denominator in each of the four terms in brackets of eq 8 corresponds to four possible combinations of spin orbitals φ^{nr} and the molecular response spinor φ^{SO}. Fortunately, in most cases, only two of these are non-negligible, as illustrated in Figure 3.
- Thanks to the shortsightedness of the function r_{HA}^{-3}, we can assume atomic-like SO splitting of the nonrelativistic spin orbitals centered primarily on the HA when a single HA is present. However, there are exceptions to this rule. In general, these exceptions occur when the SOC mixes in spin orbitals on neighboring atoms, see, e.g., the description of the trans-ligand influence in section 3.2.
- Because of the energy denominator in eq 9 and a usually large HOMO−LUMO energy gap, the SO operator mixes effectively either only occupied or only vacant molecular spinors. In the case of small HOMO−LUMO gaps or large SO-coupling integrals, there can be SO mixing between occupied and vacant spin orbitals, as illustrated by the TlH example in section 3 (Figure 19b).
- The operator $\hat{\delta}^{LA}\boldsymbol{\sigma}_u$ couples only functions with s-character on the LA. These functions are usually σ-bonding and σ-antibonding orbitals. They can enter eq 8 as the stand-alone spin orbital φ^{nr} or as part of the SO correction to the MS, φ^{SO}. Figure 3 below depicts the former case.

To illustrate these points, in Figures 2 and 3 we deal with a hypothetical system with one occupied σ-bonding MO, two nonbonding MOs and one vacant σ-antibonding MO. Figure 2 represents eq 9, i.e., the construction of the occupied MSP, φ_i^{2c} and φ_{i+1}^{2c}, from NR orbitals. The NR spatial MOs depicted on the left side of both figures are used to construct alpha/beta spin orbitals, φ^{nr}, in eqs 8 and 9. Each MS then is composed of alpha and beta spin orbitals, φ_i^{nr} and φ_{i+1}^{nr} (left gray box in Figure 2), and molecular response spinors, φ_i^{SO} and φ_{i+1}^{SO} (right gray box in Figure 2), respectively. For localized SO mixing at the HA, the SO correction φ^{SO} generally contributes to the opposite spin channel (α/β) of the total MS compared to the zeroth-order correction φ^{nr}. Figure 3 illustrates the first term in brackets on the RHS of eq 8, i.e., one part of the SO correction to the

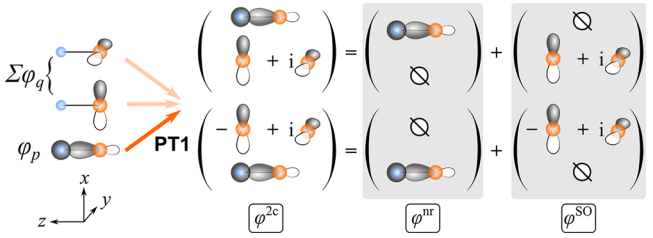

Figure 2. Graphical representation of the composition and creation of a 2c MSP from NR MOs. Every MS φ_p^{2c} is composed of an NR spin orbital φ_p^{nr} and an SO correction φ_p^{SO}. The SO correction to φ_p^{2c} is constructed from the NR spin orbitals φ_q^{nr} by SO mixing within PT1 theory (see eq 9).

isotropic paramagnetic nuclear shielding. Here only two out of four possible combinations composed of doubly degenerate spin orbitals φ^{nr} and molecular response spinors φ^{SO} give nonzero contributions. Since the MOs that make up φ^{SO} and φ^{nr} are orthonormal, the angular-momentum operator along the z-direction in Figure 3 gives zero couplings. The vanishing couplings then explain why the SO correction to the NMR shielding makes a small contribution to the tensor component parallel to the HA−LA bond.[99]

2.3.2. Perturbational Inclusion of SO Effects. As the efficiency of variational 2c and 4c methods has improved over the years, a perturbational inclusion of SO coupling has become less popular for practical calculations. A perturbational treatment does not provide quantitative accuracy for systems with atoms from the sixth period or below, and depending on the type of perturbation theory, various numerical difficulties arise (e.g., variational instabilities and singular operators).[84] On the other hand, PT treatment constitutes an excellent interpretational tool when it is based on an NR wave function. In contrast to the complex relativistic 2c or 4c MSs (see above), the use of nonrelativistic (real) molecular orbitals results in a natural language to discuss chemical phenomena. Therefore, in practice, 2c or 4c methods are used to obtain quantitative NMR shift data. Then, provided a perturbational treatment of the SO effects reproduces these results sufficiently well, one can use it to analyze the data in the more convenient framework of NR (or SR) MOs. In order to avoid any ambiguities in the nature of the perturbation operators in different SR frameworks, we will, as in the 2c case above, not use SR wave functions as a starting point in the following discussion. However, it is worth pointing out that in principle the SR wave function can also be a valid starting point for the perturbation analysis of SO effects only.

Within a single-determinantal Hartree−Fock or DFT treatment of a closed-shell singlet system, the nonrelativistic Fock (or Kohn−Sham) equations have the form

$$F^{NR}\varphi_p = \varepsilon_p\varphi_p \tag{10}$$

where the index p denotes both occupied and vacant orbitals and energies and φ_p and ε_p are the NR scalar MOs and one-electron energies, respectively, as used also in eq 6. In the nonrelativistic theory for closed-shell systems, no operator mixes the alpha and beta parts of a given spin orbital. Therefore, the alpha and beta MOs come in pairs with the same spatial part φ_p. The one-electron part of the Fock operator F^{NR} is a well-known nonrelativistic Schrödinger operator h^{NR}. To take into consideration the lowest-order ($\sim c^{-2}$) relativistic corrections in the absence of the magnetic fields, it is necessary to include

https://dx.doi.org/10.1021/acs.chemrev.9b00785
Chem. Rev. 2020, 120, 7065−7103

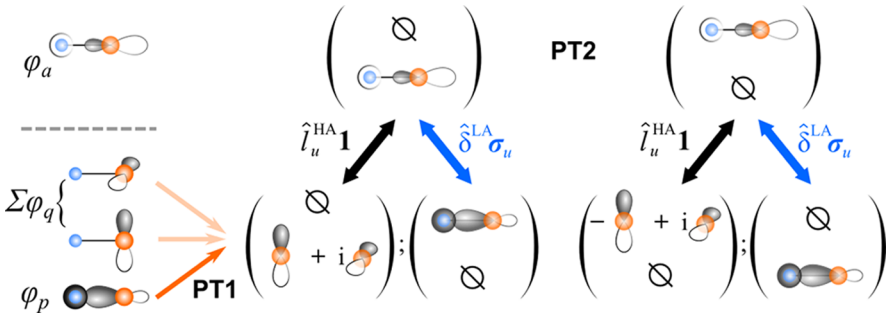

Figure 3. Graphical representation of the SO correction to isotropic paramagnetic NMR shielding at a LA in the framework of 2c relativistic theory. As an example, we schematically visualize the first term in brackets on the RHS of eq 8. The NR spin orbitals and the SO correction to the MS are coupled using PT2 theory with 2c Fermi contact $\hat{\delta}^{LA}\boldsymbol{\sigma}_u$ (in blue) and angular-moment $\hat{l}_u^{HA}\mathbf{1}$ (in black) operators.

three corrections to h^{NR}. The so-called Pauli Hamiltonian then has the form[82]

$$h^{Pauli} = h^{NR,2c} + h^{MV} + h^{DW} + h^{SO} \tag{11}$$

$$h^{MV} = -\frac{1}{8c^2}p^4\mathbf{1} \tag{12}$$

$$h^{DW} = \frac{\pi}{2c^2}\sum_{N=1}^{nuc} Z^N\hat{\delta}^N\mathbf{1} \tag{13}$$

$$h^{SO} = \frac{1}{4c^2}\sum_{N=1}^{nuc} Z^N r_N^{-3}\hat{\boldsymbol{l}}^N\cdot\boldsymbol{\sigma} \tag{14}$$

Here $\hat{\delta}^N = \hat{\delta}(\boldsymbol{r}_N)$ is the Dirac delta function centered on atom N and $\boldsymbol{r}_N$ is the electron position operator relative to the position of nucleus N. The Pauli Hamiltonian (eq 11) has a two-component structure in contrast to the scalar form of eq 10. This difference is emphasized in a slightly different definition of the Schrödinger operator, $h^{NR,2c} = h^{NR}\mathbf{1}$. Two of the relativistic operators, the mass velocity h^{MV} and Darwin h^{DW} terms, are clearly SR operators. As they contribute via the identity matrix on the diagonal of the Pauli Hamiltonian, they change only the scalar part of the two-component MOs. In other words, SR operators do not contain spin variables and are sometimes also referred to as "spin-free relativistic" operators. Examples of the well-known SR effects are the (direct) contraction of s-type core orbitals and the (indirect) expansion of valence orbitals having higher angular momentum.[103] On the other hand, the spin−orbit operator h^{SO} depends on the Pauli matrices (i.e., on spin variables) and therefore mixes the alpha and beta parts of the MOs and causes the SO splitting.

In the presence of magnetic fields, there are additional relativistic corrections to the Pauli Hamiltonian that we do not list here for the sake of brevity.[11] Within perturbation theory, the resulting isotropic paramagnetic NMR shielding can be written formally as

$$\sigma^p(\mathrm{LA}) = \sigma^{NR,p}(\mathrm{LA}) + \Delta\sigma^{REL,p}(\mathrm{LA}) \tag{15}$$

where $\sigma^{NR,p}$ is defined in eq 6 and $\Delta\sigma^{REL,p}$ contains in total 19 relativistic contributions (up to order c^{-4}) as defined in ref 11. Traditionally, the contributions containing h^{MV} or h^{DW} (h^{SO}) are termed SR (SO) relativistic corrections. The remaining contributions cannot be classified easily as SR or SO, but they can be characterized by their (in)dependence on the spin operators.[56] Fortunately, the majority of the relativistic contributions have negligible effects on the paramagnetic part of the isotropic (relative) NMR chemical shift.[56,57] One reason is that many of the SR contributions cancel out since they depend only on the core electronic structure around the LA, which is very similar for reference σ_{ref}(LA) and spectator σ(LA) isotropic NMR shielding (note the dependence of the Darwin operator, eq 13, on the Dirac delta function).[54,55]

They can nevertheless be sizable, at least for HAs from the sixth period downward (see section 4 for examples). In such cases, both SR and SO effects must be analyzed.[36−39,104] For the paramagnetic NMR shift we can write

$$\delta^p(\mathrm{LA}) = \delta^{NR,p}(\mathrm{LA}) + \Delta\delta^{REL,p}(\mathrm{LA}) \tag{16}$$

If the system contains only one HA with directly bonded LA, then there are five non-negligible relativistic contributions to δ^p(LA).[105] Two of them (arising from the mass-velocity and Darwin terms) are SR contributions, which are discussed separately (see Section 1 and below). Among the remaining three terms, fortunately in most cases only one has a major trend-defining effect on the isotropic shifts. This is the so-called spin−orbit/Fermi-contact contribution, $\sigma^{SO/FC}$.[56,60,105] The SO/FC term arises from the contact interaction (represented by the Dirac delta function) between the nuclear and electron spins, and therefore only s orbitals of the spectator LA make nonvanishing contributions to this mechanism (the analogous SO/SD term can also be sizable but does not control the main trends[106]). For the chemical concepts arising from this mechanism, see section 3. As this term depends on the SO contribution of the nearby HA, it typically will not cancel for relative shifts. Therefore, we can express the dominant relativistic contribution to the paramagnetic isotropic NMR shift as

$$\Delta\delta^{REL,p}(\mathrm{LA}) \cong \delta^{SO}(\mathrm{LA}) \cong \delta^{SO/FC}(\mathrm{LA}) = -\sigma^{SO/FC}(\mathrm{LA}) = -\frac{1}{3}\sum_{u=1}^{3}\sigma_{uu}^{SO/FC}(\mathrm{LA}) \tag{17}$$

The term δ^{SO}(LA) is referred to as the SO-HALA shift and is usually dominated by the SO/FC contribution, $\delta^{SO/FC}$(LA). In sections 3 and 4, the SO-HALA shift, δ^{SO}(LA), is calculated as the difference between the fully relativistic and scalar relativistic values as described in section 6.3. The quantitative analysis of the approximate relation $\delta^{SO}(\mathrm{LA}) \cong \delta^{SO/FC}(\mathrm{LA})$ is discussed, for example, in ref 100.

2.3.3. Third-Order Perturbation Analysis. Here we discuss the dominant SO/FC contribution to the SO-HALA shift in more detail, to provide the mathematical basis for the MO analysis described in the following sections. In the third-

https://dx.doi.org/10.1021/acs.chemrev.9b00785
Chem. Rev. 2020, 120, 7065−7103

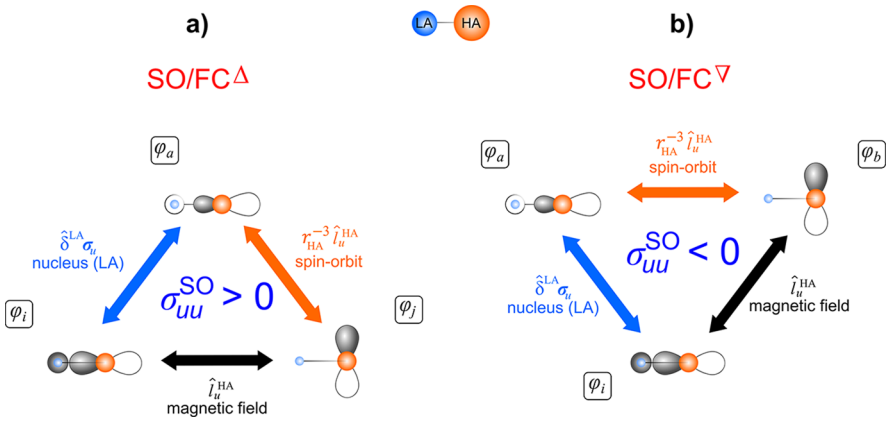

Figure 4. Example of the nonlocal nature of the SO/FC contribution to the LA shielding, which originates at the HA and propagates to the LA via either (a) the SO/FC$^{\Delta}$ mechanism involving two occupied MOs: $\varphi_i \leftrightarrow \varphi_j \leftrightarrow \varphi_a$ (see eq 18) or (b) the SO/FC$^{\nabla}$ mechanism involving two vacant MOs: $\varphi_i \leftrightarrow \varphi_a \leftrightarrow \varphi_b$ (see eq 19).[99] The interaction of an external magnetic field with the electronic orbital motion, given by an angular-momentum operator $\hat{l}^{HA}$, is color-coded in black. The perturbation caused by the nuclear magnetic moment of the LA via the FC interaction $\hat{\delta}^{LA}$ is coded in blue, and the SO coupling $r_{HA}^{-3}\hat{l}^{HA}$ originating at the HA is coded in orange. Note that in contrast to the SO-HALA shielding shown here, the SO-HALA shift discussed in sections 3 and 4 is of the opposite sign, see eq 17.

order perturbation theory (PT3) formalism, we can split $\sigma_{uu}^{SO/FC}$ into two contributions (for example, see refs 106 and 107):

$$\sigma_{uu}^{SO/FC^{\Delta}}(LA) \cong -P^{ABC}\frac{2\pi Z^{HA}}{3c^4} \sum_{i=1}^{occ}\sum_{j=1}^{occ}\sum_{a=1}^{vac} \frac{\langle\varphi_a|\hat{\delta}^{LA}|\varphi_i\rangle\langle\varphi_i|\hat{l}_u^{HA}|\varphi_j\rangle\langle\varphi_j|r_{HA}^{-3}\hat{l}_u^{HA}|\varphi_a\rangle}{(\varepsilon_i-\varepsilon_a)(\varepsilon_j-\varepsilon_a)} \quad (18)$$

$$\sigma_{uu}^{SO/FC^{\nabla}}(LA) \cong P^{ABC}\frac{2\pi Z^{HA}}{3c^4} \sum_{i=1}^{occ}\sum_{a=1}^{vac}\sum_{b=1}^{vac} \frac{\langle\varphi_i|\hat{\delta}^{LA}|\varphi_a\rangle\langle\varphi_a|\hat{l}_u^{HA}|\varphi_b\rangle\langle\varphi_b|r_{HA}^{-3}\hat{l}_u^{HA}|\varphi_i\rangle}{(\varepsilon_i-\varepsilon_a)(\varepsilon_i-\varepsilon_b)} \quad (19)$$

Here P^{ABC} is the permutation operator acting on the operators in brackets; thus, each of the two eqs 18 and 19 has three contributions (ABC + CAB + BCA). Assuming there is only one HA in the system, we have approximated the SO operator as $\sum_{N=1}^{nuc} Z^N r_N^{-3}\hat{l}_u^N \cong Z^{HA} r_{HA}^{-3}\hat{l}_u^{HA}$. We have made other approximations, such as neglecting the two-electron SO interaction, as well as first- and second-order kernels, and using a point-charge model of the charge distribution (for more details, see refs 99 and 100), which in a semilocal DFT framework makes the analysis of the HALA effect simultaneously feasible and meaningful. Note that eqs 18 and 19 are mathematically equivalent to the second term on the RHS of eq 8.

Three simple observations from eqs 18 and 19 are

A The energy denominator restricts significant contributions to frontier MOs. This restriction is even stronger for energy differences >1 *au* than in the nonrelativistic case (eq 6) due to the square-dependence of eqs 18 and 19 on these energy differences. In addition, the energy denominator is always positive, and thus it will not influence the sign of eqs 18 or 19.

B Thanks to the function r_{HA}^{-3}, MOs φ_i and φ_a must contain contributions from atomic orbitals centered at the HA.

C Similarly, thanks to the Dirac delta function $\hat{\delta}^{LA}$, MOs φ_i and φ_j in eq 18, and MOs φ_a and φ_b in eq 19 must include a contribution from s-type atomic orbitals centered on the LA.

These observations are used to analyze the NMR shifts of hydrogen and 2p atoms in the following sections.

2.4. HALA Effects on ^{1}H NMR Shifts

Considering that hydrogen as a LA uses almost exclusively its 1s orbital in bonding, and taking the above three observations into account, there are only four types of MOs making significant contributions to the summations in eqs 18 and 19 in the case of ^{1}H NMR shifts: the bonding σ_{HA-LA} and the antibonding σ^*_{HA-LA}, AO_{HA}, and AO^*_{HA}. Here AO_{HA} (AO^*_{HA}) denote occupied (vacant) molecular orbitals containing appreciable contributions from atomic orbitals at the HA. An example of AO_{HA} is a nonbonding orbital at the HA (n_{HA}), often denoted lone pair (LP), or a bonding orbital with other ligand atoms (HA–L bond). However, the latter type is typically lower in energy, and the energy denominator thus diminishes its effect. In the following, we abbreviate the sigma HA-LA orbitals as σ and σ^*, when appropriate.

Equations 18 and 19 give rise to six different terms, each of which contains three integrals. Of these, one includes a delta function, and two contain an angular-momentum operator. Two examples of such terms are visualized in Figure 4. The vertices of the triangle represent the involved MOs, while the orientation of the triangle corresponds to their energy (higher-lying vacant orbitals at the top and lower-lying occupied orbitals at the bottom). Each edge of the triangle coincides with an operator that couples the MOs across the corresponding vertices. The three operators involved in the SO/FC mechanism are the SO-coupling, Fermi-contact, and angular-momentum operators. The role of the SO-coupling term, which in analogy to the PSO term in Ramsey's equation has a rather local character, is to provide a coupling between two HA-based p-, d-, or f-type orbitals. In the following graphical representations this operator ($r_{HA}^{-3}\hat{l}^{HA}$) is color-coded in orange to highlight its origin at the HA. The Fermi-contact interaction term $\hat{\delta}^{LA}$, highlighted in blue, is particularly sensitive to the electronic structure around the LA (also shown in blue). It gives nonzero couplings only for σ-bonding and σ-antibonding orbitals since only these orbitals have a significant s-type contribution at the LA. In contrast to the

https://dx.doi.org/10.1021/acs.chemrev.9b00785
Chem. Rev. 2020, 120, 7065−7103

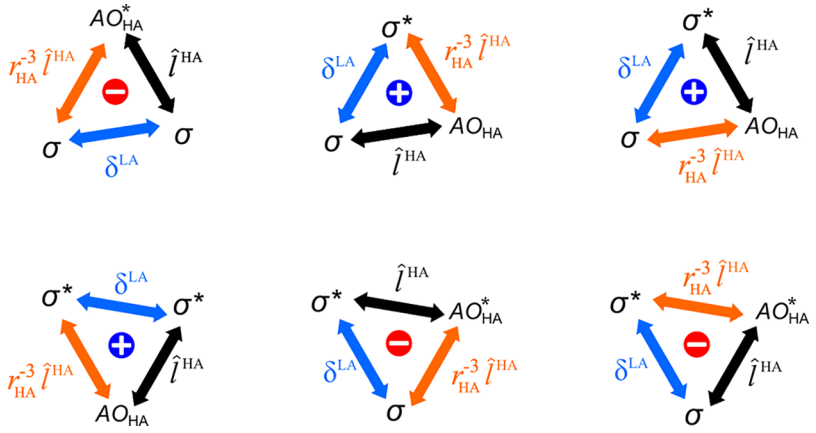

Figure 5. Schematic representation of the six MO coupling terms (triangles) active in the ^{1}H SO-HALA shielding, eq 18 (upper three triangles) and eq 19 (lower three triangles).[99] Four types of molecular orbitals are involved in the coupling, sigma HA−LA (anti)bonding MOs and occupied (vacant) MOs with significant AO_{HA} (AO^*_{HA}) contribution (examples are nonbonding MOs, n_{HA}, denoted alternatively as LP_{HA}). SO, FC, and angular-momentum operators are shown in orange, blue, and black, respectively.

PSO term (see above), the FC term represents a direct interaction of the magnetically induced electron-spin density with the LA nuclear magnetic moment. The remaining coupling term represents the applied external magnetic field through the angular-momentum operator $\hat{\boldsymbol{l}}^{HA}$ (analogous to the orbital Zeeman term in Ramsey's equation, eq 6). The mutual interplay among all three perturbations is shown schematically on an MO triangular diagram in Figure 4. Note that, while the FC and SO operators describe local interactions, their interplay results in the nonlocal nature of the SO/FC contribution to the SO-HALA shift. In the PT3 scheme, the SO/FC mechanism involves two occupied MOs and one vacant MO for the SO/FC$^\Delta$ term but one occupied MO and two vacant MOs for the SO/FC$^\nabla$ contribution, see Figure 4 and eqs 18 and 19.[99] If the FC operator couples two occupied MOs in SO/FC$^\Delta$ or two vacant MOs in SO/FC$^\nabla$, then these MOs can be identical, see the first triangle in each row in Figure 5.

To explain trends of SO-HALA NMR shifts across the Periodic Table[100] (sections 3 and 4), it is necessary to analyze eqs 18 and 19 in detail. The signs of all six terms in eqs 18 and 19 (triangles in Figure 5) can be deduced by the following reasoning. The final value of each of the six terms is invariant to the change of the phase (sign) of the molecular orbitals. Therefore, we can fix the sign of the HA AO contributing to the σ_{HA-LA} and σ^*_{HA-LA} MOs to be positive. This choice has two consequences:

1. The hydrogen 1s orbital contributes to σ_{HA-LA} and σ^*_{HA-LA} with opposite sign, which results in the following signs of the integrals involving the Dirac delta function: $\langle\sigma|\hat{\delta}^{LA}|\sigma\rangle > 0$, $\langle\sigma^*|\hat{\delta}^{LA}|\sigma^*\rangle > 0$, $\langle\sigma|\hat{\delta}^{LA}|\sigma^*\rangle < 0$, and $\langle\sigma^*|\hat{\delta}^{LA}|\sigma\rangle < 0$.

2. Second, if we assume that intra-atomic contributions dominate interatomic ones, all four integrals, $\langle X|\hat{l}^{HA}_u|\sigma\rangle$, $\langle X|\hat{l}^{HA}_u|\sigma^*\rangle$, $\langle X|r^{-3}_{HA}\hat{l}^{HA}_u|\sigma\rangle$, and $\langle X|r^{-3}_{HA}\hat{l}^{HA}_u|\sigma^*\rangle$, with X being either AO_{HA} or AO^*_{HA}, have the same sign. This assumption is less general, and we'll discuss some counterexamples below.

The second assumption is well satisfied for the SO integrals ($r^{-3}_{HA}\hat{l}^{HA}_u$), as the function r^{-3}_{HA} enhances AO contributions at the HA while those from the other atoms are quenched. Furthermore, it turns out that in practice the angular-momentum integrals ($\hat{l}^{HA}_u$) follow the same trend, even without the benefit of such a short-sighted r^{-3}_{HA} function. The second consequence is also crucial in understanding the final signs in eqs 18 and 19. It is cumbersome to determine the signs of all SO or angular-momentum integrals, but since they always appear in pairs, their signs are not needed, and their joint contribution is always positive. Combining the above arguments, the final signs of the different contributions in eqs 18 and 19 can be easily determined as illustrated in Figure 5. See section 3 for chemical interpretations.

While the determination of the signs of the different triangles described in Figure 5 works surprisingly well, there are still cases where different signs may occur:

- In the less common event that an orbital with σ-antibonding character for the HA−LA bond is occupied, i.e., when one sigma bonding orbital is replaced by an occupied antibonding orbital, the corresponding triangle will change sign. This can occur in cases where a given MO has both bonding and antibonding characteristics in nontrivial molecular systems.
- A similar situation may occur when a virtual MO has partial σ-bonding character with respect to the HA−LA bond.
- The simpler sign rules also come into question when the interatomic contributions to magnetic couplings are non-negligible (see point 2 above) as their sign is not governed by simple rules as is the case for intra-atomic contributions. This can occur when the intra-atomic contributions at HA vanish for reasons of symmetry (e.g., coupling of p- and d-atomic orbitals). One such case is the trans-ligand influence described in section 3.

2.5. HALA Effects on the NMR Shifts of 2p Atoms

In the case of NMR shifts of 2p LAs, we must also consider bonding and antibonding π orbitals (π_{HA-LA}, π^*_{HA-LA}). In this paragraph, we will discuss only arguments that are specific to the chemical shift of 2p elements, since the arguments presented above for ^{1}H shifts are applicable in this case without any changes. In most applications, we can assume that neither the bonding π_{HA-LA} nor the antibonding π^*_{HA-LA} orbital contain s-type AOs from the light atom LA. Then all π-type orbitals are excluded from couplings with the delta function $\hat{\delta}^{LA}$, and the only way π-type orbitals can influence the SO contribution to the LA shielding, $\sigma^{SO/FC}(LA)$, is through AO_{HA} and AO^*_{HA} orbitals. Note also that π-type orbitals are more likely to have non-

https://dx.doi.org/10.1021/acs.chemrev.9b00785
Chem. Rev. 2020, 120, 7065−7103

negligible interatomic contributions as is demonstrated in the discussion on trans-ligand influence in section 3.

2.6. Connection between the SO-HALA Shift and the Electron Density

In this section, we rationalize the connection of the relativistic SO contribution to the LA NMR shift, and the SO-induced electronic charge density. For closed-shell singlet systems, the first nonzero response of the electronic charge density to SO coupling is quadratic. In the following, we will refer to this function as $\rho_0^{SO,SO}$ or SO-EDD (spin−orbit-induced electron deformation density).[99] The SO-EDD does not depend on the external magnetic field. Its relation to the SO-HALA shift is thus not immediately obvious.

It has been pointed out[108] that the first-order SO effects on the NMR shielding tensor are generated exclusively by spin currents

$$\boldsymbol{j}^{\mathrm{spin}} = -\nabla \times \boldsymbol{\rho} \tag{20}$$

Here $\boldsymbol{\rho}$ represents the electron spin density. Focusing on the Fermi-contact mechanism and the fact that $\sigma^{SO/FC}(LA)$ is expressible as an integral of the spin-current $\boldsymbol{j}^{\mathrm{spin}}$ and the vector potential generated by the magnetic moment of the LA nucleus, one arrives at the relation[100]

$$\sigma^{SO/FC}(LA) = \frac{8\pi}{9c}[\rho_x^{B_x,SO}(LA) + \rho_y^{B_y,SO}(LA) + \rho_z^{B_z,SO}(LA)] \tag{21}$$

where $\boldsymbol{\rho}^{B,SO}(LA)$ denotes the bilinear response of the electron-spin density with respect to the magnetic field and the SO operator evaluated at the position of the LA. We will use the abbreviation SOM-ISD (spin−orbit-and-magnetically induced spin density)[100] for the function $\boldsymbol{\rho}^{B,SO}$.

In the case where only one HA is present in the system, a simple proportionality connection of SOM-ISD[100] and SO-EDD[99] can be derived from PT3 theory:[100]

$$\frac{Z^{HA}}{c}[\rho_x^{B_x,SO}(LA) + \rho_y^{B_y,SO}(LA) + \rho_z^{B_z,SO}(LA)] \sim \rho_0^{SO,SO}(LA) \tag{22}$$

This expression follows from the assumption that angular-momentum and SO integrals are proportional

$$\langle\varphi_p|r_{HA}^{-3}\hat{l}_u^{HA}|\varphi_q\rangle \sim \langle\varphi_p|\hat{l}_u^{HA}|\varphi_q\rangle \tag{23}$$

In practice, this assumption holds when eq 22 is evaluated at the position of (or in close proximity to) the LA. In this case the MOs involved in eq 23 arise from the set σ_{HA-LA}, σ^*_{HA-LA}, π_{HA-LA}, π^*_{HA-LA}, AO_{HA}, or AO^*_{HA}. When eq 22 is evaluated closer to the HA, other MOs, for which the proportionality of the integrals in eq 23 breaks down become involved (see Figure 13 in section 3).

Collecting the results from eqs 17, 21, and 22, we arrive at a simple, approximate connection between the isotropic SO-HALA shift, the SOM-ISD, and the SO-EDD at the position of the LA:[100]

$$\Delta\delta^{REL,p}(LA) \cong -\frac{8\pi}{9c}[\rho_x^{B_x,SO}(LA) + \rho_y^{B_y,SO}(LA) + \rho_z^{B_z,SO}(LA)] \sim -\frac{8\pi}{9Z^{HA}}\rho_0^{SO,SO}(LA) \tag{24}$$

As a result, the sign of $\Delta\delta^{REL,p}(LA)$ can be predicted just by the changes in the SO-EDD.[99,100] This argument runs parallel to typical (nonrelativistic) arguments in NMR studies that link changes in the electron density near the NMR nucleus to its shielding in different chemical environments. It is well-known,[13] however, that such correlations may fail when other aspects, such as energy denominators or angular momentum matrix elements, become important. While for the present SO case the link to the SO-EDD can likely explain the signs of the SO-HALA contributions, we anticipate that it will not hold generally when discussing more detailed trends.

3. CHEMICAL CONCEPTS: THE HA−LA INTERACTION

3.1. Mechanism, Factors Involved, and Tools for Interpretation

As has been demonstrated in the previous sections, the NMR chemical shift is intimately connected, albeit in a nontrivial way, to the distribution of electron density in the molecular or supramolecular system. Note that this does not mean just atomic charges, as frequently argued and discussed in the literature, but the full quantum electronic structure. In any case, chemists are taught to work with, and think in terms of, "chemical bonds" which somehow reflect interactions between two or more atoms in real space. A weakness of this broadly defined concept is that there is no quantum-mechanical operator that links the concept of a "chemical bond" to the quantum-mechanically defined NMR shielding constant. Yet, there have been many attempts to formulate links between the character of the HA−LA interaction and the SO-HALA NMR shift at the qualitative or semi-quantitative level. In the following we will discuss such links from the perspective of a chemist.

3.1.1. Spin−Orbit/Fermi-Contact (SO/FC) Mechanism of the SO-HALA Shift. *a). "The Fermi-contact step" of the SO/FC mechanism: the role of the s-character of the LA in the HA−LA bond.* As has been shown in section 2, the SO-HALA shift (δ_{LA}^{SO} in eq 17) is typically dominated by the Fermi-contact mechanism, SO/FC. While the spin-dipole (SO/SD) term is included in modern two- or four-component computations and thus contributes to the quantitative SO-HALA data, it tends to be less important[106] and is not considered in our qualitative reasoning throughout this review.

The conceptual analysis of the SO/FC mechanism, from the early work of Nomura et al.[19] over semiempirical implementations[30] to the first detailed treatment in DFT calculations,[26] has been described in the historical pre-2004 overview in section 1. While the individual "thought steps" elaborated below are part of one single SO/FC mechanism and thus act simultaneously, we introduce and discuss them separately for explanatory purposes and for the convenience of the reader.

Following the arguments presented in ref 26, the close and helpful analogy between the Fermi-contact mechanism of the indirect nuclear spin−spin coupling constant (J_{LA-X}^{FC}) and that of the SO-HALA shift ($\delta_{LA}^{SO/FC}$) is illustrated in Figure 6.

In both cases, the "last step" of the mechanism is linked to the Fermi-contact interaction between the induced electron-spin density surrounding the spectator NMR-active nucleus LA (not necessarily a "light atom", literally) and its nuclear magnetic moment (Figure 6, left). In the FC mechanism of J_{LA-X}, the spin density around X is generated in the "first step" by the nuclear magnetic moment of X (Figure 6, top right). In contrast, the spin density around the HA in the "first step" of the SO/FC mechanism of the SO-HALA NMR shift is induced by spin−

https://dx.doi.org/10.1021/acs.chemrev.9b00785
Chem. Rev. 2020, 120, 7065−7103

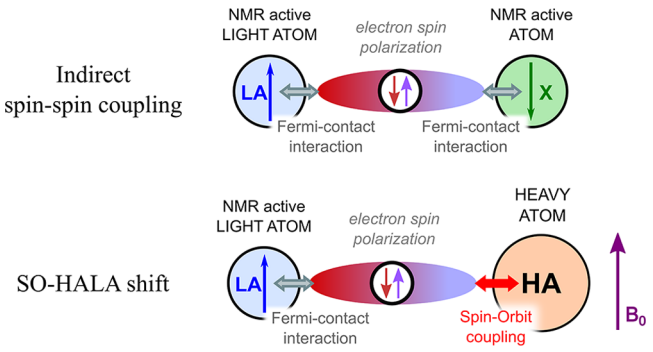

Figure 6. Schematic representation of the analogy between the Fermi-contact mechanism of the indirect spin−spin coupling constant (J^{FC}_{LA-X}) and that of the SO-HALA shift ($\delta^{SO/FC}_{LA}$) based on the idea of ref 26. Note that for consistency with the SO-HALA mechanism, the NMR spectator atom is labeled LA also in the case of indirect spin−spin coupling.

orbit coupling in the presence of a magnetic field (Figure 6, bottom right). In an "intermediate step", the induced electron-spin density around the HA (or X) is propagated throughout the system to reach the spectator LA. Here the spin density interacts with the nuclear magnetic moment of the LA via the FC interaction.

Clearly, a larger involvement of the valence *s* orbital of the LA in the HA−LA bond, i.e., a high LA s-character of the hybrid orbital employed by the LA for HA−LA bonding and efficient HA↔LA electron sharing, enables the spin-polarization mechanism to induce a larger spin density near and at the LA nucleus, causing a more significant FC interaction and enhancing δ^{SO}_{LA}. The correlation between the LA s-character of the HA−LA bond and δ^{SO}_{LA} has been demonstrated widely and for various classes of compounds, see section 1. Textbook examples of increasing s-character involve sp^3, sp^2, and sp-hybridized carbon atoms bonded to heavy halogen(s),[26] particularly iodine, as shown in Figure 7a.

Note that the effect of multiple-halogen substitution at the carbon atom on the ^{13}C SO-HALA shift is nonlinear as shown in Figure 7b. As more electronegative halogens are attached to the LA, increasing hybridization defects enhance the LA s-character of the HA−LA bond and thus lead to nonadditive behavior.[3] A similar dependence has been demonstrated for hydrides of transition-metals[95] and actinides.[97] For various examples of these effects, see Section 4.

b). "The spin-orbit step" of the SO/FC mechanism: Involvement of the HA orbitals in the HA−LA bond. In addition to the LA character of the HA−LA bond discussed above, one can look at the SO/FC mechanism from the opposite direction, studying the involvement of the HA valence orbitals in the HA−LA interaction. For example, the HA *d*-character of the HA−LA bond in transition-metal complexes has been reported to have a significant effect on the electronic structure around the HA, governing the "initial spin-orbit step" of the SO/FC mechanism.[109] This is demonstrated on a set of model PyAu(I)X (Py = pyridine) complexes with various trans substituents X which modulate the Au *d*-character of the HA−LA bond in Figure 8.

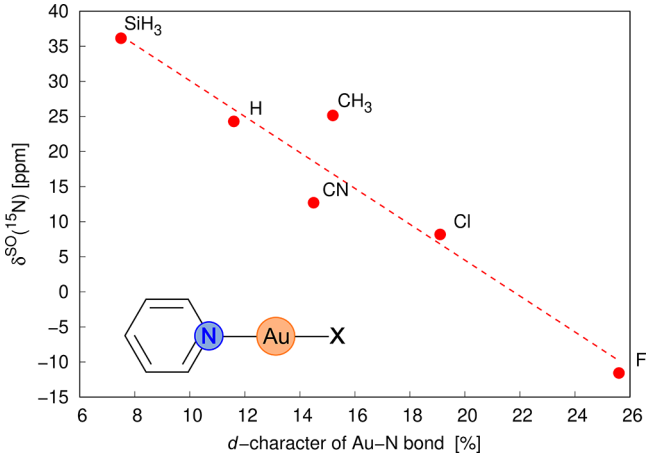

Figure 8. Relationship between the HA *d*-character[109] of the HA−LA bond in PyAu(I)X and δ^{SO}_{LA}.[99] The data were obtained using methods specified in section 6.1 (method 1), section 6.2, and section 6.3.

Two main factors influence the magnitude of the SO-based magnetically induced spin density at the HA. They are linked fundamentally to the electron *g*-factor in the EPR spectroscopy of open-shell systems:[109,110]

(i) The nuclear charge (atomic number) of the HA affects the magnitude of the relativistic spin−orbit effects as shown in eqs 14, 18, and 19. The dependence of SO splitting on the atomic number Z^{HA} can be easily understood (albeit not quantitatively) using semiclassical physical arguments. In the electron frame, the HA nucleus revolves

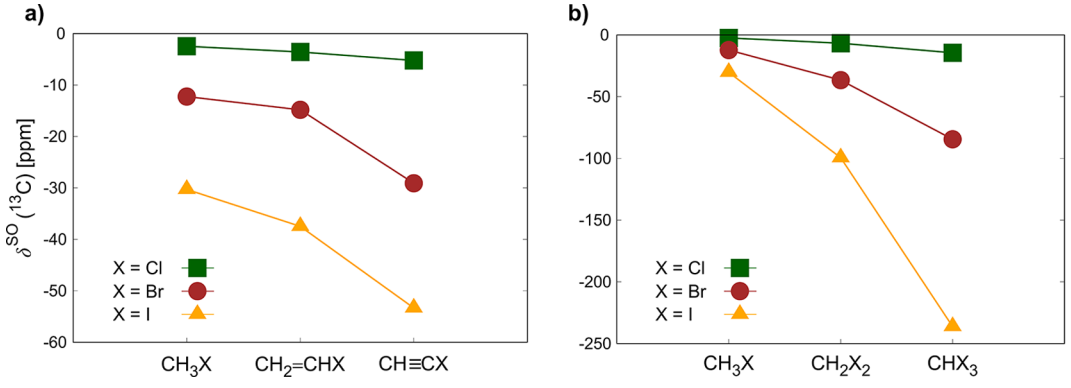

Figure 7. Effect of (a) carbon hybridization (sp^3, sp^2, and sp) and of (b) the number of halogen atoms attached (1−3) on the magnitude of the ^{13}C SO-HALA shift (δ^{SO}). The data were calculated using methods specified in section 6.1 (method 1) and section 6.3. For analogous plots based on perturbational SO treatments, see refs 3 and 26.

https://dx.doi.org/10.1021/acs.chemrev.9b00785
Chem. Rev. 2020, 120, 7065−7103

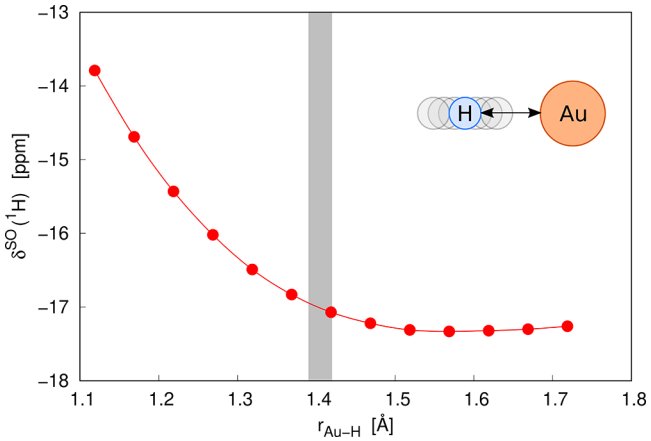

Figure 9. Effect of the interatomic HA−LA distance on the magnitude of $\delta^{SO}(^1H)$ for AuH. This can be related to a similar effect of the interatomic distance on the indirect nuclear spin−spin coupling.[112] The data were obtained using methods specified in section 6.1 (method 2) and section 6.3. The gray bar highlights the optimized equilibrium distance.

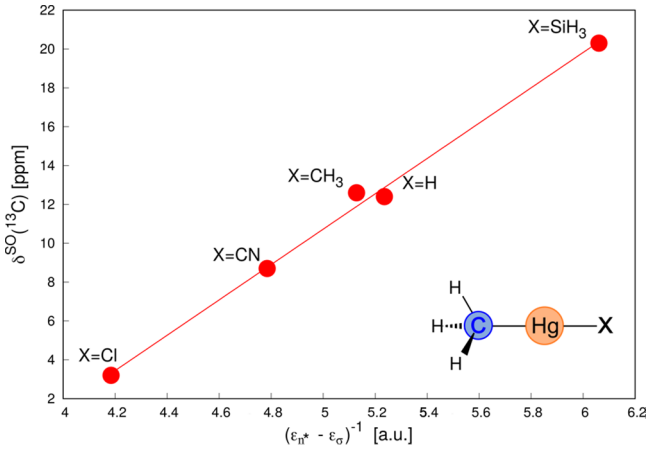

Figure 10. Correlation of $\delta^{SO}(^{13}C)$ in CH_3HgX compounds with the inverse of the energy difference between the occupied σ_{HA-LA} and vacant HA nonbonding (n^*_{HA}) Kohn−Sham orbitals involved in the dominant $\sigma_{HA-LA} \leftrightarrow n^*_{HA}$ MO coupling. Data from ref 38.

around the electron and generates an effective magnetic field at the position of the electron. This magnetic field depends linearly on the nuclear charge (Z^{HA}) and, coupled with the spin of the electron, gives the SO interaction (an effective nuclear charge may be used when also accounting for two-electron SO contributions).

(ii) The type of frontier MOs at the HA governs their SO splitting. That is, SOC does not directly influence the s orbitals, whereas valence p, d, and f orbitals are affected to different extents, depending also on their principal quantum number, for example, inner $(n - 1)$d orbitals vs outer np orbitals.

Considering (i), the nuclear charge is essentially a physical property, not a chemical concept. However, different HAs can exhibit principally different bonding with the LA, or with linking atoms for effects across more than one bond, see section 3.1.4. Naturally, larger relativistic effects are expected going down the Periodic Table (albeit energy gaps may counteract this trend for transition metals, see the inverted V-shape dependence below), whereas shell-structure effects cause the largest SO effects in each period to be found toward the right side of the Periodic Table, albeit exceptions do exist in the p-block, see section 4. Concerning (ii), the composition of the relevant valence MOs in terms of contributing angular momentum at the HA is crucial. For example, heavier elements of groups 2 (alkaline earth metals) and 12 (zinc group) exhibit notable $(n - 1)$d- and np-character, respectively, in their chemical bonding. As a result, they share many features with d(p) elements while formally being considered s(d)-block HAs. For examples and effects on δ^{SO}_{LA}, see section 4.

c). Link between the FC and SO steps: Covalency of the HA−LA bond. The efficiency with which the electron-spin density induced by SO coupling at the HA in the presence of a magnetic field is propagated to the spectator LA nucleus is tightly connected to the degree of electron sharing between the atomic basins of the HA and the LA, and thus to the covalency of the HA−LA bond.[104,111,114] This aspect can be considered a third piece of the puzzle in our understanding of the SO-HALA mechanism, in addition to the individual characters of the HA and the LA. Note, however, that the HA and LA character of the HA−LA bonding, and the HA−LA covalency are mutually interconnected. Naturally, the electron sharing for the HA−LA interaction depends on the interatomic HA−LA distance as does δ^{SO}_{LA},[47] but this dependence is clearly nonlinear (see Figure 9).

The magnitude of electron sharing between the HA and the LA can be described as follows:

(i) The covalency of the HA−LA bond is reflected in the relative positions of the frontier-orbital energies, in particular the gap between the occupied MOs dominating the HA−LA interactions and the associated vacant MOs of appropriate symmetry (see PT3 theory in section 2). A clear correlation between the energy gap of the "HALA MOs" and δ^{SO}_{LA} has been demonstrated for a series of CH_3HgX complexes,[38] Figure 10.

The role of the energy gap has also been used to explain the rather striking observation of a counterintuitive "inverted V-shape" dependence[95,113] of the SO-HALA effect down group 9, an example of which is shown in Figure 11. This is due to the generally smaller ligand-field splitting in 3d systems caused by the absence of a radial node in the 3d shell and the resulting stretched-bond situation.[46] This reduces the (square) energy denominators in the PT3 expressions (eqs 18 and 19 in section 2) and renders the SO-HALA effects larger in 3d compared to

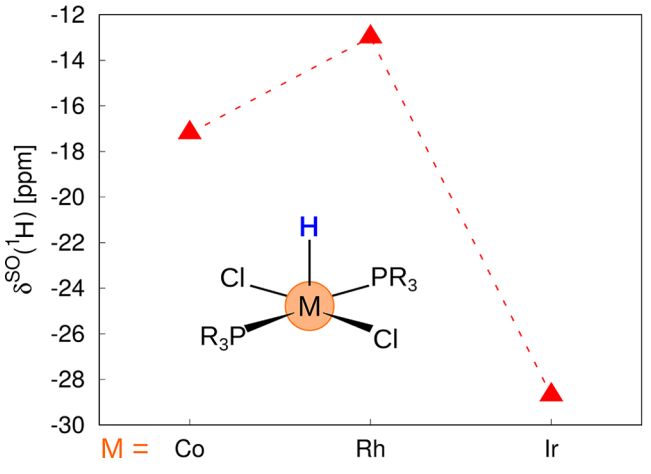

Figure 11. "Inverted V-shape" dependence of $\delta^{SO}(^1H)$ for a set of group 9 model compounds. Data from ref 95.

https://dx.doi.org/10.1021/acs.chemrev.9b00785
Chem. Rev. 2020, 120, 7065−7103

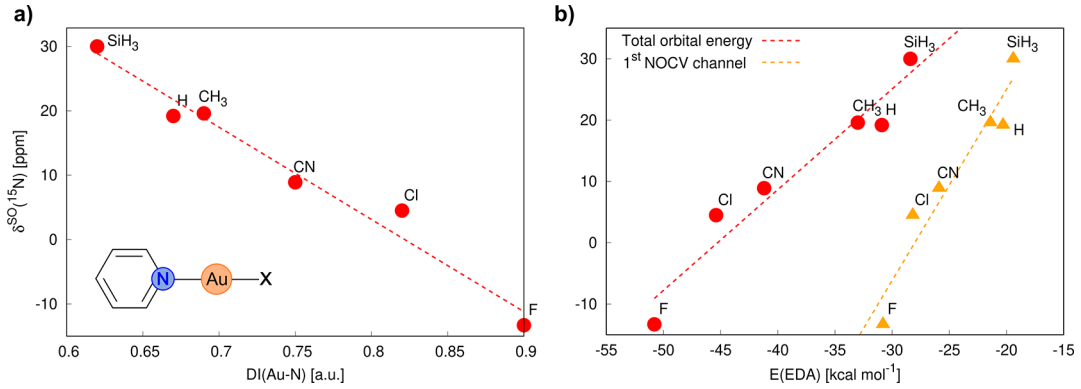

Figure 12. Relationship between the ^{15}N SO-HALA shifts (δ_{LA}^{SO}) in PyAuX compounds and (a) the delocalization index (HA ↔ LA) for the HA−LA bond[114] and (b) the orbital contribution to the EDA[116] bond energy (red) and ligand donation (orange) as quantified by the first NOCV-channel[117] of the EDA/NOCV analysis (see section 6.2).[99] Data from ref 99.

the analogous 4d complexes. Indeed, the Rh complex exhibits a less negative δ_{LA}^{SO} than its Co analog (Figure 11), as has also been found for smaller three-bond ^{1}H NMR effects in a series of polyamine complexes. While the energy denominators increase further from Rh to Ir due to the SR expansion of the 5d orbitals, the effect is more than compensated by the larger SO splitting of the 5d element, leading, overall, to the inverted V-shape.

(ii) Second, the covalency of the HA−LA bond can be quantified by electron sharing between the atomic basins of the HA and the LA as described, for example, by the delocalization index (DI, HA↔LA)[114] of the Quantum Theory of Atoms in Molecules (QTAIM). A larger covalency is reflected directly in a larger DI as has been demonstrated for a series of transition-metal complexes,[114,115] for which the DI correlates with the SO-HALA shifts, Figure 12a.

In a complementary fashion, the covalent character of the HA−LA bond has been investigated by energy decomposition analysis (EDA) and natural orbitals for chemical valence (NOCV) analysis, with the results also linked to δ_{LA}^{SO},[99] Figure 12b. Here, the larger covalency is reflected in both the more negative orbital stabilization energy and the more negative energy of the first NOCV bond channel, which reflects the ability of the ligand containing the LA (pyridine in Figure 12) to make a σ-donation to the Au-X unit.

3.1.2. Visualization Tools: SOM-ISD and SO-EDD. The propagation of the spin density induced at the HA by SO and the magnetic field during the "initial SO step" through to the last "Fermi-contact step" at the LA can be visualized by the real-space distribution of the SO-and-magnetically induced spin density (SOM-ISD, eq 24 in section 2)[100] shown in Figure 13a for model Au^{I}H and PhHg^{II}H systems as examples. These plots clearly demonstrate that the induced α or β spin density around the spectator hydrogen LA is reflected in a negative or positive sign of $\delta^{SO}(^1H)$, respectively.

It has also been shown previously that the SO-HALA shift can be correlated with the SO-induced electron deformation density (SO-EDD)[99] around the spectator NMR-active nucleus. This is the change in the total ground-state charge density due to SO coupling (section 2) and is shown in Figure 13b for the same two systems. Despite the different patterns in electronic structure around the HA, the SO-induced charge density (SO-EDD) surrounding the LA parallels the SOM-ISD patterns.

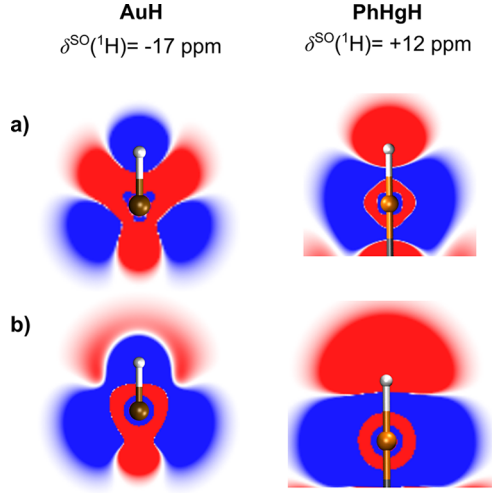

Figure 13. (a) Visualization of the SOM-ISD in Au^{I}H (left) and PhHg^{II}H (right). The local spatial predominance of α or β induced spin density is shown in blue and red, respectively. The calculated ^{1}H SO-HALA shifts (δ_{LA}^{SO}) are also shown for comparison. (b) Visualization of the SO-EDD in Au^{I}H and HHg^{II}Ph. The accumulation and depletion of electron density induced by SO coupling is shown in blue and red, respectively. The data were obtained using methods specified in section 6.1 (method 1), section 6.3, and section 6.4.

3.1.3. Structural and Electronic Influence of a trans Ligand. Particularly in the case of the HA being a transition metal, the character of the HA−LA bond can be substantially altered by the nature of the substituent or ligand bonded to the HA in the trans-position relative to the LA (labeled as TL or X), as had already been noted early on for d^{10} LA-Hg-TL systems.[38] The structural and electronic trans-ligand influence (TLI, also known as thermodynamic trans-effect or structural trans-effect) on the SO-HALA shift can be modeled computationally by changing the HA−TL bond length as has been demonstrated first for an octahedral Ir(III) complex.[118] While both scalar-relativistic and spin−orbit contributions to the NMR shifts are affected by the changes in the HA-TL distance, the modulation of the SO-HALA contribution is by far the more significant (see also section 4). The effect of the Au-TL distance on the ^{1}H SO-HALA shift of the trans hydride in HAu^{I}TL is shown in Figure 14. Note the reversal of the sign of the SO-HALA shift near the equilibrium distance of about 1.95 Å, highlighted by a gray vertical bar. The structural and electronic TLI is also reflected in

https://dx.doi.org/10.1021/acs.chemrev.9b00785
Chem. Rev. 2020, 120, 7065−7103

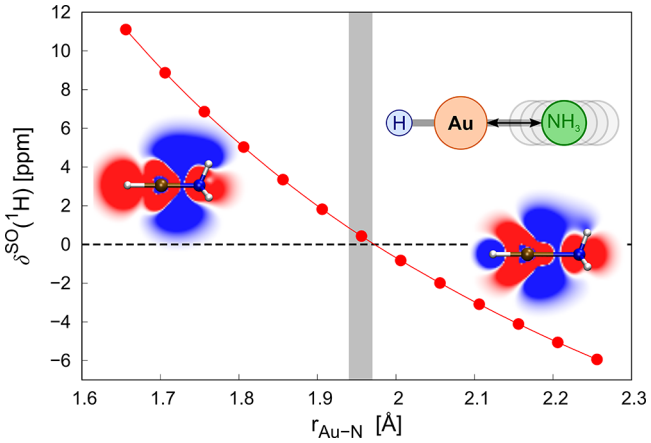

Figure 14. Effect of the HA-TL distance on the SO contributions[118] to the ^{1}H NMR shift in $HAuNH_3$. Note the change in the sign of the SO-HALA contribution around the equilibrium distance (indicated by a gray vertical bar). The SOM-ISD calculated for the short and the long HA-TL distances is shown on the left and the right, respectively. Note the change in color (opposite induced spin density) around the hydrogen atom. The data were calculated using methods specified in sections 6.3 and 6.4.

an inverted spin density around the LA as shown by the SOM-ISD for the short (left) and long (right) HA-TL distance.

The TLI on the SO-HALA shift has been elaborated upon extensively in a series of papers on iridium, platinum, gold, and mercury complexes.[99,109,114,115,119,120] The electronic TLI has been rationalized by the simultaneous involvement of a central HA orbital with both the TL and the LA. In other words, the two trans-arranged ligands share a single HA atomic orbital (AO) in their bonding. As a result, the polarization of HA-centered AOs by one of the substituents (e.g., the TL) induces a significant repolarization of the same orbital on the side of the second substituent (e.g., the LA).[99] The two substituents thus mutually influence the character of their bonding with the HA center, where the increasing polarity of the bond to the TL (smaller HA AO character in the HA−TL bond for a weaker trans-ligand) results in a more covalent bonding with the LA. The effect of the nature of the TL on the SO-HALA shift is shown in Figure 15.

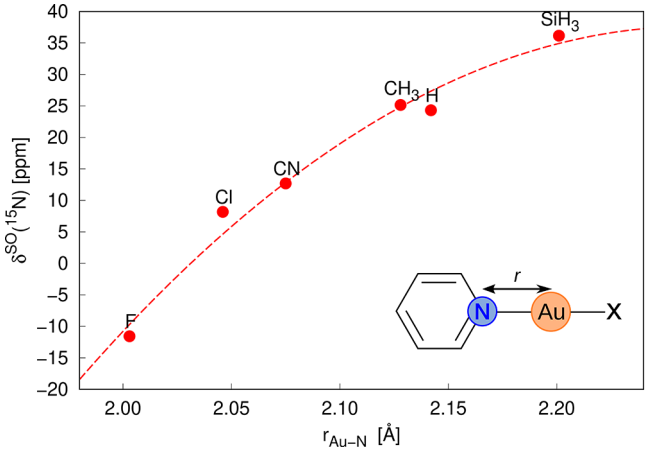

Figure 15. Influence of the trans-ligand (X) on the equilibrium HA−LA distance, r, and the SO contribution to the ^{15}N NMR shift (δ^{SO}_{LA}) for a pyridine ligand.[99] The data were obtained using methods specified in section 6.1 (method 1) and section 6.3.

We note that matters are rather different for actinide systems, where the intrinsically ungerade character of the 5f-AOs, as opposed to the gerade character of d-type AOs in transition-metal complexes, is known to contribute to an inverse TLI for structural and electronic properties.[121−124] Such an inverse TLI has been found to affect ^{13}C SO-HALA shifts in U^{VI} complexes in a relatively complicated manner.[97] As the valence p-orbitals are also intrinsically ungerade in nature, substituents in different positions likely affect SO-HALA shifts differently in heavy p-block compounds, although this has yet to be investigated in detail.

3.1.4. Long-Range SO Effects. As shown in Figure 6 above, there is a clear parallel between the FC mechanism of SO-HALA shifts and the FC contribution to indirect nuclear spin−spin couplings (see also Introduction). Thus, the SOM-induced spin density around the HA (see section 3.1.1) for the SO-HALA effect and the spin density around the X atom induced by the nuclear magnetic moment in case of J-coupling are propagated similarly by spin-polarization mechanisms, governed by exchange interactions, to generate a spin density at the position of the spectator LA. The schematic representation of the propagation of spin polarization from the HA to the LA via one, two, and three chemical bonds as governed by the Pauli principle and Hund's rule is shown in Figure 16a. The SOM-ISD

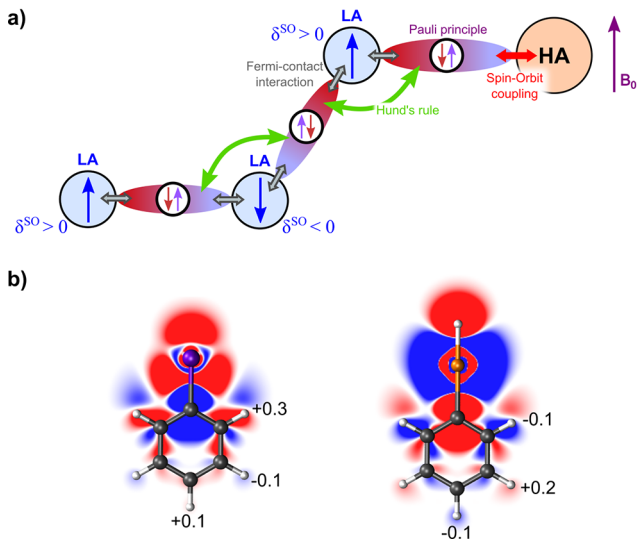

Figure 16. (a) Schematic representation of the propagation of spin polarization from the HA to the LA via one, two, and three bonds using the Dirac vector model, which is also commonly used to rationalize the alternation of the sign of indirect spin−spin coupling constants. (b) DFT-calculated distribution of SOM-ISD in PhI[26] (left) and $PhHg^{II}H$[130] (right). The spatial predominance of α and β SOM-ISD is shown in blue and red, respectively. The data were obtained using methods specified in section 6.1 (method 1), section 6.3, and section 6.4.

distributions in iodobenzene[26] and in PhHgH highlight the local predominance of α (blue) or β (red) induced spin density and its alternation throughout the conjugated system, resulting in alternation of the sign of δ^{SO}_{LA} for different atoms, see Figure 16b. We note in passing that a similar analogy applies to the pathways of spin-density propagation in the context of hyperfine couplings.[21,125,126] This has led to the definition of new 3D quantities termed "coupling electron deformation density"[127,128] and "hyperfine structure deformation density".[129]

https://dx.doi.org/10.1021/acs.chemrev.9b00785
Chem. Rev. 2020, 120, 7065−7103

Further examples of long-range SO-HALA effects are given in Section 4.

In analogy to the Fermi-contact mechanism of indirect nuclear spin−spin coupling, the Fermi-contact mechanism of SO-HALA shifts is governed by the electronic structure on the interaction path between the HA and the spectator LA. Thus, the Karplus-like torsion dependence of three-bond δ_{LA}^{SO} effects has also been rationalized by its analogy to nuclear spin−spin coupling pathways.[26] An example of the conformational dependence of $\delta^{SO}(^1H)$ for a "three-bond" interaction in Te═CH−CH_3 is shown in Figure 17. More examples are provided in section 4.

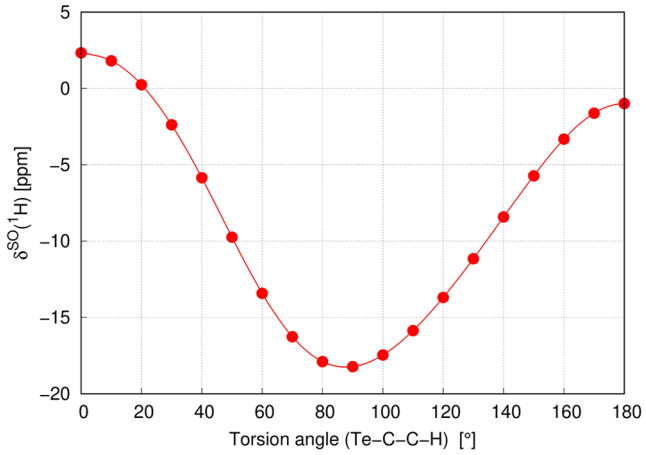

Figure 17. Karplus-like dependence of three-bond $\delta^{SO}(^1H)$ in Te═CH-CH_3 on the rotation of the central C−C bond. The data were obtained using methods specified in section 6.1 (method 1) and section 6.3.

3.1.5. "Through-Space" Supramolecular Effects. The propagation of the spin density induced during the above-mentioned SO step (section 3.1.1) toward the LA can also occur in various supramolecular interactions such as hydrogen, halogen, or chalcogen bonding. Note that this requires an uninterrupted pathway of sufficiently large electron density between the HA and the LA that can be polarized. In principle, this can be observed for various supramolecular bonding, nonbonding, and antibonding situations. However, the most efficient currently known examples of this effect are those exhibiting supramolecular covalency (orbital interaction and HA↔LA electron sharing),[131] which can also make a significant contribution to the total binding energy. As an example of this phenomenon, we plot (i) δ_{LA}^{SO}, (ii) the change in the NMR shift, calculated at the SR level, induced by the formation of a supramolecular bond ($\Delta\delta_{LA}^{SR/SB}$), and (iii) the SOM-ISD map in Figure 18 for a) the hydrogen-bonded (HB) ion-pair complex $NH_4^+\cdots I^-$ and b) the halogen-bonded (XB) complex $NH_3\cdots$IF. We note that in the first case, the SO-HALA effects reduce the overall (positive) complexation shift somewhat, whereas in the second case, the (negative) complexation shift is enhanced by the SO contributions.

3.2. Unifying the Chemical Concepts

3.2.1. PT2 Analysis Based on Molecular Spinor Pairs. A PT2 analysis of SO-HALA effects based on molecular spinors calculated at the two-component (or four-component) level is analogous to the standard NR or SR analysis of paramagnetic contributions to the NMR shift within the Ramsey formalism,

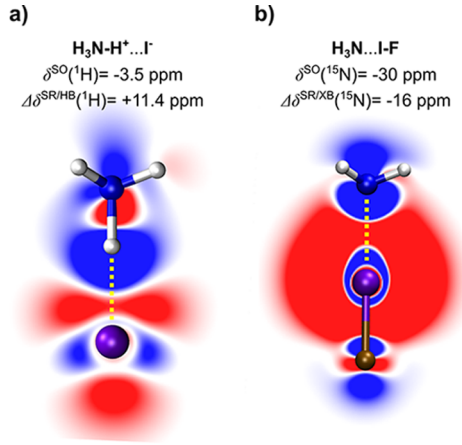

Figure 18. (a) $\delta^{SO}(^1H)$, $\Delta\delta^{SR/HB}(^1H)$, and a plot of the SOM-ISD for the hydrogen-bonded complex between NH_4^+ and I^- (for the H atom involved in the hydrogen bond). (b) $\delta^{SO}(^{15}N)$, $\Delta\delta^{SR/XB}(^{15}N)$, and a plot of the SOM-ISD for the halogen-bonded complex between NH_3 and IF. The predominance of α and β induced spin density is shown in blue and red, respectively. The data were obtained using methods specified in section 6.1 (method 1), Section 6.3, and section 6.4.

except that in the presence of SO coupling the perturbation operators for the nuclear magnetic moment include the FC and SD hyperfine contributions that underlie the SO-HALA effect (see section 2). The analysis for diamagnetic (closed-shell) systems is typically done using molecular spinor pairs (MSPs), also known as Kramers pairs. This allows an MSP ↔ MSP* coupling analysis while accounting for SO effects and provides differences from the analogous SR (or NR) values for the relevant MO ↔ MO* couplings.

A comparison between the MOs (NR or SR level) and MSPs (2c or 4c level) can be used to estimate the role of mixing MOs of different symmetry by SO coupling for the magnetic response of the system. This mixing in turn can be obtained from the nonrelativistic MOs using first-order perturbation theory (PT1), as demonstrated in Figure 2. As an example, we show the SO-induced mixing of occupied σ-bonding and nonbonding (n_{HA}) MOs at the HA for AuH in Figure 19a. The resulting MSP (HOMO−3) of mixed σ and π character dominates ($\Sigma\delta^{SO}$ = −16 ppm) the enhancement of the paramagnetic ^{1}H NMR shielding by SO coupling (reflected in the δ_{tot}^{SO} = −13 ppm relative to the SR data). The efficient and most significant magnetic coupling of the HOMO−3 with the LUMO (δ^{SO} = −14 ppm) is shown schematically in Figure 19a. In contrast to AuH, the SO-induced mixing of vacant (n_{HA}^*) MOs at the HA in TlH results in an extremely efficient deshielding HOMO↔LUMO magnetic coupling (δ^{SO} = +107 ppm),[132] which dominates the total SO-HALA shift (δ_{tot}^{SO} = +122 ppm), Figure 19b.

The advantage of the PT2 analysis is that SO effects are included variationally and thus more accurately and completely. A disadvantage is that the MSPs are complex quantities (see Figure 2) that are difficult to visualize and interpret completely, see section 2. One needs to transform the data in order to visualize them. For example, within the two-component ZORA implementation in the ADF code,[133,134] only one real function is typically displayed (Figure 19) instead of the required two complex functions. This has been used previously to interpret the roles played by the electronic structure around the metal atom[114] and the TLI[99,119] on the SO-HALA shifts in various transition-metal complexes. To relate the MSPs to the NR MOs

https://dx.doi.org/10.1021/acs.chemrev.9b00785
Chem. Rev. 2020, 120, 7065−7103

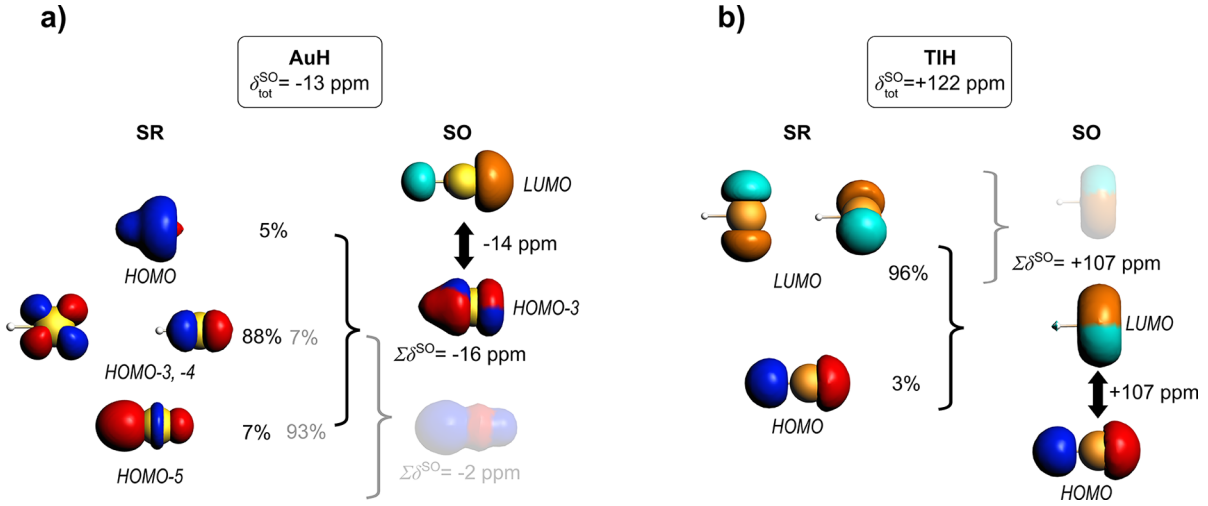

Figure 19. SO-induced (a) mixing of the occupied σ-bonding (HOMO and HOMO−5) and nonbonding (n_{HA}, HOMO−3, HOMO−4) SR MOs for AuH, and an example of the MSP↔MSP* coupling of the resulting HOMO−3 MSP with a LUMO MSP having significant LA s-character, and (b) mixing of two vacant n^*_{HA} MOs (LUMOs) and the occupied σ-bonding HOMO for TlH, and an example of the MSP*↔MSP coupling of the resulting LUMO MSP with an HOMO MSP having significant LA s-character. The contributions to δ^{SO}_{LA} are shown for the individual MSPs. The data were obtained using methods specified in section 6.1 (method 1) and section 6.5 (PT2).

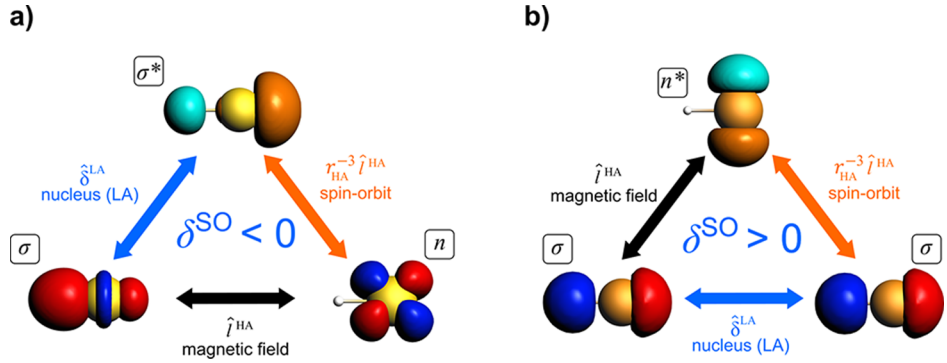

Figure 20. Schematic graphical representation of the SO/FC$^{\Delta}$ mechanism involving two occupied MOs (see also eq 18 and Figure 4).[99] (a) The shielding SO contribution that dominates the negative $\delta^{SO}(^1H)$ in AuH, and (b) the deshielding SO contribution that dominates the positive $\delta^{SO}(^1H)$ in TlH. The occupied MO in TlH can be viewed as a superposition of two MOs, antibonding s(Tl)-s(H) and bonding p(Tl)-s(H). Because s functions of the Tl atom have no effect on magnetic and SO coupling integrals, this occupied MO is considered as a σ-bonding orbital in the PT3 analysis. The data were obtained using the method specified in section 6.5.

and thus obtain further insight, one would have to apply PT1 to the MSPs (Figure 2 and section 2) and thus to sacrifice the higher accuracy of the two- or four-component treatment. Moreover, the mechanism and sign of the SO-HALA shift are not fully transparent in Figure 19. To understand the sign and mechanism of the SO-HALA effect in more detail, we must resort to the PT3-based analysis of δ^{SO}_{LA}, which is elaborated in the following section.

3.2.2. Transparent PT3 Analysis Based on Non-relativistic MOs. The PT3 scheme starts from nonrelativistic (NR) or scalar-relativistic (SR) MOs and adds SO coupling as another perturbation (section 2). It provides a particularly transparent and fine-grained interpretation in terms of standard nonrelativistic MOs, decoding their role in the magnetic response of the system.

As described in detail in section 2, the three perturbations involved in the SO/FC mechanism are the SO-coupling, Fermi-contact, and angular-momentum operators. The mutual interplay of all three perturbations has been discussed thoroughly in section 2 and is shown schematically in Figure 20, for examples of the triangular diagrams[99] that dominate the shielding and deshielding SO/FC contributions to δ^{SO}_{LA} in AuH and TlH, respectively. For the convenience of the reader, the interaction of an external magnetic field with the electronic orbital motion, given by the angular-momentum operator $\hat{\boldsymbol{l}}$, is color-coded in black. The perturbation caused by the nuclear magnetic moment of the spectator atom LA via the Fermi-contact (FC) interaction is coded in blue, and the SO coupling originating at the HA is coded in orange.

In the PT3 scheme, the SO/FC mechanism involving two occupied MOs and one vacant MO for the SO/FC$^{\Delta}$ term (within the reasonable approximations discussed in section 2) results in a shielding SO contribution ($\delta^{SO} < 0$, Figure 20a) unless both occupied MOs are of σ(HA−LA)-bonding character, which changes the overall sign ($\delta^{SO} > 0$, Figure 20b).[99] The two examples shown in Figure 20 are directly related to the PT2 analysis of AuH and TlH shown in Figure 19.

Given the PT3 examples in Figure 20, we now proceed to analyze the sign of the SO-HALA contribution to the NMR shift, as it relates to the electronic structure of the HA, which is crucially important to understanding the periodic trends discussed in section 4.[100] As discussed in section 2, the leading

https://dx.doi.org/10.1021/acs.chemrev.9b00785
Chem. Rev. 2020, 120, 7065−7103

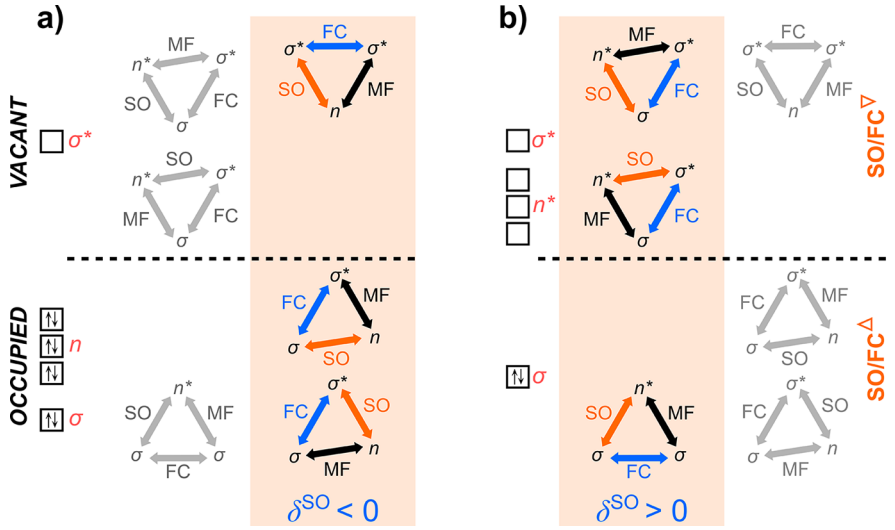

Figure 21. Schematic representation of two limiting electronic configurations at the HA with (a) occupied (n, left) and (b) vacant (n^*, right) HA-based nonbonding orbitals.[100] The sign of $\delta_{LA}^{SO/FC}$ is governed by the availability of occupied/vacant HA-based orbitals of suitable energy as shown by the MO coupling triangles for the SO/FC$^{\Delta}$ (bottom) and SO/FC$^{\nabla}$ (top) mechanisms.[99] Triangles shown in gray are not accessible for a given electronic configuration. Note that MF stands for the interaction of an external magnetic field (B_0) with the electronic orbital motion given by the angular-momentum operator $\hat{l}$ (see section 2), and $\sigma^{(*)}$ in the text stands for σ and σ^*, which are both present in all of the triangles due to the role of the FC operator (shown in blue).

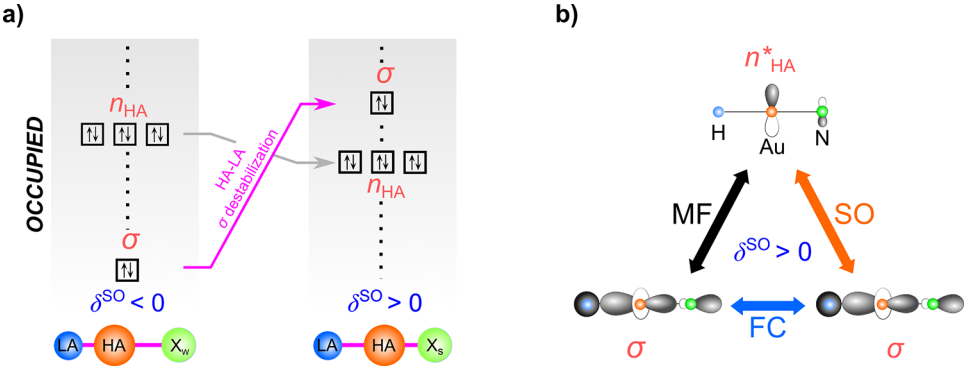

Figure 22. (a) Structural and electronic trans-ligand influence of a weak X_w like F or a strong X_s like CH_3 on the relative energy of the σ_{HA-LA} MO entering the coupling triangles and affecting the SO-HALA shift as discussed above.[99,119] (b) The PT3 coupling triangle governing $\delta_{LA}^{SO}(^1H) > 0$ in $HAuNH_3$ for a short Au−N distance (strong X), which highlights the role of 2p AOs of the trans nitrogen atom (shown in green), cf. Figure 14. MF stands for the interaction of an external magnetic field (B_0) with the electronic orbital motion, given by the angular-momentum operator $\hat{l}$ (see section 2). The data were obtained using the method specified in section 6.5.

MO↔MO couplings must arise from the frontier MOs, i.e., high-lying occupied and low-lying vacant MOs. Furthermore, the electronic structure around the HA can be analyzed in terms of MOs with significant coefficients from AOs on the HA (AO_{HA}). These AO_{HA}s are represented by nonbonding orbitals at the HA (n_{HA}, or lone electron pair - LP), π_{HA-LA} and δ_{HA-LA} bond types, and σ_{HA-L} with another ligand (L). For the sake of simplicity, let us consider the simplest HA−H example with only a σ(HA−H) bond and with nonbonding orbitals at the HA (e.g., AuH). Four types of frontier orbitals then play roles in the SO-HALA mechanism: nonbonding orbitals at the HA, including both occupied (n_{HA}) and vacant (n_{HA}^*) MOs, and occupied HA−LA bonding (σ_{HA-LA}) and vacant antibonding (σ_{HA-LA}^*) MOs. We denote them for simplicity as n, n^*, σ, and σ^*.

The two limiting cases of electronic configurations at the HA are shown in Figure 21. A representative electronic configuration with an available occupied nonbonding orbital n at the HA (n_{HA}) but without n_{HA}^* is shown in Figure 21a, whereas one without n_{HA} but with an available vacant nonbonding orbital n_{HA}^* is shown in Figure 21b. The presence of filled nonbonding MOs in the valence shell of the HA (Figure 21a) causes the active shielding contributions ($\delta_{LA}^{SO} < 0$) described as $n_{HA} \leftrightarrow \sigma_{HA-LA}^{(*)}$ in the SO/FC mechanism (examples are transition-metal complexes with d^2−d^8 configurations and halogen compounds, section 4). Note that $\sigma^{(*)}$ in the text stands for σ and σ^*, which are both present in all of the triangles due to the role of the FC operator. In the absence of occupied nonbonding MOs, only deshielding contributions ($\delta_{LA}^{SO} > 0$) labeled $\sigma_{HA-LA}^{(*)} \leftrightarrow n_{HA}^*$ in Figure 21b are nonzero, as found, for example, for p^0, d^0, and f^0 configurations at the HA in the molecule (not necessarily the atomic ground state of the HA).[100]

In general, both the SO deshielding and shielding contributions may be active simultaneously, with the total δ_{LA}^{SO} value governed by the energy separations between the relevant frontier MOs and the coupling MO matrix elements.[99] Excellent examples representing a delicate balance between two contributions of opposite sign are d^{10} systems (e.g., Au(I) complexes),[99,119] where the properties of the ligand trans to the

https://dx.doi.org/10.1021/acs.chemrev.9b00785
Chem. Rev. 2020, 120, 7065−7103

LA can modulate or even invert the overall sign of δ^{SO}_{LA}, see Figure 15. For weak trans-ligands (X_w) in a linear LA-HA-X complex of gold(I), the HA−LA bond is relatively strong; and the corresponding MO of σ_{HA-LA} character is energetically stabilized and thus plays a marginal role in the SO-HALA mechanism. In this case, the SO-HALA shift is governed by many small shielding SO contributions (negative δ^{SO}_{LA}) originating in $n_{HA} \leftrightarrow \sigma^{(*)}_{HA-LA}$ type (HA-based 5d ↔ 5d*) couplings. A strong trans-ligand (X_s, covalent HA−X bond) destabilizes the HA−LA bond by a structural and electronic trans-ligand influence (TLI), and the energy of the corresponding σ_{HA-LA} orbital is increased, Figure 22a. It therefore contributes significantly, and it typically governs the SO deshielding (positive δ^{SO}_{LA}).

The PT3 mechanism of this SO-HALA deshielding particularly highlights the role of the *trans* ligand as shown for $HAuNH_3$ in Figure 22b. The SO (and angular-momentum) operator couples the occupied and vacant MOs with the following AO contributions: $2p^{\sigma}_{N} \leftrightarrow 2p^{\pi}_{N}$, $2p^{\sigma}_{N} \leftrightarrow 6p^{\pi}_{Au}$, and $5d^{\sigma}_{Au} \leftrightarrow 2p^{\pi}_{N}$, all involving the trans-nitrogen atom and contributing to the SO deshielding. The SO-and-magnetically induced electron-spin density interacts with the magnetic moment of the LA nucleus via the FC operator, acting on occupied MOs with s-character at the hydrogen (LA) atom. Induction and propagation of spin density thus involve AOs of the trans atom X, particularly for strong TLs (Figure 15) and short HA-TL distances (Figure 14).

The trans-ligand influence shown in Figure 22b is a good example of an arrangement where one of the assumptions we used to derive the rules for the sign of the SO-HALA effect (Figure 5) does not hold. Specifically, the MO ↔ MO couplings between the occupied and vacant HA AOs vanish, and the SO ($r^{-3}_{HA}\hat{\boldsymbol{l}}^{HA}$) and MF ($\hat{\boldsymbol{l}}$) coupling is dominated by the interatomic contributions. Here, the FC coupling (the occupied MOs are identical) and the product of SO and MF coupling (equal signs) are both positive. The final SO-HALA deshielding (positive δ^{SO}_{LA}) is then given by the negative sign in eq 18.

The theoretical foundations of the SO-HALA shift summarized in section 2 and demonstrated in this section on selected examples in terms of chemical concepts allow for a more complete understanding of previously observed trends across the Periodic Table of the Elements (PTE)[100] than had hitherto been possible. In section 4 we will focus on these general trends and selected examples from the time period 2004−2019 to illustrate the usefulness of these concepts and to reveal the broad importance of such effects throughout the Periodic Table.

4. TRENDS IN SO-HALA SHIFTS ACROSS THE PERIODIC TABLE

As shown in sections 2 and 3, SO-HALA NMR effects are connected to the electronic structure of the neighboring heavy atom (HA) and its ligand sphere.[99,100,119] With few exceptions, trends in SO-HALA effects have been investigated using relatively small groups of HA compounds. Recent efforts to understand the phenomenon on a wider scale encompass three large studies[99,100,119] that have revealed in detail how the sign of the SO-HALA shift relates to the electronic structure at the HA and how the position of the HA within the PTE, its oxidation state, and its bonding environment (e.g., the TLI in transition-metal complexes), influence the sign and magnitude of δ^{SO}. The link between the electron configuration of the HA and the SO-HALA shift was generalized when the triangular PT3 concept[99] was applied systematically to compounds of the sixth-row[100] to determine whether or not the SO-HALA effect shows periodic trends. A large set of ^{1}H NMR shifts for compounds containing HAs of the sixth period, ranging from Cs^I to At^I, has been analyzed, with periodic trends in the sign of $\delta^{SO}(^1H)$ revealed and rationalized.[100] Most importantly, it has been shown that the sign of δ^{SO}(LA) correlates systematically with the presence of occupied/vacant nonbonding orbitals centered at the HA (this is valid also for heavier atoms such as ^{13}C and ^{15}N), as will be discussed in detail in this section. Note that throughout section 4 we will use the notation LA for light atoms and also for heavier spectator NMR atoms (e.g., Se or Te) in the vicinity of an even heavier HA. Based on refs 51, 91, 95, 97, 99, 100, 111, 113, 115, 119, and 132−138, the following general rules can be derived for periodic trends in the SO-HALA shifts:

1. A formally empty valence shell at the HA (p^0, d^0, or f^0 configuration) gives rise to SO-HALA deshielding of LA(s) bonded directly. This is the case particularly for HAs with $5d^0$ and a positive oxidation state Cs^I−Os^{VIII}, for $6p^0$ Hg^{II}−Bi^{III} (the $6s^2$ shell is present but unimportant in this context), and for $6d^05f^0$ Ac^{III}−U^{VI}.[51,100,132,137,138] For the corresponding lighter analogs, the effect exists in diminished form (Figure 23). (Note that the electronic state relates to the HA bonded in a molecule not its atomic ground state.) In such cases, the SO-HALA deshielding is dominated by the $\sigma^{(*)}_{HA-LA} \leftrightarrow n^{*}_{HA}$ coupling mechanism (Figures 5 and 21b), which requires the presence of a low-lying vacant orbital(s) at HA.[100,132]
2. Partially filled, energetically high-lying valence subshells (d^2−d^8, p^2−p^4) at the HA induce SO-HALA shielding at the LA, particularly in $5d^{2n}$ (Hf^{II}−Au^{III}) or $6p^{2n}$ (Bi^I−At^I) compounds and, in diminished form, for their corresponding lighter analogs (Figure 23).[51,95,100] The SO-HALA shielding is dominated by the $n_{HA} \leftrightarrow \sigma^{(*)}_{HA-LA}$ coupling mechanism (Figures 5 and 21a) and requires the presence of one or more nonbonding (n_{HA}, or lone electron pair, LP_{HA}) orbitals at the HA. This effect is to a certain extent additive when more than one suitable nonbonding MO is present, for example, along the $5d^2$ through $5d^4$ to $5d^6$ and $6p^2$ to $6p^4$ series of hydride complexes.[51,95,100,132] A considerably smaller shielding effect is observed when the HA AOs are not LPs but are involved in bonding interactions to ligands other than the LA or the trans ligand (see rule 4), for example, in σ_{HA-L} bonds.[100]
3. The oxidation state of the HA is related directly to the occupation of n_{HA} and thus determines δ^{SO}(LA), according to rules 1 and 2 above.[99,100,132] For instance, an LA in a $5d^2$ complex of W^{IV} experiences SO-HALA shielding, i.e., a negative δ^{SO}(LA), while SO-HALA deshielding, i.e., positive δ^{SO}(LA), would be expected in a $5d^0$ W^{VI} complex.[100] In most cases, the above-mentioned mechanisms act simultaneously, and one usually dominates the other. Sometimes, for example in Bi^{III} ($6p^0$) and Au^I ($5d^{10}$) systems, these two mechanisms are so similar in magnitude that the sign of the SO NMR shift can be dictated by other factors, or the SO-HALA effect can be vanishingly small (see rule 4).
4. Additional factors, such as the trans-ligand influence,[99,109,115,118,119] (TLI, section 3.1.3) and a recently described cis-ligand influence[120] further modulate the δ^{SO}. The TLI influences the relative energies and compositions of frontier $\sigma^{(*)}_{HA-LA}$ orbitals, thereby

https://dx.doi.org/10.1021/acs.chemrev.9b00785
Chem. Rev. 2020, 120, 7065−7103

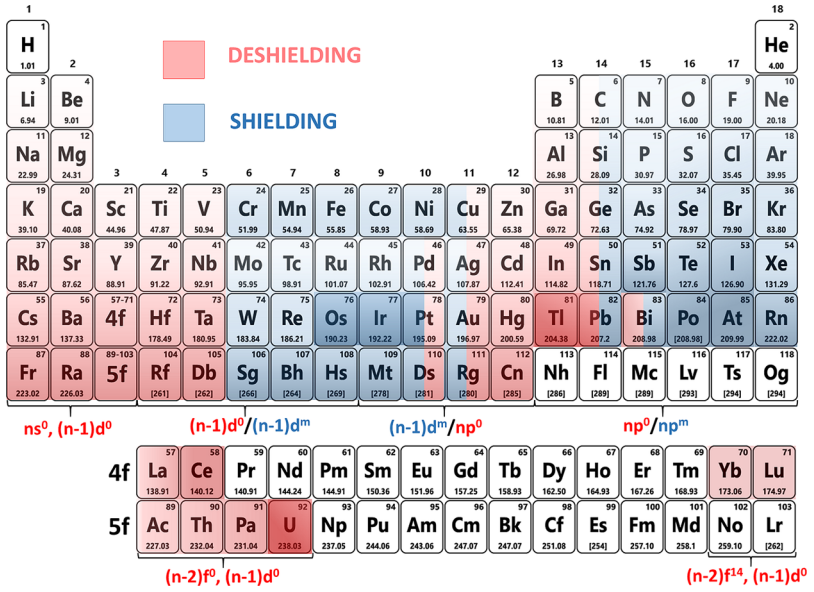

Figure 23. General trends in SO-HALA NMR shifts across the Periodic Table. Red shows SO-HALA deshielding ($\delta^{SO} > 0$) and blue SO-HALA shielding ($\delta^{SO} < 0$) for a given HA in its typical oxidation state(s). The relative magnitude of the SO-HALA effect is represented by lighter (less) and darker (more) shading. HAs for which SO-HALA effects have not yet been evaluated or for which closed-shell complexes are unknown, are indicated by a white background. The color-coded configurations presented beneath the 7th period and beneath actinides indicate which of the elements in the groups above can occur in $(n-2)f^0/(n-1)d^0/np^0$ configurations (n is principal quantum number), which may lead to deshielding SO-HALA effects caused by vacant valence p-, d-, or f-orbitals, and which of the more electron-rich situations tend to be more shielded (d^m/p^m configurations, index m represents even-numbered electron configuration).

affecting the SO-HALA mechanism. Strong trans ligands may even invert the sign of δ^{SO}, particularly in d^8 and d^{10} complexes, see below.[99,115,119] The effects of cis and/or other than trans ligands are typically smaller than the TLI but should be considered, e.g., for Bi^{III} ($6p^0$) and Au^{I} ($5d^{10}$) complexes (see below).

5. The vertical trends for HAs of the s- and p-blocks follow the expected dependence of relativistic effects on Z_{HA} (the atomic number of the HA nucleus).[56] The trend is analogous to the well-known normal halogen dependence (NHD, i.e., the SO shielding increases going down the given group for the HA, section 1) observed for groups 14−18, whereas the opposite behavior (growing SO deshielding going down the group) is observed for compounds with HAs of s-block[100,139] and group 13.[51] The latter trend is analogous to inverse halogen dependence (IHD, section 1)[42] but its origin is different (the SO-HALA effect instead of scalar paramagnetic shielding). For HAs with partially filled d-shells, particularly for octahedral d^6 and square-planar d^8 complexes, the SO-HALA effects generally follow an inverted V-shape trend,[113,138,140] resulting from competition between the growing SO splittings and the likewise growing energy denominators down the PTE (explained in section 3 and Figure 11).

For convenience, we have collected the available occurrences of typical SO-HALA (de)shielding from the studies reviewed here and presented them schematically throughout the Periodic Table (Figure 23). Red and blue are used to show SO-HALA deshielding and shielding effects, respectively, in compounds of a given HA in its typical (closed shell) oxidation state(s). The color-coded description of electronic configurations located beneath the seventh period has been added to further emphasize the elements which can, at least hypothetically, be found in an $ns^0(n-1)d^0$ or np^0 configuration. In that case, vacant valence p- or d-orbitals lead to deshielding SO-HALA effects, while the more electron-rich configurations at the HA feature partially occupied orbitals and thus make shielding SO contributions. For instance, deshielding SO-HALA effects are expected in W^{VI} complexes with a $6s^05d^0$ configuration, whereas SO-HALA shielding is expected in W^{IV} ($5d^2$) and W^{II} ($5d^4$) complexes, increasingly so for the latter. The same applies for the majority of early transition-metal complexes. Similarly, transition-metal configurations for which the SO-HALA effects are influenced considerably by the availability of *n*p orbitals[99,114,119] are denoted $(n-1)d^m$, np^0. Here d^m corresponds to an even-numbered d-configuration, i.e., d^6, d^8, or d^{10}. The influence of a TLI (see sections 2 and 3), which can switch the sign of the SO-HALA effect for some HAs, is emphasized by both red and blue stripes for the given element (see, e.g., Pt and Au). The red and blue stripes in group 14 and Bi emphasize the possible large deshielding SO-HALA effects in HA^{II} when the HA is a group 14 element and in Bi^{III} complexes (compared to shielding for higher oxidation states, HA^{IV} and Bi^{V}).[91,132] Exceptions to these elaborated general trends may occur in specific cases (e.g., exotic oxidation states, involvement of the atom in a cluster, strong TLI).

More detailed descriptions of the known SO-HALA trends in s-, d-, p-, and f-block compounds are given in sections 4.1−4.5 below, together with an overview of the individual works dealing with calculating and predicting SO and (where available) SR contributions to LA NMR shifts in heavy-element compounds. As outlined in section 1, SR effects have not been investigated extensively, and only a few general concepts have been derived for them, although some basic observations are outlined in the text. Schematic illustrations of the known ranges of SO-HALA shifts for complexes of a given element (group), collected from the works covered in this comprehensive review, are presented at the beginning of each subsection. These are accompanied by

https://dx.doi.org/10.1021/acs.chemrev.9b00785
Chem. Rev. 2020, 120, 7065−7103

examples of applications of SO-HALA effects in the elucidation of molecular and electronic structure and chemical reactivity.

4.1. HAs of the s-Block

4.1.1. General Aspects. SO-HALA effects of HAs of the s-block have scarcely been investigated, likely because the ns valence orbitals themselves do not contribute to SO effects. However, low-lying $(n\text{-}1)$d orbitals of the heavy alkaline earth elements (Ca, Sr, Ba, and Ra) participate in their chemical bonding, making them "honorary d-elements".[141] As a result, the low-lying $(n-1)$d HA orbitals contribute to the SO-HALA mechanism in a way similar to that for genuine d^0 systems (as well as for the lanthanides), particularly to the $\sigma^{(*)}_{HA-LA} \leftrightarrow n^*_{HA}$ deshielding (Figure 23).[100] An example of such deshielding orbital magnetic coupling (OMC) involving contributions from 5d and 5d* orbitals in BaH_2 is illustrated in Figure 24.[100]

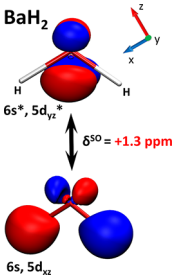

Figure 24. Example of the 5d-5d* $\sigma^{(*)}_{HA-LA} \leftrightarrow n^*_{HA}$ deshielding orbital magnetic coupling in $5d^06s^0$ $Ba^{II}H_2$, adapted from ref 100. Copyright 2018 American Chemical Society.

Because of the d^0 character, weakly deshielding SO-HALA effects are found in heavier, formally ns^0 complexes. The range of currently known $\delta^{SO}(^1H)$ values[100] for hydrides of these elements is shown in Figure 25.

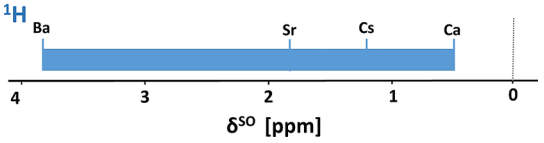

Figure 25. Range of computed ^1H SO-HALA shifts in s-block hydride complexes (LA bonded directly to the HA).[100]

We note in passing that alkalide anions from Na^- through Cs^- with the electronic configuration ns^2 at the HA have been observed experimentally, including NMR measurements,[142] but no data regarding SO-HALA effects or LA NMR shifts have been reported. We speculate that the SO-HALA effects in such compounds are in any case small, because of the strongly ionic nature of alkalide bonding.

4.1.2. Groups 1 and 2: Alkali and Alkaline-Earth Metals. Computational analysis of ^1H NMR shifts in gas-phase s-block hydrides[100] has shown that in group 2 hydrides the SO-HALA effect increases by about 4 ppm from CaH_2 to BaH_2,[100] see Figure 25. This correlates well with experimental ^1H NMR shifts in the solid-state hydrides, which increase by 4.2 ppm, from 4.5 ppm (CaH_2) to 8.7 ppm (BaH_2).[143] While earlier attempts to explain this trend using classical arguments, such as the electronegativity of the alkaline earth metal, were not convincing,[143] the SO-HALA effect provides a natural explanation for the observations.

Relativistic deshielding of ^1H NMR resonances can also be found in relatively complex materials. For instance, the hydride signals in hydride-doped strontium mayenite have been found experimentally at δ_{tot} up to +6 ppm, a region that is usually associated with the ^1H NMR resonances of OH groups.[144] These results could not be reproduced using scalar relativistic calculations, although the inclusion of scalar-relativistic corrections slightly improved the agreement with experiment.[144] Clearly, the inclusion of SO-HALA effects in the calculations is necessary to reproduce the ^1H NMR spectra of hydride-doped materials of the heavier s-block metals.

Relativistic effects were also calculated for ^{19}F NMR shifts in solid-state Li, Na, Ca, Rb, Sr, Cs, and Ba fluorides.[139] The reported $\delta^{SO}(^{19}F)$ values were between −3 ppm (CaF_2) and +2 ppm (CsF). The relatively small SO-contributions are likely due to the high polarity and particularly to the low s-character of the fluorine in the M−F bond. That $\delta^{SO}(^{19}F) = -3$ ppm for CaF_2 may reflect the numerical uncertainties of these calculations (differences between SO-ZORA and SR-ZORA data) is suggested in the original work.[139]

4.2. HAs of the d-Block

4.2.1. General Aspects. Due to the high sensitivity of ^1H shifts to SO-HALA effects (efficient SO/FC mechanism, see section 3), and the ensuing spectacular ^1H shifts, relativistic contributions to the ^1H NMR shifts in transition-metal hydride complexes have been at the center of various computational analyses of SO-HALA effects.[95,100,115,120,137,145] Indeed, many general SO-HALA trends in d-block systems have been derived primarily from hydride NMR shifts. While not as spectacular in magnitude, due to the larger "standard" NMR spectral ranges, similar trends are also found for other LAs, such as carbon and nitrogen, provided an efficient SO/FC mechanism is operative.[96,99,100,109,114,119,130,146,147] Calculated ranges of the SO-HALA shift for ^1H, ^{13}C, and ^{15}N nuclei in transition-metal complexes are summarized in Figure 26. The data were collected from the works covered in section 4.2.

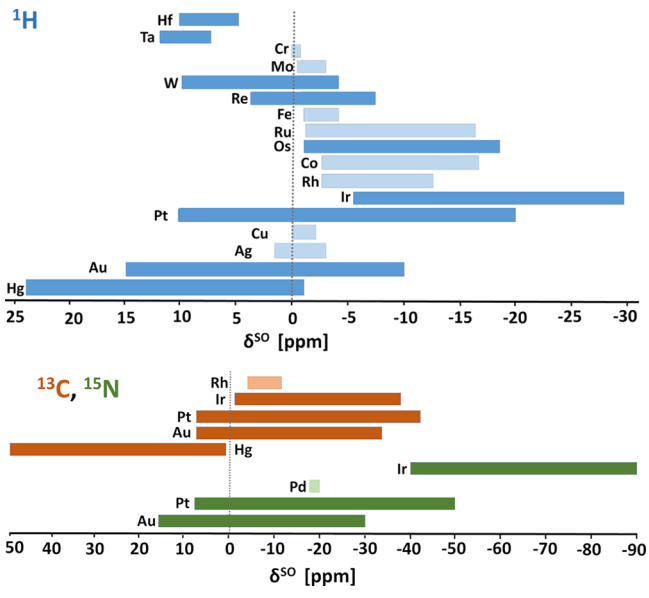

Figure 26. Ranges of the computed ^1H, ^{13}C, and ^{15}N SO-HALA shifts for individual d-block metal HAs (LA bonded directly to the HA). Note that lighter shades are used for 3d and 4d to highlight the trend in δ^{SO}(LA) for compounds of 5d elements.

https://dx.doi.org/10.1021/acs.chemrev.9b00785
Chem. Rev. 2020, 120, 7065−7103

In early transition-metal complexes with d^0 configuration, the deshielding $\sigma^{(*)}_{HA-LA} \leftrightarrow n^*_{HA}$ orbital coupling dominates the SO-HALA shifts. Hence, positive SO-HALA contributions are found in Figure 26 for early transition-metal complexes featuring d^0 configurations (mainly from groups 3−8). As the d-shell becomes populated in d^2, d^4 d^6, and d^8 systems, the shielding $n_{HA} \leftrightarrow \sigma^{(*)}_{HA-LA}$ coupling mechanism becomes dominant.[100] This trend, together with additional shielding due to the Buckingham-Stephens effect[148,149] (shielding at the LA, caused by off-center paramagnetic ring currents from the incomplete valence shell of the HA and found particularly in hydride complexes), is responsible for the predominantly low-frequency ^{1}H NMR signals in d^2 to d^8 d-metal hydrides (Figure 26). A local extremum in $\delta^{SO}(^1H)$ for d-block hydrides is observed for $5d^6$ Ir^{III} complexes with a computed δ^{SO} of −30 ppm (and even more negative overall shifts).[95,100] We note that the lowest total ^{1}H NMR shift ever experimentally observed was −59.1 ppm in a $5d^6$ Ir^{III} porphyrin hydride complex.[150]

Vacant HA 6p orbitals start to play an important role for SO-HALA effects in $5d^8$ complexes, see Pt and Au in Figure 26.[114] These orbitals mix into the frontier MOs and thus participate in the deshielding $\sigma^{(*)}_{HA-LA} \leftrightarrow n^*_{HA}$ mechanism that reduces the overall SO-HALA shielding. The 6p-6p*-based $\sigma^{(*)}_{HA-LA} \leftrightarrow n^*_{HA}$ mechanism then typically dominates the SO-HALA effects in d^{10} compounds and beyond (particularly in group 12, see Hg in Figure 26) causing largely positive δ^{SO}(LA) values.[99,130,151] For borderline cases, such as $5d^{10}$ Au^I complexes, both mechanisms play similar roles and can be strongly modulated by the TLI (section 3.1.3).[99,109,115,118,119] Hence the broad range of SO-HALA shifts in Pt and Au complexes shown in Figure 26.

Except for the d^0 and d^{10} configurations, the vertical trends in the SO-HALA shift in the d-block tend to be characterized by an inverted V-shape dependence (Figure 11),[95,113] although this can be affected by TLI when a strong trans ligand is present.[99,119] The inverted V-shape reflects greater (shielding) SO-HALA contributions for the 3d and 5d compared to the 4d transition-metal complexes, due to the increase in ligand-field splitting with respect to 3d analogs and thus the relevant energy denominators for the 4d case (section 3.1.1). A detailed explanation of the V-trend can be found in the discussion of group 9 complexes below.

Before we discuss individual examples for d-block HA systems, it should be noted that a number of the computational studies of SO-HALA shifts in transition-metal complexes mentioned in the following discussion used a higher admixture of exact exchange in the DFT functional (typically 40%), to obtain better agreement with the experimental NMR shifts at the two-component SO-ZORA level, e.g., refs 104, 109, 114, 118, 137, 147, and 152 However, the need for a higher exact-exchange admixture was later identified as an artifact caused by the absence of an exchange-correlation kernel in the SO-ZORA implementation used.[96,97,153] Such a high exact-exchange admixtures should be avoided when using computational codes that treat the kernel properly.[134,154]

4.2.2. Early Transition Metals. The SO-HALA effects in early transition-metal complexes have not been investigated as much as those of the late transition metals but a short overview of relativistic NMR effects in d^0 complexes of early transition metals was contained in a recently published larger review.[138] Available data confirm that the SO-HALA effects for d^0 complexes are uniformly deshielding, in contrast to the increasingly shielding contributions in d^2 and d^4 systems.[100,137,146,155]

An analysis of the relativistic ^{13}C NMR shifts in early transition-metal complexes was used to elucidate the link between the NMR shifts and the electronic structure in d^0 Schrock alkylidene methathesis catalysts based on Mo, Ta, W, and Re.[156] The high-frequency ^{13}C signals in these complexes were attributed to the large paramagnetic contributions caused by the small energy separations between the σ_{M-C} and π^*_{M-C} orbitals. In addition, the orientations of some of the components of the ^{13}C shielding tensor were found to be influenced by the angle between the metal atom and the ═C−H fragment. These factors are very similar to those responsible for the modulation of SO-HALA effects, particularly the influence of energy denominators. Also, the relevant orbital couplings resemble those of the deshielding $\sigma^{(*)}_{HA-LA} \leftrightarrow n^*_{HA}$ mechanism, see Figure 21b.

4.2.3. Group 8: Ruthenium and Osmium. The hydride ^{1}H NMR shift in $4d^6$ Ru complexes with *N*-heterocyclic carbenes increases from −41 ppm to +5 ppm with increasing TLI (trans ligand: none, F^-, Cl^-, MeCN, N_2, H_2, H^-, P_4, SO_2, CO, and O_2).[157] A striking outlying value ($\delta(^1H)$ = +5 ppm) has been experimentally observed for an Ru complex with an η^2-O_2 ligand in the trans position. Detailed analysis revealed strong π-type interactions between the O_2 2p and the Ru $5d_{xy}$ orbitals (HOMO) along with substantial destabilization of the Ru $5d_{yz}$ orbital. The Ru $5d_{yz}$ orbital, occupied in other complexes, becomes the LUMO in the O_2 complex. The original LUMO, which is in fact the σ^*_{Ru-H} MO, thus becomes less available for the shielding $n_{Ru} \leftrightarrow \sigma^{(*)}_{Ru-H}$ magnetic coupling, which diminishes the SO shielding mechanism (the SO contribution remains negative). Simultaneously, paramagnetic deshielding couplings between the Ru $5d_{xz}$ HOMO and the Ru $5d_{yz}$ LUMO further increase the total NMR shift at the hydrogen nuclei in question.

The SO-HALA shielding contribution to the ^{29}Si NMR signals of − SiX_3 groups (X = H, C, and Cl) in $4d^6$ Ru silyl complexes[158] was found to increase with the electronegativity of substituent X, with the maximum SO-HALA value of −35 ppm for X = Cl.[158] It has been suggested that this could be due to a smaller energy gap between the occupied and vacant MOs. However, an alternative explanation would be that the electronegative substituents increase the positive charge at Si and thus also the hybridization defects that increase the 3s-character of Si in the Si−M bond,[46] thereby enhancing the SO/FC mechanism of the SO-HALA effect (section 3.1.1).[26]

A recent detailed study of the effect of TLI on the mechanism of ^{1}H SO-HALA shifts in a series of transition-metal complexes also included d^6 osmium(II) compounds.[119] This study is discussed more thoroughly with groups 10 and 11 below.

4.2.4. Group 9: Cobalt, Rhodium, and Iridium. An experimental solid-state NMR study of ^{1}H shift tensors in $4d^6$ Rh^{III} and $5d^6$ Ir^{III} hydride complexes[159] revealed that the unusual low-field isotropic shifts are accompanied by very large chemical shift anisotropies (CSAs), particularly for the Ir systems, confirming predictions based on large computed SO-HALA anisotropies.[95] These arise from the tensor components perpendicular to the M−H bond, increasing from Rh to Ir.[159]

Four-component relativistic computations of the ^{1}H NMR shifts of iridium hydride, shifted to a lower frequency by SO-HALA effects, were used to elucidate the mechanism of the hydrosilylation of carbonyl compounds using Brookhart's iridium pincer complex.[160] A detailed comparison of the calculated ^{1}H NMR shifts of nine different hydride complexes with experimental ^{1}H NMR data revealed a fast equilibrium between a dihydride-silane Ir^{III} complex and a trihydride silyl Ir^V

https://dx.doi.org/10.1021/acs.chemrev.9b00785
Chem. Rev. 2020, 120, 7065−7103

complex formed by oxidative addition of the silane.[160] Similar computational predictions of relativistic ^{1}H NMR shifts for hydride complexes and intermediates have been reported for Si−H activation across an Ru−S bond.[161] These results could not be verified experimentally because of rapid decomposition reactions.

Two-component relativistic calculations of ^{1}H and ^{13}C NMR chemical shifts in d^8 Ir^{I} and Rh^{I} complexes[145] interacting with methane were performed to provide an insight into the mechanisms of activation of the C−H bond. δ^{SO} has been found to dominate the overall ^{1}H and ^{13}C NMR shifts, causing considerable shielding (overall shifts exceeding −40 ppm) of both types of nuclei. Only proper treatment of SO-HALA effects and consideration of long-range-corrected DFT functionals enabled identification of the correct structures of methane σ-complex intermediates, assignment of their signals in the NMR spectra, and explanations for the underlying reaction mechanism.[145]

Solid-state NMR and relativistic DFT calculations of a hexairidium cluster[162] provided explanations for unusually shielded ^{13}C NMR resonances of bridging carbonyl ligands resonating at +191 ppm. Analyses showed that this is caused by a $\delta^{SO}(^{13}C)$ for the bridging carbonyls (−27 ppm) much larger than that for the terminal ligands (−2 ppm). This is likely due to the bonding of the bridging carbon atom to two iridium centers.[163,164] A higher covalency of the bridging Ir−CO bonds due to stronger back-bonding may also contribute via a more efficient SO/FC mechanism (section 3.1.1).[109,114]

Systematic studies of three-bond SO-HALA effects in group 9 chelates have been carried out[113,140] to understand experimental ^{1}H NMR titration results in a series of d^6 Co, Rh, and Ir polyamine complexes. Upon deprotonation of the aqua, alcohol, or polyalcohol (carbohydride) coligands in these systems, one would have expected better charge donation by the anionic coligand (OH) generated upon deprotonation to enhance shielding of all CH_2 protons within the polyamine ligand. However, for certain methylene positions trans to the deprotonation site, substantial deshielding was observed. This can even lead to a nonmonotonous pH-dependence of the ^{1}H shift titration curves for multiple deprotonation sites. Computations at NR levels could not reproduce the observations, while inclusion of a PT3 treatment of SO-HALA effects provided the correct trends and insights.[113,140] Interruption of SO/FC pathways from the metal center to the methylene proton site by the larger TLI of the deprotonated coligand combined with the antiperiplanar M−N−C−H arrangement in the protonated system enabling maximal SO/FC contributions (rationalized by a Karplus-type dependence, section 3.1.4) explained the differential SO-HALA effects causing the observed anomalous pH dependencies. Notably, smaller SO-HALA effects were found for the $4d^6$ Rh complexes compared to both the $3d^6$ Co and $5d^6$ Ir analogs, indicating for the first time the inverted V-shape dependence (section 3.1.1) of the SO-HALA effects down the group, due to the increased ligand-field splittings (energy denominators) partly counteracting larger SO coupling (cf. eq 18 in section 2).[98] While the larger energy gap renders the SO-HALA effects smaller for the Rh compared to the Co system, the still much larger SO splitting explains the largest SO-HALA shifts for the Ir complex. This rationalization has been confirmed subsequently in other studies, e.g., for d^8 metallasilatrane complexes,[111] and for d^6−d^{10} transition metal hydrides.[95]

A modulation of $\delta^{SO}(^{15}N)$ of about 25 ppm caused by changing the metal trans-ligand distance was computed in an octahedral $5d^6$ Ir^{III} complex.[118] Notably, SR and NR contributions both changed by only 6 ppm in total. This initiated the first systematic study of the mechanisms of TLI in the SO-HALA effects. It was performed on a set of model d^6 Ir^{III} complexes featuring different oxygen- and sulfur-based trans ligands,[109] and found a linear correlation of δ^{SO}(LA) with the Ir 5d-character of the HA−LA bond (section 3.1.1). Essentially, covalently bound trans substituents tend to diminish the metal d-character in the HA−LA bond because they compete for the available metal d-orbitals. In contrast, substituents bound more ionically leave a larger fraction of the HA d-orbitals available for HA−LA bonding, thus increasing the metal d-character in the HA−LA bond. The analysis also provided a link between the SO/FC part of the SO-HALA shielding and the g- and A-tensors of EPR spectroscopy, which are known to be modulated by the metal d-character. The role of the metal d-character was later embedded into a more general relationship between covalency and the magnitude of the SO-HALA effects (section 3.1.1).[114] This concept has been developed further by several studies of the TLI (see below).[99,115,119,120]

4.2.5. Groups 10 and 11: Platinum, Gold. As discussed above, SO-HALA effects in platinum and, especially, gold complexes are strongly influenced by contributions from the frontier 6p-orbitals participating in the SO/FC mechanism and by TLI. Overall, the LAs are more shielded in Pt complexes than in Au systems, partly due to the predominance of d^8 Pt^{II} in the examples studied (a d^{10} configuration would require Pt^0 complexes, which tend to be very reactive). However, even for d^{10} Au^{I}, a weak TLI can lead to shielding SO-HALA effects (see Figure 26).

Interest in computational studies of SO-HALA shifts in Pt and Au complexes peaked in 2011 with three independent works. One study used relativistic DFT methods to investigate SR and SO-HALA effects on the ligand atoms of 2-phenylpyridine ligands in related square-planar Pt and Au complexes.[104] Large SR effects on ^{13}C and ^{15}N NMR shifts (δ^{SR}) up to −28 ppm were calculated for the Au system, likely reflecting the well-known "gold maximum" of SR effects.[58] Relativistic contributions to the ^{13}C and ^{15}N NMR shifts in the Pt system were, in contrast, dominated by the SO-HALA effects. The much smaller ^{15}N SO-HALA shift in the Au complex (near 0 ppm) compared to the Pt system (−18 ppm) was rationalized by the rather ionic (less covalent) character of the Au−N bonds (due in part to differences in the trans ligand, as was shown later[114]). Alternating signs of the long-range SO-HALA effects correlating with indirect spin−spin couplings have also been noted (cf. Figure 16 in section 3.1.4).

The unusually shielded ^{29}Si resonances in certain metallasilatrane complexes[165] were interpreted in terms of SO-HALA shielding effects influenced by TLI when the trans-ligand was changed from Cl to I. A role for the Si−M bond covalency in the propagation of the SO-HALA was hinted at. The calculated values of $\delta^{SO}(^{29}Si)$ = −20, −17, and −33 ppm for Ni, Pd, and Pt complexes, respectively, follow the inverted V-shape dependence[165] (cf. Figure 11 in section 3.1.1).

A third study in 2011 focused on the well-known high-field hydride ^{1}H NMR shifts in heavy transition-metal hydride complexes.[95] In the 1960s, the shielded hydride resonances had been attributed to off-center paramagnetic ring-current effects in the Buckingham-Stephens model.[148,149] That model was confirmed by SR-DFT calculations in 1996.[77] The 2011 work

https://dx.doi.org/10.1021/acs.chemrev.9b00785
Chem. Rev. 2020, 120, 7065−7103

showed that for the heaviest d^6 and d^8 systems, including Pt and Ir complexes, up to two-thirds of these spectacular high-field shifts can be due to SO-HALA effects. This was contrasted to the deshielding SO-HALA effects in d^{10} group 11 and 12 hydride complexes. This work also clearly confirmed the inverted V-shape dependence of SO-HALA shifts for the d^6 and d^8 cases.[95]

Pt and Au complexes were also central to subsequent studies on the importance of the covalency of the HA−LA bond for SO-HALA effects and TLI.[114,115] Reference 114 correlated ^{13}C and ^{15}N SO-HALA shifts with the covalence of the HA−LA bond expressed by the delocalization index of QTAIM (DI; cf. Figure 12). This work further established the role of 6p-type HA orbitals (and the effect of decreasing 5d character in bonding) in SO-HALA deshielding contributions in Au complexes, an effect that becomes even more pronounced in group 12 systems. In the second study,[115] the ^1H shifts in a series of square-planar $5d^8$ Pt hydride complexes trans-H-PtL_2X (L = PMe_3, X = trans ligand) were studied systematically as a function of the strength of the trans ligand. It was found that, while paramagnetic shieldings also contributed to the experimentally well-known larger shielding with weaker trans ligands, the SO-HALA contributions dominated the trend. While greater shielding also correlates with the Pt−H distances, closer analysis has established that both trends are consequences of the stronger trans ligands competing for the metal 5d orbitals with the hydride bond and thereby weakening it.[115]

Two independent computational studies from our groups in 2017 used complementary analytical tools to shed more light on the TLI for SO-HALA effects.[99,119] While ref 119 relied on two-component spinors from ZORA computations and applied PT2 analyses, ref 99 in addition to PT2 introduced PT3 analysis of δ^{SO} based on NR MOs to understand the electronic-structure origins of the SO-HALA trends (section 2.3.3). The systems studied in these two works overlapped to some extent, allowing a comparison of the insights gained from PT2 analysis based on MSPs (molecular spinor pairs, section 2) and PT3 analysis based on NR MOs. The generality of the TLI for SO-HALA effects for ^1H, ^{13}C, and ^{15}N shifts all the way from $5d^6$ Os^{II} and Pt^{IV} complexes via $5d^8$ Pt^{II} and Au^{III} systems to $5d^{10}$ Au^I and Hg^{II} compounds with a broad range of *trans* ligands was demonstrated in these works. For $5d^8$ Pt^{II} and d^{10} Au^I, the TLI may even change the sign of the SO-HALA contribution (and even the sign of the total ^1H hydride shifts) from shielding for weak trans ligands to deshielding for strong trans ligands.[119] Interestingly, a comparison of linear d^{10} Cu, Ag, and Au complexes showed, that the V-shape dependence of SO-HALA shifts down the group for d^6 and d^8 systems extends to the d^{10} case for weak trans ligands but changes to a monotonous increase for strong trans ligands,[119] due to enhanced SO-HALA deshielding contributions. Modulation of the sign of the SO-HALA contributions by the interplay of the metal center and the trans ligand has also been correlated with SO effects on the electron density (SO-EDD,[99] see sections 2 and 3).

A recent study of the interplay between cis- and trans-ligand effects on SO-HALA shifts in a series of square-planar d^8 Au^{III} hydride complexes explained the broad span of experimentally observed ^1H NMR signals from −8.5 ppm to +7 ppm.[120] The cis and trans ligands influence the $\delta^{SO}(^1H)$ in opposite way. That is, stronger ligands in the *cis* position stabilize the higher-lying σ_{Au-H} bonding MOs and hence weaken the SO-HALA deshielding mechanism. The largest deshielding due to the cis ligand (up to +5 ppm) was therefore found for neutral weak σ-donors (S-, N-, and O-based ligands and CO). As in previous studies, the ^1H NMR shifts were found to correlate with the Au−H distance and the ionicity of the bond, which in turn correlated with trends in reactivity.

Combined DFT and experimental solid-state NMR investigations were performed for a diphosphacyclobutadiene cobaltate sandwich complex of Au^I.[166] Inclusion of relativistic effects (both SR and SO-HALA effects) in the DFT computations was crucial for the correct assignment of the ^{31}P NMR resonances. For instance, the nonrelativistic ^{31}P NMR chemical shift of the Au^I-bound phosphorus atoms was −64 ppm (using an SR-ECP at gold), while the relativistic two-component SO-ZORA value was +23 ppm, indicating substantially deshielding SO-HALA effects. The need to revisit the ^{31}P NMR spectra assignments of similar compounds using relativistic DFT calculations was pointed out by the authors.

A sizable $\delta^{SO}(^{14}N)$, −45 ppm, was calculated at the N_α atom of an azide ligand directly bound to Pt.[167] Significant SO-HALA shielding was also predicted for N_β (−21 ppm) and N_γ (−7 ppm) as a result of the high electron delocalization within the azide ligand. However, in spite of the large $\delta^{SO}(^{14}N)$, the N_α and N_β nuclei have experimental NMR chemical shifts similar to those in free N_3^-. Analysis showed that the SO-HALA shielding contributions at the N_α and N_β nuclei partly compensate the paramagnetic deshielding contributions because electron density is withdrawn upon formation of the Pt−N_α bond, including trans ligand effects. The authors suggested the term *hidden heavy-atom effect* when strong SO-HALA effects are present but are disguised in the spectrum by other contributions.

Probably the most dramatic example of a TLI for SO-HALA shifts can be found in a 2005 computational study,[168] where the unusually low $\delta(^{13}C)$, 135.2 ppm, of a carbon atom trapped inside a phosphine-ligand-stabilized Au_6 cluster was investigated, see Figure 27. Signals of interstitial carbon atoms in

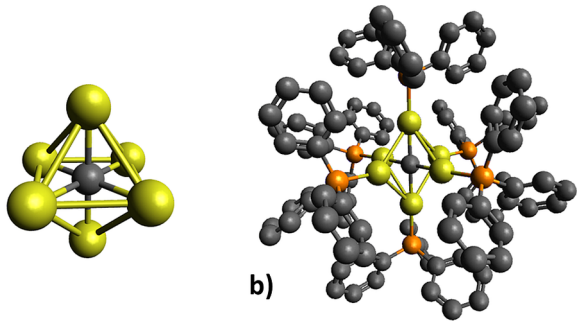

Figure 27. Structures of (a) the central CAu_6^{2+} cluster and (b) the entire cluster stabilized by phosphine ligands. Data from ref 168.

"non-d^{10}" transition-metal clusters tend to resonate at rather high frequencies, above +400 ppm.[168] Computations on the unsubstituted parent CAu_6^{2+} cluster gave $\delta^{SO}(^{13}C)$ = −240 ppm (Figure 27a), which would lead to the even more exotic $\delta^{tot}(^{13}C)$ of −288 ppm. Inclusion of the phosphine ligands into the model resulted in $\delta^{SO}(^{13}C)$ = +28 ppm (see Figure 27b), which means that more than 300 ppm of the total chemical shift at the interstitial carbon results from the combined TLI of the six phosphine ligands! Inversion of the sign of $\delta^{SO}(^{13}C)$ due to the presence of strong trans ligands in Au complexes is now well-known,[99,114,119] but in 2005 it prompted Le Guennic et al. to carefully re-examine their computational methodology. The large SO-HALA effects were confirmed, with a "final" calculated $\delta^{tot}(^{13}C)$ of +129 ppm, in excellent agreement with experiment.

https://dx.doi.org/10.1021/acs.chemrev.9b00785
Chem. Rev. 2020, 120, 7065−7103

While the origin of the large shielding of the interstitial carbon atom was not explained, the observed modulation of δ^{SO} is remarkable.

4.2.6. Group 12: Mercury. While we discuss the group 12 elements in the d-block section, we note that they are often viewed as "post transition-metal" or "representative" p elements, as their $(n-1)$d-orbital participation in bonding tends to be minor. Indeed, the SO-HALA effects for Hg^{II} complexes are dominated by the *n*p orbitals, leading to considerable SO-HALA deshielding, Figure 26, which is due to the 6p ↔ 6p*-based $\sigma^{(*)}_{HA-LA} \leftrightarrow n^{*}_{HA}$ deshielding mechanism (Figure 20b).[26,99,100,114] Building on the pre-2004 work discussed in section 1,[38] more recent (experimental and computational) studies of relativistic effects (both SR and SO) on the ^{13}C NMR shielding constants in organomercury compounds have shown deshielding SO contributions up to +52 ppm (for sp-hybridized carbon atoms).[130] Notably, SR deshielding effects were observed at the LA in contrast to the shielding δ^{SR} in Pt and Au complexes discussed above.[104] Alternating signs of Hg-derived long-range SR effects on neighboring atoms were noted,[130] with δ^{SR} = +28 ppm, −10 ppm, and +2 ppm for C_α, C_β, and C_γ, respectively. While the alternation of the sign of δ^{SR} resembles the oscillations of δ^{SO} that have been linked to FC-based *J*-coupling mechanisms,[26] the SR effects likely operate via inductive effects, polarizing the intervening bonds. Notably, a $\delta^{SR}(^{13}C_\alpha)$ of only +1 ppm has been calculated at the sp-hybridized acetylide *α*-carbon in CH_3HgCCH, compared to the much larger $\delta^{SR}(^{13}C_\alpha)$ of +20 ppm for the sp^3 hybridized methyl group. This is the exact opposite of δ^{SO} (cf. Figure 7), which is enhanced by the increasing LA s-character in the HA−LA bond. A TLI on the ^{13}C NMR shifts in $LAHg^{II}X$ complexes was noted earlier[38] and has been analyzed in detail in the $PhHg^{II}X$ series[99] (see discussion of groups 10 and 11 above).

4.3. HAs of the p-Block

4.3.1. General Aspects. The periodic trends of the SO-HALA effect in the p-block are governed predominantly by the occupation or vacancy of *n*p n_{HA}/n^{*}_{HA} orbitals, which directly relates to the oxidation state of the HA.[100] Calculated SO-HALA NMR shift ranges in p-block element complexes, based on references discussed in this section, are summarized in Figure 28.

The presence of the low-lying vacant *n*p n^{*}_{HA} orbitals together with a small HOMO−LUMO energy separation maximizes the SO-HALA deshielding mechanism (Figure 20b) in group 13 and 14 compounds with the HA in oxidation state I and II, respectively. Maximum deshielding (up to several hundreds of ppm for ^{13}C LAs) has been computed for Tl^{I} and Pb^{II} compounds.[91,132] Increased deshielding was also calculated for In^{I} complexes.[169] On the other hand, involvement of the HA *n*s orbitals in bonding (incomplete hybridization of s and p orbitals of rather different orbital sizes) disrupts the efficient orbital overlaps in the magnetic couplings and increases the HOMO−LUMO separation, which results in SO-HALA effects in Tl^{III} and Pb^{IV} compounds that may be an order of magnitude smaller than for their Tl^{I}/Pb^{II} counterparts.

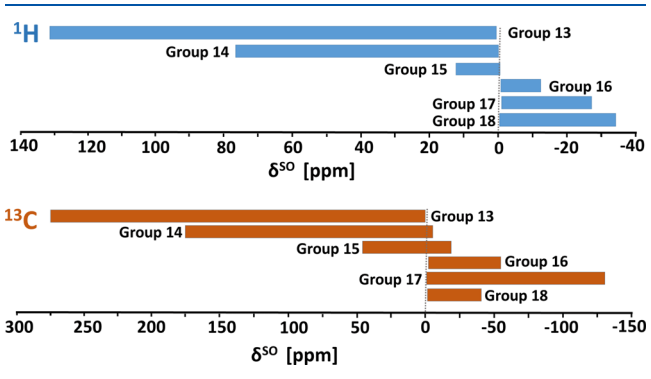

Figure 28. Computed ranges of the ^{1}H and ^{13}C SO-HALA shifts for individual groups in the p-block (LA bonded directly to the HA).

Vertical trends in the p-block using typical oxidation states are compared in Figure 29 for the $\delta^{SO}(^{13}C)$ of the sp-hybridized C_α atoms of acetylide substituents bound to different p-block HAs.[51] Note that nonbonding MOs are absent from the group 13 and 14 examples. In the former, the $\sigma^{(*)}_{HA-LA} \leftrightarrow n^{*}_{HA}$ deshielding mechanism (Figure 21b) dominates and leads to an inverse dependence, while the group 14 HA^{IV} compounds lack low-lying n^{*}_{HA} orbitals and thus exhibit small shielding contributions which originate in the $\sigma_{HA-L} \leftrightarrow \sigma^{*}_{HA-LA}$ contributions (see rule 2 in the beginning of this section).

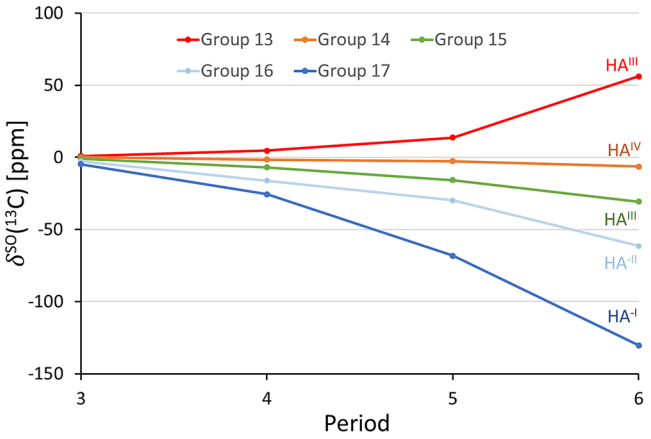

Figure 29. Comparison of trends in $\delta^{SO}(^{13}C_\alpha)$ for acetylide substituents bound to heavy p-block elements (with 0, 0, 1, 2, and 3 n_{HA} for groups 13, 14, 15, 16, and 17, respectively). Data from ref 51.

We recall that the absence of larger shielding SO-HALA contributions due to inefficient SO/FC pathways may lead to a trend that is inverse to halogen dependence for certain LAs with small s-character in the HA−LA bond, such as early d-block elements in their halide complexes. In that case the IHD is mostly of paramagnetic origin.[42] However, for HAs of group 13, the inverse trend (analogous to IHD) down the group is due to increasingly deshielding SO-HALA effects (Figure 29). This has been termed a *triel dependence*.[51]

In groups 15−17, the SO-HALA shielding increases with the group number and with decreasing oxidation state of the HA, i.e., with an increasing number of occupied $LP_{HA}(s)$. Group 15 compounds actually represent a borderline where the SO-HALA mechanisms of deshielding and shielding largely compensate each other, often resulting in a small overall (in absolute value) δ^{SO}.[51,100] Maximum SO-HALA shielding at the LA is observed in group 17 complexes in low oxidation states, i.e., halogens in oxidation state + I/-I with two occupied *π*-type LPs at the HA.[49,51,100] Regarding group 18, LA SO-HALA shifts were studied only for Xe compounds and are generally smaller than in group 17 compounds, except the outlier $\delta^{SO}(^{1}H)$ in HXeF, which explains the extended ^{1}H NMR range in Figure 28.

https://dx.doi.org/10.1021/acs.chemrev.9b00785
Chem. Rev. 2020, 120, 7065−7103

4.3.2. Groups 13 and 14: Triels and Tetrels. The SO-HALA-induced ^{13}C chemical shifts in group 13 HA^{III} and group 14 HA^{IV} complexes have been thoroughly investigated using model ethane-, ethene-, and ethyne-substituted systems.[51] Distinct SO-HALA deshielding was noted down the group 13 HA^{III} complexes, ranging from $\delta^{SO}(^{13}C)$ = +0.9 ppm in $H_2Al^{III}(CCH)$ to $\delta^{SO}(^{13}C)$ = +57 ppm in $H_2Tl^{III}(CCH)$. Comparatively smaller shielding $\delta^{SO}(^{13}C)$ was calculated in group 14 $H_3M^{IV}(CCH)$ complexes (M = Si^{IV} to Pb^{IV}) ranging from −0.3 ppm to −6 ppm in $H_3Pb^{IV}(CCH)$.[51] This is not surprising, as the availability of low-lying HA-centered unoccupied MOs, important for the SO-HALA deshielding mechanism, is diminished as we move from tricoordinated group 13 to tetra-coordinated group 14 systems, and the SO-HALA shielding effects originating in $\sigma_{HA-L} \leftrightarrow \sigma^*_{HA-LA}$ mechanism prevail. Notably, the overall reported relativistic contributions to the ^{13}C NMR resonances in group 14 HA^{IV} systems are deshielding (up to +11 pm) as a result of dominant deshielding SR effects (δ^{SR} up to +17 ppm for the C_α of an alkyl Pb^{IV} complex), which are only partially compensated by SO-HALA shielding contributions (δ^{SO} = −6 ppm in the same complex).[51] Similar results had been reported previously for group 14 hydrides ($HA^{IV}H_4$, HA = C, Si, Ge, Sn, and Pb) using complete active space self-consistent field (CASSCF) calculations,[170] where small ^1H SO-HALA shieldings and over-compensating deshielding δ^{SR} contributions were reported. A deeper PT2 analysis of those model Pb^{IV} systems, performed for the purpose of this review, reveals a number of small SO-HALA shielding and deshielding MO couplings balanced by several factors, mostly related to the substituents present.

A delicate dependence of both SR and SO-HALA effects on electronic structure has also been pointed out in a fully relativistic DFT study of $\delta(^{13}C)$ in group 14 (M^{IV}) alkynyl compounds.[92] For instance, a deshielding δ^{SR} up to +16 ppm and a shielding δ_{SO} up to −13.5 ppm were calculated for C_α in tetra-alkynyl complexes of Pb^{IV}, in good agreement with previous findings.[51,170] However, when three out of the four alkynyls were replaced by methyl groups, the signs of both the SR and the SO contributions on the remaining alkynyl C_α switched, to δ^{SR} = −7 ppm and δ^{SO} = +4 ppm. No explanation for this observation was given in that work, but we speculate that it may be related to a larger covalency of the Pb−CH_3 than the Pb−alkynyl bonds, influencing the energy and composition of the Pb−L bonding orbitals (particularly orbitals with π-character relative to the Pb−LA bond) and thus also affecting the corresponding orbital magnetic couplings. In summary, the SO-HALA effects in the $M^{IV}L_4$ tetrel complexes of group 14 are relatively small, and their sign depends heavily on the substituents present.

Moving to the lower oxidation states in groups 13 and 14, the recently predicted extremely deshielding δ^{SO}(LA) in Tl^I and Pb^{II} compounds[91,132] can be up to +200 ppm for ^{13}C, to +1000 ppm for ^{29}Si, and to +80 ppm for ^1H NMR chemical shifts. The origin of this extraordinarily large SO-HALA contribution relates to the geometrical and electronic structures of Tl^I and Pb^{II} compounds. Large deshielding $\sigma^{(*)}_{HA-LA} \leftrightarrow n^*_{HA}$ orbital magnetic couplings arise from the interplay of occupied and vacant 6p-based MOs, which are rotated by 90 degrees relative to each other (Figure 20b). This results in nearly perfect magnetically induced orbital overlap, further complemented by rather small energy gap(s) between σ_{HA-LA} and n^*_{HA} MOs.[132]

Extreme deshielding SO-HALA effects readily explain why certain NMR signals were absent in the experimental spectra of some previously studied Tl^I and Pb^{II} compounds; such signals lie far outside the typical NMR spectral ranges,[132] see Figure 28. Hence, only a few months after the computational prediction,[91] a record ^1H NMR shift of more than 35 ppm in a dinuclear Pb^{II} hydride was experimentally confirmed.[171] Since then, a growing number of new experimental studies have been motivated by the discovery of extreme SO-HALA effects in Pb^{II} compounds, and old attempts to prepare the Pb^{II} hydrides and investigate their chemistry have been revived.[171−173]

An analogous but an order of a magnitude smaller deshielding δ^{SO} has been calculated for some Sn^{II} compounds.[91,132] It should be noted, however, that in certain circumstances, such as the involvement of the HA in clusters, relatively large shielding SO-HALA effects can also be found for Sn^{II} species. In earlier computations on Sn−P cages,[174] sizable SO-HALA shielding contributions to the ^{31}P shifts were calculated (−80 ppm at the phosphorus atoms adjacent to three Sn^{II} centers). This is a rather extreme example of the influence of structural aspects on the SO-HALA effect.

The magnitude of $\delta^{SO}(^1H)$ in both Sn^{II} and Pb^{II} hydrides has been reported to depend on the coordination number of the central atom.[91] This was rationalized by the variable involvement of Sn and Pb np^* orbitals in ligand binding, making them less accessible for the SO-HALA deshielding mechanism in case of higher coordination numbers of the HA. SO-HALA shifts in Sn^{II} and Pb^{II} compounds thus sensitively probe the coordination sphere of the central metal atom. A practical application of the dependence of the SO-HALA effect on electronic structure[175] showed that a sizable decrease of $\delta^{SO}(^{13}C_\alpha)$ in cyclic plumbanes from ∼80 to ∼20 ppm can be used to probe the formation of adducts with Lewis bases. This decrease results from the involvement of the Pb 6p* orbitals in adduct formation, which increases the energy denominators in the SO/FC formula (section 2.3.3).[175]

Four-component relativistic DFT calculations of the NMR chemical shifts in a dimeric plumbylene,[176] [Fe{(η5-C_5H_4)-$NSiMe_3$}$_2$Pb:], which can activate aromatic C−H bonds under normal conditions, revealed a large difference between the $\delta^{SO}(^{15}N)$ values of the two nitrogen atoms bound directly to the lead center (76 ppm vs 9 ppm). This difference was rationalized based on the covalency of the individual Pb−N bonds, which was in turn used to explain the unexpected shielding of one of the ^{207}Pb resonances.

4.3.3. Group 15: Pnictogens. The SO-HALA effects in compounds with an HA of group 15 are mostly shielding, and the role of the oxidation state of the HA seems less pronounced (so far it is reported to be notable only for bismuth). For instance, the calculated[51] SO-HALA shielding at $^{13}C_\alpha$ alkynyl atoms ranges from δ^{SO} = −1 ppm in $H_2P^{III}CCH$ to δ^{SO} = −31 ppm in $H_2Bi^{III}CCH$. A weak ^1H SO-HALA shielding of −0.2 ppm for hydrogen atoms bound to phosphorus has been noted.[65] The rovibrational, thermal, and relativistic corrections to the ^{19}F shielding constants in group 15 trifluorides (NF_3, PF_3, and AsF_3) have been investigated using a combination of nonrelativistic coupled-cluster with single, double, and triple excitations (CCSDT) and relativistic DFT calculations.[177] Weakly shielding $\delta^{SO}(^{19}F)$ up to −4 ppm was observed. A similarly large SO-HALA ^{13}C shielding down to δ^{SO} = −4 ppm was calculated at a carbon atom bound to As in a number of naturally occurring organo-arsenic compounds, including a variety of isomers of Arsenicin A, for which an adamantane-like structure has been proposed.[178] Inclusion of SO-HALA effects in the calculations was found necessary in order to distinguish

https://dx.doi.org/10.1021/acs.chemrev.9b00785
Chem. Rev. 2020, 120, 7065−7103

between the individual isomers of Arsenicin A, enabling the confirmation of the adamantane-like structure.

A rather small SO-HALA shielding $\delta^{SO}(^{13}C) = -4$ ppm was predicted at $^{13}C_{ipso}$ in triphenylbismuth.[179] The C_{ipso} of phenyl (Ph) substituents was later used to study the dependence of the SO-HALA effect on the oxidation state of Bi in $Bi^{III}PhCl_2$ and $Bi^{V}PhCl_4$.[132] Small SO-HALA shielding at C_{ipso} was predicted in $PhBi^{V}Cl_4$ ($\delta^{SO} = -2$ ppm), probably resulting from a low availability of low-lying LP* MOs for the SO-HALA deshielding (compare to Pb^{IV} compounds above) and stabilization of the HA-L MOs, which diminishes the SO-HALA shielding mechanism.[132] A notably larger SO-HALA deshielding (δ^{SO} = +50 ppm) was calculated for $PhBi^{III}Cl_2$. The latter value is nearly an order of magnitude larger than the one predicted for the same ligand C_{ipso}(Ph) in triphenylbismuth (see above).[179] The reasons for this effect are explained at the bottom of next paragraph.

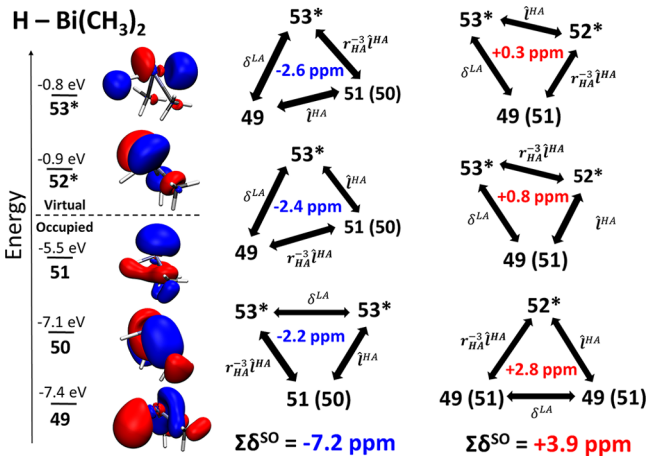

Figure 30. Schematic PT3 visualization of the $\delta^{SO}(^{1}H)$ deshielding (top) and shielding (bottom) orbital magnetic couplings computed for $HBi(CH_3)_2$. Adapted from ref 100. Copyright 2018 American Chemical Society.

Another example of the importance of the ligand sphere for SO-HALA shifts can be found for Bi^{III} hydrides. The simple hydride $HBi^{III}(CH_3)_2$ (Figure 30) has an ^{1}H NMR shift of 2.1 ppm,[180] with a small $\delta^{SO}(^{1}H)$ of 0.7 ppm.[100] Replacing the methyl groups with a pair of large terphenyl substituents[181] results in a total ^{1}H shift of 19.4 ppm and in $\delta^{SO}(^{1}H) = 14.4$ ppm (presented in this work, calculated at the same level as used in ref 91). The delicate dependence of δ^{SO} on the nature of the substituents can be rationalized by a competition between the shielding and deshielding SO-HALA mechanisms in Bi^{III} compounds, which has been explained for a Bi^{III} hydride using PT3 theory,[100] see Figure 30. Essentially, differences in the covalency of the Bi−L bonds promote one mechanism at the expense of the other. More electron-donating substituents (i.e., the terphenyl group in these hydrides) stabilize those Bi-L bonding orbitals that contribute most to the SO shielding mechanism. This diminishes the negative, shielding $\sigma_{HA-L} \leftrightarrow \sigma^{*}_{HA-LA}$ SO-HALA contributions, while the positive (deshielding) SO-HALA contributions remain largely unaffected. Hence, considerably larger SO deshielding may be observed at the LA when more charge-withdrawing substituents are present in the molecule. This applies also to the Pb^{IV} compounds, see above.

4.3.4. Group 16: Chalcogens. The SO-HALA effects in heavy chalcogen compounds have been well investigated, at least partly because the favorable spin 1/2 of ^{77}Se and ^{125}Te nuclei give rise to experimental multinuclear NMR studies that frequently also include the lighter nuclei. Relativistic effects on the NMR chemical shifts in heavy chalcogen compounds have been studied mostly by relativistic DFT methods.[51,164,182−185] Generally, the SO-HALA shielding increases uniformly with Z_{HA} down group 16 and also increases with the number of occupied LPs at the HA, i.e, for a lower HA oxidation state. Maximal SO-HALA shieldings (>50 ppm) are reached for the heavier chalcogen compounds (Se and Te) in oxidation state − II, when a double bond to the LA is present (as in seleno- and telluroketones).[164,182,185] This bonding situation clearly favors the propagation of the SO-HALA effects from the HA to the LA in p-block species and additionally involves small energy denominators. Even a relatively "light" HA like sulfur can induce an overall δ^{SO} shielding of −8 ppm at the adjacent ^{13}C nuclei of CS_2 via the C═S double bonds.[164,185] In addition to the two factors mentioned above, a large carbon 2s character in the C−S bonds (formal sp^2 hybridization) also aids this shielding. A thorough study of the SO-HALA effects in heavy chalcogen complexes at the Coupled-Cluster with Single and Double and Perturbative Triple excitations CCSD(T) and Breit-Pauli Perturbation Theory (BPPT) levels of theory was performed to evaluate secondary isotope effects on nuclear shielding in CSe_2.[185,186]

Large SO-HALA effects propagating over several bonds in experimentally known seleno- and telluro-ketones were calculated using relativistic DFT methods.[187] The long-range SO-HALA effects on the ^{13}C shifts were found to be −23, +18, and −9 ppm for C_α, C_β, and C_γ, respectively. This alternation of the sign reflects the analogy of the SO/FC mechanism with that of J-coupling[26] (section 3.1). Moreover, $\delta^{SO}(C_\gamma)$ fulfilled the Karplus double-cosine dependence on the M-C_α-C_β-C_γ dihedral angle, also known for J-coupling.[26,140] In a follow-up study,[188] the authors found similar relations (sign alternation and Karplus dependence), for H_β and H_γ nuclei in analogous systems. These results confirm earlier findings[113,140] that, when sufficiently large, δ^{SO} can be used to determine dihedral angles and isomerism.

4.3.5. Group 17: Halogens. The first mentioned[19,20] and most intensively studied SO-HALA effect is the normal halogen dependence (NHD), which refers to the increasing SO-HALA shielding at the LA with increasing Z_{HA} of an adjacent halide substituent for both organic and inorganic compounds. While we saw analogous dependencies throughout groups 14−17 (see Figure 29 in section 4.3.1), the SO-HALA effects and thus the NHD-type behavior tends to be most pronounced for HAs from group 17. Given that the SO-HALA effect depends on the number of halogen LPs,[49] NHD has been studied largely for halide substituents, and the number of studies is so large that we do not attempt a comprehensive coverage of the literature in this case. For example, since 2004, computational investigations of NHD for ^{1}H and ^{13}C NMR shifts have targeted hydrogen[189] and methyl[135,189] halides, halogen-substituted acetonitrile,[190] cyclohexane,[191] pyran,[191] purines,[105] and carbazoles.[192] Studies of NHD on the NMR chemical shifts and shielding tensors of ^{11}B, ^{19}F, and ^{29}Si nuclei at various levels of theory[193−195] led to essentially the same trends and conclusions as for ^{1}H and ^{13}C nuclei. Higher halogen oxidation states have been mentioned in Section 1.[49]

https://dx.doi.org/10.1021/acs.chemrev.9b00785
Chem. Rev. 2020, 120, 7065−7103

One of the computationally most advanced and detailed studies focused on the ^{13}C and ^{1}H shift tensors in the methyl halides using combined ab initio and DFT analyses with perturbation theory (PT), complemented by vibrational corrections and thermal averaging.[135] The SO origin of the NHD was confirmed (the SO/FC term dominates the PT contributions), although SR effects of opposite sign (deshielding) were found important in order to obtain quantitative agreement with experiment. Note that the SR effects do not follow the SO-HALA trends but tend to be generally deshielding for HAs of the p-block. Relativistic DFT and BPPT computational approaches were also applied to the propagation of SO-HALA effects in heteroaromatic 6-halopyridines.[105] The authors concluded that relativity, solvent effects, and the choice of reference compound are important for achieving quantitative agreement between theory and experiment. Long-range relativistic effects were also studied, and the previously discussed sign alternation of the SO-HALA contributions[47] was also seen in these heterocyclic systems.

Interestingly, the magnitude of the SO-HALA effect induced by heavy halide substituents depends on the conformation of stereoisomers. The propagation of the SO-HALA effect was diminished in halogenated hydrocarbons[191] when strong hyperconjugative interactions involving σ^*_{C-X} orbitals (X = halogen) were present. The authors calculated various conformers of halocyclohexanes and 2-halo-tetrahydropyran and analyzed the SO-HALA effects on the ^{13}C shifts. The SO contribution in the axial conformer of iodo-cyclohexane with stronger hyperconjugative interactions was found to be 7 ppm lower than in the equatorial conformer (δ^{SO} = 15.8 ppm vs 22.8 ppm), confirming the experimentally observed difference of 8 ppm. Hyperconjugation was shown to stabilize the occupied LP_{HA} orbitals and to thereby increase the relevant energy denominators. The changes in the SO-HALA effect thus determine the observed differences in shift and may be used to distinguish individual conformers. The authors pointed out, however, that this may apply only to structurally similar groups of molecules (conformers, isomers) where other factors influencing the SO-HALA effect (e.g., hybridization at the LA) are comparable. Subsequent work on the influence of stereoelectronic interactions on the SO and paramagnetic contributions to the ^{13}C NMR shielding tensors in dihaloethenes[196] came to similar conclusions: the hyperconjugative interactions involving the halogen LPs and σ^*_{C-X} antibonding orbitals (X = halogen), together with steric interactions between the halogen atoms, were found to be a major cause of the difference in $\delta(^{13}C)$ between the cis vs trans isomers. These two studies nicely demonstrate the possible use of SO-HALA shifts to investigate isomerism and hyperconjugation in compounds with heavy halogen substituents.

4.3.6. Group 18: Aerogens. For obvious reasons, SO-HALA effects originating from noble-gas (Ng) heavy atoms have been studied less than those for group 17 HAs. A combination of ab initio and relativistic DFT levels for noble-gas hydride cations (NgH^+; Ng = Ne−Xe)[136] found the total relativistic effect on the ^{1}H shifts (the SO-HALA was not investigated separately) to range from ca. 0 ppm in NeH^+ to ca. −18.1 ppm in XeH^+. A perturbational treatment of relativistic effects typically gave smaller SO-HALA effects for a series of HXeY[197,198] compounds than for HI,[189] probably due to the lower covalency of the Rg−H bonds. The HXeF system with an extreme value of $\delta^{SO}(^{1}H)$ = −35 ppm, probably caused by the TLI of fluorine, was an exception.[197,198]

While no structure-related applications of SO-HALA effects have yet been reported for Ng compounds, the known correlations between δ^{SO} and the covalency of the HA−LA bond[114] can be useful in determining the character of Ng−LA bonds and the oxidation state of the Ng by using a combination of relativistic calculations and NMR studies, as suggested in refs 197 and 198.

4.4. HAs of the f-Block

4.4.1. General Aspects. Investigation of the SO-HALA trends in lanthanide and actinide complexes has been limited to the closed-shell $4f^0$ (La^{III}, Ce^{IV}), $4f^{14}$ (Lu^{III}), and $5f^0$ (Th^{IV}, Pa^{V}, and U^{VI}) electronic configurations, as others typically feature paramagnetic metal centers and thus different physics of nuclear shielding. In these closed-shell configurations, the f-elements have formally empty, low-lying valence (n-1)d and/or (n-2)f shells. Hence, the deshielding $\sigma^{(*)}_{HA-LA} \leftrightarrow n^*_{HA}$ coupling mechanism dominates, similar to the p^0 and d^0 cases (Figure 23).[97,100,137,199] A relatively small deshielding $\delta^{SO}(^{1}H) \approx +5$ ppm, has been calculated for La^{III} and Lu^{III} hydrides.[100] This is comparable to $5d^0$ transition-metal hydrides, which may reach

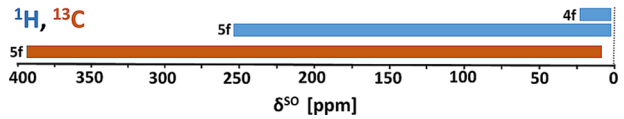

Figure 31. Computed ranges of the ^{1}H and ^{13}C SO-HALA shifts in 4f and 5f complexes (LA bonded directly to the HA).

$\delta^{SO}(^{1}H)$ values up to ca. + 10 ppm (e.g., Hf^{IV}, Ta^{V}, W^{VI}, and Re^{VII}, Figure 26). A larger deshielding effect of $\delta^{SO}(^{1}H) \approx +20$ ppm was predicted for a Ce^{IV} hydride, see below. The ranges of the SO-HALA ^{1}H and ^{13}C shifts in 4f and 5f complexes that have been predicted are summarized in Figure 31.

The availability of low-lying 5f-orbitals and the involvement of the 5f-shell in chemical bonding is decisive for the $5f^0$ systems. Moderately deshielding SO-HALA effects (5−12 ppm), comparable to $5d^0$ systems, are found for Th^{IV} complexes[137,200] because 6d and 7s orbitals dominate Th^{IV} bonding with only minor involvement of the relatively diffuse 5f orbitals.[137,200] A protactinium model hydride complex $[HPaF_5]^-$ has been predicted to have $\delta^{SO}(^{1}H) > +50$ ppm, which indicates that 5f-orbitals which are more available can strongly enhance the deshielding SO-HALA effects.[12] This effect is further enhanced for U^{VI} hydride complexes with $\delta^{SO}(^{1}H)$ predicted to be well over +200 ppm in model hydrides and $\delta^{SO}(^{13}C)$ of nearly +400 ppm for carbon atoms directly bound to the U^{VI} centers in organometallic complexes (see below).[95,97,201]

The oxidation state again plays a potentially important role in the size and sign of the SO-HALA effects, as it does for the d- and p-block elements. In contrast to the large deshielding δ^{SO}(LA) in $5f^06d^0$ U^{VI} complexes, a strongly shielding $\delta^{SO}(^{1}H)$ of −37 ppm has been predicted for a hypothetical closed-shell $5f^26d^0$ U^{IV} complex.[100] While this $5f^2$ model system is unlikely to reflect any real U^{IV} ground-state complex, the computations confirm that the general mechanism outlined above (SO shielding due to LPs at the HA)[100] can also be applied to 5f actinide systems. The δ^{SO} of this hypothetical closed-shell U^{IV} complex is not included in Figure 31 because no closed-shell $5f^2$ complexes are known to exist.

4.4.2. Selected Examples and Applications. SO-HALA effects in lanthanide complexes have, until now, been

https://dx.doi.org/10.1021/acs.chemrev.9b00785
Chem. Rev. 2020, 120, 7065−7103

investigated only very sparsely, probably due to a limited number of known closed-shell species.[100,199] Very small SO-HALA effects (<1 ppm) were computed for the nitrogen atoms of a phenanthroline ligand bound directly to lanthanum, probably due to the highly ionic La−N bonding.[199] On the other hand, a large ^{1}H SO-HALA deshielding (δ^{SO} = +20 pm, δ^{tot} ≈ +31 ppm) has been predicted for a Ce^{IV} hydride[100] and rationalized by the involvement of formally vacant Ce 4f orbitals in the Ce−H bonding and thus also in the $\sigma^{(*)}_{HA-LA} \leftrightarrow n^{*}_{HA}$ deshielding mechanism, in analogy to U^{VI}, see Figure 32. However, neither this prediction for Ce^{IV} nor the U^{VI} case described below has been confirmed experimentally.

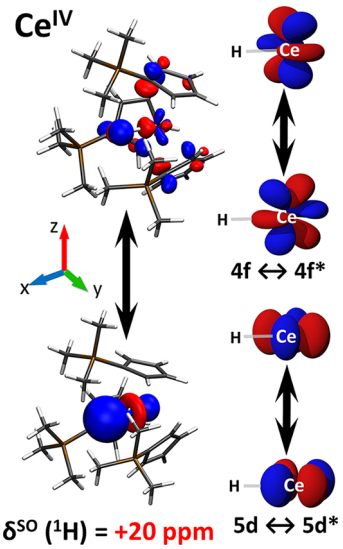

Figure 32. Example of the orbital magnetic coupling in a Ce^{IV} hydride complex (top) and schematic representation of the AOs contributing to the SO deshielding (bottom). Adapted from ref 100. Copyright 2018 American Chemical Society.

The NMR shifts of closed-shell actinide complexes have been studied extensively over the years. Early relativistic DFT computations of the ^{19}F shifts in U^{VI} fluoride complexes gave modest SO-HALA shifts up to about 30 ppm,[41,202] because the low fluorine 2s-character in the U−F bond disfavors the FC mechanism. Much of the early work focused on the challenges of computing the NMR shifts for actinide complexes, e.g., choosing the sizes of the ECP cores and the exact-exchange admixtures to use in the DFT functionals.[97,137,201] The calculation of ^{19}F NMR shifts in actinide systems has been reviewed critically.[203]

A two-component ZORA study of the ^{1}H shifts in U^{VI} hydride complexes[137] was aimed explicitly at investigating potentially large SO-HALA shifts. The results indeed suggested giant deshielding of more than +100 ppm in some of the model systems studied. As no experimental NMR data for such species are yet available (the only known U^{VI} hydride complex, H_2UO_2, has been studied only by matrix-isolation IR spectroscopy),[204] selecting a suitable functional to make valid predictions required that other reference data be available. These were the ^{13}C NMR shifts of some U^{VI}-bound carbon atoms in organometallic complexes. Except for the system discussed in the next paragraph, comparison with the available experimental ^{13}C data suggested the use of a hybrid functional with 40% exact-exchange admixture. Notably, this was due to the absence of an exchange-correlation kernel in the 2-component ZORA implementation used at the time.[96,97,153] A systematic reinvestigation of the ^{1}H and ^{13}C NMR shifts in U^{VI} complexes including the exchange-correlation kernel (in comparison with 4-component results)[97] suggested that functionals with a lower exact-exchange admixture (20−25%) are more appropriate. Nevertheless, the giant SO-HALA shifts were confirmed.

The one ^{13}C case for which the predictions of ref 137 disagreed starkly with the available experimental data was an unusual U^{VI}-hexaalkyl complex. Here the uranium-bound methylene ^{13}C NMR shift had been assigned originally to a signal at +34 ppm, which was likely a contaminant in the *in situ* spectrum,[205] while the computations suggested values closer to 400 ppm because of the extremely large SO-HALA shifts. Such shifts are completely outside the usual expectations for an alkyl carbon atom, and consequently the original measurements had been restricted to a range between −50 and +130 ppm. A new measurement with a larger spectral range gave a value of 434 ppm,[201] in line with the computational predictions, and confirming the existence of giant SO-HALA shifts of more than +300 ppm. The predictive quality of the computational methods suggested a blind test of computed and measured ^{13}C NMR shifts for a newly found tetraalkyluranylate complex. The computed shift of +250 ppm agreed excellently with the independently measured value of +243 ppm, again with sizable SO-HALA contributions of about +177 ppm.[201]

These results were still obtained with 40% exact-exchange admixture and without a kernel in the perturbation treatment. The above-mentioned reinvestigation of ref 97 with a kernel and other functionals confirmed overall the large SO-HALA shifts also for these cases while providing some corrections to the quantitative data. That study also gave further predictions, in particular an extension of the range of U^{VI}-bound ^{13}C NMR shifts up to +550 ppm (δ^{SO} = +390 ppm) for organometallic model complexes, and it suggested the positions of missing signals in experimentally characterized complexes.[97] Systematic analyses correlated the SO-HALA shifts with the covalency of the U−C bond and the position of the LA in the complex. For example, atoms opposite to strong π-donors (e.g., in uranyl complexes) were found to have smaller SO-HALA shifts than nuclei positioned *trans* to less π-donating ligands, e.g., in the above-mentioned hexaalkyl complex.[97]

Covalency was also studied in rare actinide-chalcogen Th^{IV} and U^{VI} complexes by ^{77}Se and ^{125}Te NMR.[206] Curiously, selenium and tellurium constitute the "LA" in these systems, and their chemical shifts include SO-HALA effects arising from the actinide center. The $\delta^{SO}(^{77}Se)$ and $\delta^{SO}(^{125}Te)$ were found to increase linearly with the covalency of the actinide−chalcogen bond (R^2 = 0.92−0.99) expressed as the delocalization index. In one of the U^{VI} complexes studied, a ^{77}Se NMR shift of 4900 ppm was measured, which extends the known chemical shift range for this nucleus in diamagnetic systems from the previous record of 3300 ppm. Even larger ^{77}Se shifts, up to 8000 ppm, have been predicted computationally.[206]

Uranyl ^{17}O NMR chemical shifts have been investigated recently[207] by combined experimental and computational approaches. The *ab initio* calculations revealed that the ^{17}O resonances were very sensitive to the local environment, a fact which could be used to provide better understanding of the structure and crystal packing of such compounds in the solid state. A thorough evaluation of the DFT approaches to calculating various properties of uranium complexes, including computation of the relativistic NMR shift, has been reported recently.[208]

https://dx.doi.org/10.1021/acs.chemrev.9b00785
Chem. Rev. 2020, 120, 7065−7103

4.5. Superheavy Elements (SHEs) as HAs

Given the short half-lives of SHEs, the chances for experimental NMR studies of their compounds are slim at best. Therefore, computational studies have also been almost nonexistent. So far, only one set of computations (done at four- and two-component levels) is available for a number of postactinide complexes with $6d^6$, $6d^8$, and $6d^{10}$ HA configurations.[209] Interestingly, the SO-HALA shifts in the $6d^6$ complexes are slightly smaller or only marginally larger (in absolute value) than in their $5d^6$ analogs. This is due to greater ligand-field splitting (caused by the improved bonding interactions of the relativistically expanded 6d-orbitals) counteracting the larger SO matrix elements.[113] The SO-shifts in $6d^8$ complexes are somewhat larger than in their $5d^8$ analogs. Notably, the ligand-field effects do not apply to the d^{10} configuration, and in consequence the deshielding SO-HALA shifts are notably enhanced in the $6d^{10}$ hydrides compared to their $5d^{10}$ analogs, e.g. + 23.7 ppm for [HRg(NHC)] vs +3.3 ppm for [HAu(NHC)] (NHC is the simplest possible imidazolium-based N-heterocyclic carbene-model ligand, Rg is roentgenium) or +33.1 ppm for [HCnPh] (Cn is copernicium) compared to +9.0 ppm for [HHgPh].[209] All data given are predictions based on two-component SO-ZORA computations.[134]

4.6. Weak Interactions and "Through-Space" SO-HALA Effects

The above-mentioned studies concentrated mostly on SO-HALA effects at an LA chemically bound to the HA (or involved in a covalent bonding network including the HA). However, in the same way as the FC mechanism of *J*-coupling operates via the polarization of the spin density even in the absence of "chemical bonds" ("through-space" *J*-coupling),[210] one can expect this to hold also for the SO-HALA chemical shifts, see section 3.1.5.

The possibility of "through-space" propagation of SO-HALA effects in pyridinium halide ionic liquids has been investigated computationally.[211] Using various computational models, $\delta^{SO}(^{13}C)$ up to +3 ppm was predicted at the pyridinium carbon atoms when pyridinium was involved in an ion pair with I_3^-, but this effect vanished with the Cl_3^- analog. The authors concluded that it may be challenging to find experimental evidence to support these computational predictions, owing to the short lifetime of the investigated ion pairs in a liquid environment. Notably, in contrast to typical shielding SO-HALA effects for bonded halogen substituents, the through-space SO-HALA contribution from X_3^- to the pyridinium carbon nuclei was found to be deshielding. This would correspond to an IHD, and the authors argued that the spin polarization is transmitted via the π-system.

Spectroscopic and computational evidence of an intramolecular $Au^I\cdots H-N$ hydrogen bond in a gold carbene complex was reported recently.[212] While the SO-HALA effect can propagate only via an Au···H hydrogen bond, δ^{SO} values of −6 ppm and −0.1 ppm were predicted for the ^{15}N and ^1H nuclei, respectively, involved in the $Au^I\cdots H^+-N$ hydrogen bond. The SO-EDD[99] calculated for this system is shown in Figure 33. The low stability of the molecule in solution prohibited detailed experimental NMR investigations.

During the revision of this review, solid-state ^1H NMR and DFT study of a series of 4-(dimethylamino)pyridinium with Cl, Br, and I counteranions has been reported.[213] Discrepancy between the experimental and theoretical NMR shifts was attributed to an absence of the SO effects in the calculations of hydrogen-bonded ion pairs at the SR DFT level. However, agreement between the theoretical and experimental NMR data was significantly improved at the SO level that demonstrated propagation of the SO effects through hydrogen bonding which resulted in "through-space" SO-HALA shifts.

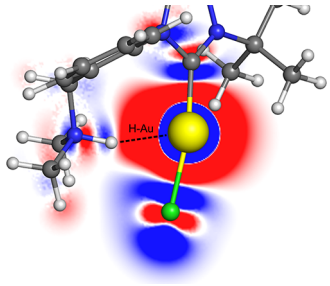

Figure 33. SO-EDD[99] for an intramolecular $Au^I\cdots H-N$ hydrogen bond in a gold carbene complex.[212] The SO-induced increase and decrease in the electron density, which correspond to the sign of SO-HALA shift, are shown in blue and red, respectively.

The involvement of the HA in weak interactions may also indirectly influence the δ^{SO} at a bonded LA. As heavier halogens, particularly iodine, induce considerable (shielding) δ^{SO} at an adjacent LA, their involvement in halogen bonding modulates the size of δ^{SO} in analogy to the TLI reported for transition-metal complexes (see above), thus providing another tool to investigate halogen bonding.[214] Already in 2004,[215] following still earlier work,[216,217] the effect of halogen bonding on the ^{13}C NMR chemical shifts of C_α in haloarenes in different solvents was studied. The authors noted that nonrelativistic deshielding of 6−8 ppm at C_α caused by the formation of a halogen bond was compensated by an induced SO-HALA shielding of similar size. One might thus mistakenly assume the absence of halogen bonding based on the total observed $^{13}C_\alpha$ NMR chemical shift.

Recently, a multinuclear solid-state NMR study investigated halogen bonding in various cocrystals.[218] The carbon atoms attached to a heavy halogen ($^{13}C_\alpha$) were found to be deshielded by +6 ppm when iodine derivatives were involved in halogen bonding. Two-component relativistic SO-ZORA calculations showed that modulation of both the paramagnetic and SO-HALA contributions to the $^{13}C_\alpha$ chemical shifts was the main cause of the observed deshielding. The relativistic ^{13}C NMR chemical shift was proposed as a possible indicator of halogen bonding, although the exact mechanism was not investigated. The calculated deshielding correlated with increasing C−I and C−Br bond lengths, as confirmed by other studies.[219] We speculate that the main cause of the observed deshielding is a decrease of the p-character/covalency of the C−X bond upon formation of the halogen bond,[114,132] which in turn weakens the SO/FC propagation of the SO-HALA effect.[114]

4.7. Emerging Applications

In Section 4, we have explained and summarized how the SO-HALA shifts relate to the electronic structure of the heavy atom across the Periodic Table, that is, the periodic trends in SO-HALA effects. We hope the examples provided show that applications of SO-HALA shifts are not limited to merely aiding the assignments of experimental spectra or to improving the agreement between experimental and computational data. As demonstrated in sections 3 and 4, the SO-HALA shifts sensitively reflect—and thus can be used to study—various chemical phenomena, such as the structural trans and cis influences, the covalency of the HA−LA bond, molecular

https://dx.doi.org/10.1021/acs.chemrev.9b00785
Chem. Rev. 2020, 120, 7065−7103

conformation and isomerism, and weak supramolecular interactions. The SO-HALA shifts also provide insights and links to chemical reactivity and may guide experimental efforts by revealing new and exotic ranges of NMR chemical shifts. A thorough understanding of the SO-HALA shift thus represents a powerful tool for probing the structure and chemical properties of heavy-element compounds.

5. SUMMARY AND PROSPECTS

Relativistic effects can influence the neighbor-atom NMR shifts in heavy-element compounds appreciably, with substantial and often analytically characteristic consequences for the NMR spectra. Relativistic neighbor-atom effects on NMR shifts are typically dominated by spin−orbit and magnetically induced spin polarization arising at the heavy atom and propagating to the spectator nucleus via a Fermi-contact-type interaction. This phenomenon, generally known as the spin−orbit heavy-atom effect on the light-atom NMR shift (SO-HALA shift), has been known for some time but is still underappreciated in the NMR community. Significant progress in our understanding of these effects across the Periodic Table since the last general review in 2004 and the recent availability of powerful MO-by-MO analysis and interpretative tools rooted in third-order perturbation theory called for a new and comprehensive exposition and critical overview of the theoretical background of SO-HALA shifts, of the conceptual tools available, and of the trends observed throughout the Periodic Table of the Elements.

Throughout this review we have compared both second-order perturbation theory based on relativistic molecular spinor pairs and third-order perturbation theory based on nonrelativistic (or scalar relativistic) MOs. The latter offers a more fine-grained analysis of SO-HALA shifts, in particular regarding the question of the sign of the effect−shielding vs deshielding. Provided a perturbational treatment of the SO effects does not cause too large errors, the PT3 treatment gives the clearer picture. It has been central to clarifying many of the concepts laid out in this overview. The terms obtained in the PT3 framework for the SO/FC mechanism of SO-HALA shifts can be connected directly to the bonding and electronic structure of the given system and can be displayed in a pictorial representation based on triangles linking the MOs and their energetics, as well as the perturbation operators. Further graphical insights can be provided by comparisons to the spin−orbit and magnetically induced spin density (SOM-ISD) and to changes in charge density induced by spin−orbit coupling (spin−orbit electron deformation density, SO-EDD). Together, these analyses and graphical tools allow for chemically intuitive interpretations of the SO effects on the neighbor-atom NMR shifts. This understanding is expected to greatly assist experimental chemists and NMR spectroscopists in estimating the ranges of the NMR shifts for unknown compounds, in the identification of intermediates in catalysis or other processes, in analyzing conformational aspects or intermolecular interactions, and in the prediction of trends in series of compounds throughout the Periodic Table.

Given the substantial progress made since the 2004 review referred to in section 1 and the fast-growing literature with ever more examples of relativistic neighbor-atom effects on NMR shifts and their utilization in many fields of chemistry, it seems safe to expect further insights and a further widening of this topic over the coming years.

6. TECHNICAL AND COMPUTATIONAL DETAILS

To have a consistent data set on which to base our discussion, and to illustrate the concepts in Section 3, new data were calculated using the methods given below.

6.1. Optimization of Structure

Method 1: The structures were optimized using the Turbomole program (releases 6.3 or 7.3).[220] The PBE0 functional,[221] scalar-relativistic effective core potentials (ECPs) for the HA, and def2-TZVPP basis sets were used.

Method 2: The structures were optimized using the ORCA 4.1 program.[222] The scalar-relativistic all-electron DKH approach, the PBE0 functional, and def2-TZVPP basis sets were employed.

6.2. Molecular orbital and bonding analysis

6.2.1. Natural Bonding Orbital (NBO) Analysis. Contributions of the AOs (e.g., d orbitals) to the HA−LA bond were calculated using the NBO 3.1[223] module as implemented in Gaussian16.[224] The PBE0 functional, an ECP for the HA, and def2-TZVPP basis sets were used.

6.2.2. Energy Decomposition Analysis-Natural Orbitals for Chemical Valence (EDA-NOCV).[225] Charge and energy analysis of orbital contributions to the binding energy was performed in the ADF 2014 program.[226] The computational setup was based on the ZORA/PBE0/TZP level of theory.

6.3. Calculation of SO-HALA Shifts

The SO-HALA data calculated for this work were obtained as the difference between four-component relativistic DFT calculations of NMR shifts[73] and calculations neglecting spin−orbit coupling (scalar-relativistic values - the contribution of the SO operator was down-scaled to 0),[110] as implemented in the ReSpect program.[93,154] The Dirac-Kohn−Sham (DKS) approach was used with the PBE0[221,227] functional, Dyall-vtz basis sets[228−230] for the HA, and pcS-2 basis sets[231,232] for the other atoms (DKS/PBE0/Dyall-vtz/pcS-2 level).

6.4. Calculation and Visualization of the SO-and-Magnetically Induced Spin Density (SOM-ISD) and the Spin−Orbit Electron Deformation Density (SO-EDD)

The SOM-ISD maps[100] were calculated as implemented in the ReSpect program.[93,154] The SO-EDD maps[99] were obtained as differences between the 3D electron density maps calculated at four-component and scalar-relativistic levels (to obtain scalar-relativistic values, the contribution of the SO operator was down-scaled to 0).[110]

6.5. Analysis of SO-HALA Shifts

6.5.1. Second-Order Perturbation Analysis (PT2). The SO-HALA shifts were obtained as the difference between 2c-ZORA and 1c-ZORA values calculated in the ADF program. The analysis of MO ↔ MO and MSP ↔ MSP couplings was used as implemented in the ADF program.[134] The composition of 2c MSPs in terms of 1c-ZORA MOs was determined by employing standard fragment analysis.[134] The graphical display of MSPs used only one real function of the complex, transformed spinor of a given Kramers pair.

6.5.2. Third-Order Perturbation Analysis (PT3). The SO-HALA shifts were calculated and analyzed using the PT3 approach as implemented[99] in the ReSpect program.[93,154] This implementation follows the third-order response theory of ref 107 for the static (perturbation-free) case. The applied analysis considers only the one-electron contributions to the SO/FC NMR shielding and neglects all HF and DFT kernels. Assuming the presence of a single heavy atom in the system

https://dx.doi.org/10.1021/acs.chemrev.9b00785
Chem. Rev. 2020, 120, 7065−7103

allows us to approximate the SO operator as $\sum_{N=1}^{nuc} Z^N r_N^{-3} \hat{l}_u^N \cong Z^{HA} r_{HA}^{-3} \hat{l}_u^{HA}$, see section 2.3.3. The unperturbed wave function has been calculated at the PBE/Dyall-vtz/pcS-2 level.

AUTHOR INFORMATION

Corresponding Authors

Michal Straka − *Institute of Organic Chemistry and Biochemistry, Czech Academy of Sciences, CZ-16610 Prague, Czechia;* orcid.org/0000-0002-7857-4990; Email: straka@uochb.cas.cz

Martin Kaupp − *Institute of Chemistry, Technische Universität Berlin, D-10623 Berlin, Germany;* orcid.org/0000-0003-1582-2819; Email: martin.kaupp@tu-berlin.de

Radek Marek − *CEITEC - Central European Institute of Technology and Department of Chemistry, Faculty of Science, Masaryk University, CZ-62500 Brno, Czechia;* orcid.org/0000-0002-3668-3523; Email: radek.marek@ceitec.muni.cz

Authors

Jan Vícha − *Centre of Polymer Systems, Tomas Bata University in Zlín, CZ-76001 Zlín, Czechia;* orcid.org/0000-0003-3698-8236

Jan Novotný − *CEITEC - Central European Institute of Technology, Masaryk University, CZ-62500 Brno, Czechia;* orcid.org/0000-0002-1203-9549

Stanislav Komorovsky − *Institute of Inorganic Chemistry, Slovak Academy of Sciences, SK-84536 Bratislava, Slovakia;* orcid.org/0000-0002-5317-7200

Complete contact information is available at: https://pubs.acs.org/10.1021/acs.chemrev.9b00785

Notes

The authors declare no competing financial interest.

Biographies

Jan Vícha studied inorganic chemistry at the Masaryk University in Brno and received his Ph.D. in biochemistry under the supervision of Radek Marek in 2014. After a postdoctoral stay at the Central European Institute of Technology, Brno, he moved to Tomas Bata University in Zlín, where he obtained a position as a Senior Researcher in 2017. His research interests focus on the chemistry of heavy-element complexes with anticancer activity and on better understanding the relationship between the electronic structure and relativistic effects in NMR spectroscopy.

Jan Novotný studied biomolecular chemistry at the Masaryk University in Brno. He obtained his Ph.D. with Radek Marek in 2015. As a postdoc in the group of Radek Marek, he received the Petr Sedmera Award in NMR spectroscopy in 2018. He is currently teaching NMR spectroscopy, biophysical chemistry, and computational quantum chemistry at the Masaryk University. His main research interests include NMR spectroscopy, paramagnetic and relativistic effects in NMR, structure and spectroscopic properties of transition-metal complexes, supramolecules, and noncanonical forms of nucleic acids.

Stanislav Komorovsky studied theoretical physics at the Comenius University in Bratislava. He received his Ph.D. in chemical physics at the Comenius University with Vladimír Malkin in 2009. After postdocs in Toulouse with Trond Saue and in Tromsø with Kenneth Ruud, he was awarded a Marie Curie Fellowship at the Slovak Academy of Sciences. His research focuses on the development of relativistic methods for the calculation of spectroscopic properties with stress on the magnetic properties of open-shell systems. He is one of the main authors of the ReSpect program (respectprogram.org), a computer simulation package dedicated to predicting and understanding molecular properties obtained by first-principle relativistic DFT calculations.

Michal Straka received his M.Sc. in physical chemistry at the Comenius University in Bratislava in 1996 and his Ph.D. with Pekka Pyykkö at the University of Helsinki in 2001. After a postdoc with Martin Kaupp at the University of Würzburg and a Marie Curie Fellowship with Juha Vaara at the University of Helsinki, he moved to Prague, where he became a senior researcher at the Czech Academy of Sciences. He enjoys solving theoretical problems on the border of inorganic, physical, and organic chemistry. His research interests include theoretical spectroscopy, chemical bonding, heavy-atom compounds, relativistic effects, and endohedral fullerenes.

Martin Kaupp studied chemistry at universities in Stuttgart and Cincinnati. He obtained his Ph.D. at Universität Erlangen-Nürnberg with Paul v. R. Schleyer. After postdocs in Stuttgart with Hans-Georg von Schnering and in Montreal with Dennis Salahub, he completed his Habilitation in Stuttgart before starting his first professorship at Universität Würzburg in 1999, teaching inorganic and theoretical chemistry. Since 2010, he has led the quantum chemistry unit at Technische Universität Berlin, and since 2017 he has been the deputy director of the institute of chemistry at TU. His awards include the Heinz-Maier-Leibnitz-Preis 1994, the DFG Heisenberg and FCI Docent Scholarships in 1998, as well as the Dirac medal of WATOC (2001). The research interests of M.K. cover a wide range of topics in computational and theoretical chemistry, including method development in magnetic-resonance parameter computations, relativistic quantum chemistry and new density functionals, and various applications in catalysis, materials research, fundamental questions of chemical bonding, and different kinds of spectroscopies.

Radek Marek is a Professor of Chemistry at the Masaryk University in Brno. During his chemistry studies, he spent several months with Roger Dommisse at the University of Antwerp and obtained his Ph.D. with Milan Potáček in 1995. After a postdoc in NMR spectroscopy with Vladimír Sklenář he completed his Habilitation in 2004 before starting his professorship at the Masaryk University in 2011, teaching NMR spectroscopy and structural and computational chemistry. He received the Prix de Chimie (Jean-Marie Lehn Prize) for the best PhD thesis in chemistry (1996), the Alfred Bader Prize (Sigma-Aldrich Comp.) for the top young researcher in bioorganic chemistry (2002), and the Petr Sedmera Award in NMR spectroscopy (2018). The main research areas of R.M.'s group at the Central European Institute of Technology (CEITEC) and Faculty of Science, MU are NMR spectroscopy, paramagnetic and relativistic effects in NMR, fundamental aspects of chemical bonding, DFT applied to bonding and molecular properties, supramolecular structure and interactions, host−guest chemistry, and anticancer metallodrugs.

ACKNOWLEDGMENTS

This work has received support from the Czech Science Foundation (Grant No. 18-05421S); the Ministry of Education, Youth, and Sports of the Czech Republic (Grant Nos. LQ1601, LO1504, and LTAUSA19148); the Grant Agency of the Masaryk University (Grant No. MUNI/E/1335/2019); and the Slovak Grant Agencies VEGA and APVV (Contract Nos. 2/0116/17 and APVV-15-0726). Work in Berlin has benefitted from funding by the Deutsche Forschungsgemeinschaft (DFG, German Research Foundation) under Germany's Excellence Strategy, EXC 2008/1-390540038, and by the DFG collaborative research center CRC1349 ("Fluoro-specific interactions",

Project 387284271). Computational resources were provided by the CESNET (Grant No. LM2015042), the CERIT Scientific Cloud (Grant No. LM2015085), and the IT4Innovations National Supercomputing Center (Grant No. LM2015070).

TABLE OF ABBREVIATIONS

1c	one-component
2c	two-component
4c	four-component
A2C	approximate two-component
AO	atomic orbital/occupied atomic orbital
AO*	vacant atomic orbital
BP	Breit-Pauli
BPPT	Breit-Pauli perturbation theory
CASSCF	complete active space self-consistent field
CCSD(T)	coupled-cluster with single and double and perturbative triple excitations
CCSDT	coupled-cluster with single, double, and triple excitations
CGO	common gauge origin
DFT	density-functional theory
DHK	Douglas−Kroll−Hess
DI	delocalization index
ECP	effective core potential
EDA	energy decomposition analysis
EPR	electron paramagnetic resonance
FC	Fermi-contact
GIAO	gauge-including atomic orbitals
HA	heavy atom
HAHA	heavy-atom on the heavy-atom effect
HALA	heavy-atom on the light-atom effect
HB	hydrogen bond
HF	Hartree−Fock
HOMO	highest occupied molecular orbital
IHD	inverse halogen dependence
KS	Kohn−Sham
LA	light atom
LP	lone electron pair
LUMO	lowest unoccupied molecular orbital
Me	methyl
MF	magnetic field (external, B_0)
MO	molecular orbital/occupied molecular orbital
MO*	vacant molecular orbital
MS	molecular spinor
MSP	molecular spinor pair
NBO	natural bonding orbital
Ng	noble gas
NHC	*N*-heterocyclic carbene
NHD	normal halogen dependence
NMR	nuclear magnetic resonance
NOCV	natural orbitals for chemical valence
NR	non-relativistic
Ph	phenyl
PSO	paramagnetic spin−orbit
PT1	first-order perturbation theory
PT2	second-order perturbation-theory
PT3	third-order perturbation-theory
PTE	Periodic Table of Elements
Py	pyridine
QTAIM	quantum theory of atoms in molecules
RHS	right-hand-side
SD	spin-dipolar
SFR	spin-free relativity
SHE	super-heavy elements
SO	spin−orbit
SO/FC	spin−orbit/Fermi-contact term
SO/FC$^{\nabla}$	spin−orbit/Fermi-contact term involving one MO and two MO*s
SO/FC$^{\Delta}$	spin−orbit/Fermi-contact term involving two MOs and one MO*
SOC	spin−orbit coupling
SO-EDD	spin−orbit induced electron deformation density
SO-HALA	spin−orbit heavy-atom effect on the light-atom (NMR shift)
SOM-ISD	spin−orbit-and-magnetically induced spin density
SR	scalar relativity/scalar relativistic
TL	trans-ligand
TLI	trans-ligand influence
X2C	exact two-component
XB	halogen bond
Z	atomic number
ZORA	zeroth-order regular approximation

REFERENCES

(1) Pyykkö, P.; Görling, A.; Rösch, N. A Transparent Interpretation of the Relativistic Contribution to the N.M.R. 'Heavy Atom Chemical Shift.'. *Mol. Phys.* **1987**, *61*, 195−205.
(2) Edlund, U.; Lejon, T.; Pyykkö, P.; Venkatachalam, T. K.; Buncel, E. ^{7}Li, ^{29}Si, ^{119}Sn, and ^{207}Pb NMR Studies of Phenyl-Substituted Group 4 Anions. *J. Am. Chem. Soc.* **1987**, *109*, 5982−5985.
(3) Kaupp, M. Relativistic Effects on NMR Chemical Shifts. In *Theoretical and Computational Chemistry*; Schwerdtfeger, P., Ed.; Elsevier: Amsterdam, 2004; Vol. *14*, pp 552−597.
(4) Truflandier, L. A.; Sutter, K.; Autschbach, J. Solvent Effects and Dynamic Averaging of Pt-195 NMR Shielding in Cisplatin Derivatives. *Inorg. Chem.* **2011**, *50*, 1723−1732.
(5) Autschbach, J.; Ziegler, T. Relativistic Computation of NMR Shielding and Spin-Spin Coupling Constants. In *Encyclopedia of Nuclear Magnetic Resonance*; John Wiley and Sons: Chichester, U.K., 2002; Vol. *9*, pp 306−323.
(6) Fukui, H.; Baba, T.; Inomata, H. Calculation of Nuclear Magnetic Shieldings. X. Relativistic Effects. *J. Chem. Phys.* **1996**, *105*, 3175−3186.
(7) Fukui, H.; Baba, T.; Inomata, H. Erratum: Calculation of Nuclear Magnetic Shieldings. X. Relativistic Effects [J. Chem. Phys. 105, 3175 (1996)]. *J. Chem. Phys.* **1997**, *106*, 2987−2987.
(8) Visscher, L.; Enevoldsen, T.; Saue, T.; Jensen, H. J. A.; Oddershede, J. Full Four-Component Relativistic Calculations of NMR Shielding and Indirect Spin-Spin Coupling Tensors in Hydrogen Halides. *J. Comput. Chem.* **1999**, *20*, 1262−1273.
(9) Schreckenbach, G.; Wolff, S. K.; Ziegler, T. NMR Shielding Calculations across the Periodic Table: Diamagnetic Uranium Compounds. 1. Methods and Issues. *J. Phys. Chem. A* **2000**, *104*, 8244−8255.
(10) Schreckenbach, G. NMR Shielding Calculations across the Periodic Table: Diamagnetic Uranium Compounds. 2. Ligand and Metal NMR. *Inorg. Chem.* **2002**, *41*, 6560−6572.
(11) Melo, J. I.; Ruiz de Azua, M. C.; Giribet, C. G.; Aucar, G. A.; Romero, R. H. Relativistic Effects on the Nuclear Magnetic Shielding Tensor. *J. Chem. Phys.* **2003**, *118*, 471−486.
(12) Gómez, S. S.; Romero, R. H.; Aucar, G. A. Relativistic Mass-Corrections to the Heavy Atom Nuclear Magnetic Shieldings. Analysis of Contributions in Terms of Localized Orbitals. *Chem. Phys. Lett.* **2003**, *367*, 265−269.
(13) Kaupp, M. Interpretation of NMR Chemical Shifts. In *Calculation of NMR and EPR Parameters: Theory and Applications*; Kaupp, M., Buhl, M., Malkin, V. G., Eds.; Wiley: Weinheim, 2004; pp 293−306.
(14) Lantto, P.; Romero, R. H.; Gómez, S. S.; Aucar, G. A.; Vaara, J. Relativistic Heavy-Atom Effects on Heavy-Atom Nuclear Shieldings. *J. Chem. Phys.* **2006**, *125*, 184113−184114.

https://dx.doi.org/10.1021/acs.chemrev.9b00785
Chem. Rev. 2020, 120, 7065−7103

(15) Autschbach, J.; Zheng, S. *Relativistic Computations of NMR Parameters from First Principles: Theory and Applications*; Webb, G. A., Ed.; *Annu. Rep. NMR Spectrosc.*; 2009; Vol. *67*.
(16) Autschbach, J. Relativistic Effects on NMR Parameters. In High Resolution NMR Spectroscopy: Understanding Molecules and Their Electronic Structures; *Science and Technology of Atomic Molecular Condensed Matter and Biological Systems*; Contreras, R. H., Ed.; Elsevier: Amsterdam, 2013; pp 69−117.
(17) Vaara, J. Theory and Computation of Nuclear Magnetic Resonance Parameters. *Phys. Chem. Chem. Phys.* **2007**, *9*, 5399−5418.
(18) Autschbach, J. Density Functional Theory Applied to Calculating Optical and Spectroscopic Properties of Metal Complexes: NMR and Optical Activity. *Coord. Chem. Rev.* **2007**, *251*, 1796−1821.
(19) Nomura, Y.; Takeuchi, Y.; Nakagawa, N. Substituent Effects in Aromatic Proton Nmr Spectra. III Substituent Effects Caused by Halogens. *Tetrahedron Lett.* **1969**, *10*, 639−642.
(20) Nakagawa, N.; Sinada, S.; Obinata, S. *6th NMR Symp.*, Kyoto, 1967, 8−12.
(21) Kaupp, M.; Köhler, F. H. Combining NMR Spectroscopy and Quantum Chemistry as Tools to Quantify Spin Density Distributions in Molecular Magnetic Compounds. *Coord. Chem. Rev.* **2009**, *253*, 2376−2386.
(22) Vaara, J. Chemical Shift in Paramagnetic Systems. In *High resolution NMR spectroscopy: understanding molecules and their electronic structures*; Contreras, R. H., Ed.; Elsevier: Amsterdam, 2013; pp 41−67.
(23) Pell, A. J.; Pintacuda, G.; Grey, C. P. Paramagnetic NMR in Solution and the Solid State. *Prog. Nucl. Magn. Reson. Spectrosc.* **2019**, *111*, 1−271.
(24) Bleaney, B. Nuclear Magnetic Resonance Shifts in Solution Due to Lanthanide Ions. *J. Magn. Reson.* **1972**, *8*, 91−100.
(25) Golding, R. M.; Pyykkö, P. On the Theory of Pseudocontact N.M.R. Shifts Due to Lanthanide Complexes. *Mol. Phys.* **1973**, *26*, 1389−1396.
(26) Kaupp, M.; Malkina, O. L.; Malkin, V. G.; Pyykkö, P. How Do Spin-Orbit-Induced Heavy-Atom Effects on NMR Chemical Shifts Function? Validation of a Simple Analogy to Spin-Spin Coupling by Density Functional Theory (DFT) Calculations on Some Iodo Compounds. *Chem. - Eur. J.* **1998**, *4*, 118−126.
(27) Ejchart, A.; Gryff-Keller, A. On the Spin−Spin Coupling Constants of Trimethylsilylated Iodoacetylene. *Chem. - Eur. J.* **1998**, *4*, 2072−2072.
(28) Morishima, I.; Endo, K.; Yonezawa, T. Effect of the Heavy Atom on the Nuclear Shielding Constant. I. The Proton Chemical Shifts in Hydrogen Halides. *J. Chem. Phys.* **1973**, *59*, 3356−3364.
(29) Volodicheva, M.; Rebane, T. Effect of Spin-Orbit Coupling on Magnetic Shielding of Proton in Hydrogen Halides. *Theor. Exp. Chem.* **1979**, *14*, 348−354.
(30) Cheremisin, A. A.; Schastnev, P. V. Effects of Spin-Orbital Interactions on ^{13}C NMR Chemical Shifts in Halogen-Substituted Methanes. *J. Magn. Reson.* **1980**, *40*, 459−468.
(31) Schastnev, P. V.; Cheremisin, A. A. Quantum-Chemical Calculation of NMR Chemical Shifts. *J. Struct. Chem.* **1982**, *23*, 440−472.
(32) Tripathi, G. S.; Misra, C. M.; Misra, P. K. Relativistic Effects on the Chemical Shift in Solids: Important Points of a New Contribution. *J. Phys. C: Solid State Phys.* **1985**, *18*, L935−L939.
(33) Pyykkö, P. On the Relativistic Theory of NMR Chemical Shifts. *Chem. Phys.* **1983**, *74*, 1−7.
(34) Pyper, N. C. The Relativistic Theory of the Chemical Shift. *Chem. Phys. Lett.* **1983**, *96*, 204−210.
(35) Zhang, Z. C.; Webb, G. A. On the Relativistic Molecular Orbital Theory of Diamagnetism and NMR Chemical Shifts. *J. Mol. Struct.: THEOCHEM* **1983**, *104*, 439−444.
(36) Kaupp, M.; Malkin, V. G.; Malkina, O. L.; Salahub, D. R. Scalar Relativistic Effects on ^{17}O NMR Chemical Shifts in Transition-Metal Oxo Complexes. An Ab Initio ECP/DFT Study. *J. Am. Chem. Soc.* **1995**, *117*, 1851−1852.
(37) Kaupp, M.; Malkina, O. L.; Malkin, V. G. The Calculation of ^{17}O Chemical Shielding in Transition Metal Oxo Complexes. I. Comparison of DFT and Ab Initio Approaches, and Mechanisms of Relativity-Induced Shielding. *J. Chem. Phys.* **1997**, *106*, 9201−9212.
(38) Kaupp, M.; Malkina, O. L. Density Functional Analysis of C-13 and H-1 Chemical Shifts and Bonding in Mercurimethanes and Organomercury Hydrides: The Role of Scalar Relativistic, Spin-Orbit, and Substituent Effects. *J. Chem. Phys.* **1998**, *108*, 3648−3659.
(39) Vaara, J.; Malkina, O. L.; Stoll, H.; Malkin, V. G.; Kaupp, M. Study of Relativistic Effects on Nuclear Shieldings Using Density-Functional Theory and Spin-Orbit Pseudopotentials. *J. Chem. Phys.* **2001**, *114*, 61−71.
(40) Bühl, M.; Kaupp, M.; Malkina, O. L.; Malkin, V. G. The DFT Route to NMR Chemical Shifts. *J. Comput. Chem.* **1999**, *20*, 91−105.
(41) Straka, M.; Kaupp, M. Calculation of F-19 NMR Chemical Shifts in Uranium Complexes Using Density Functional Theory and Pseudopotentials. *Chem. Phys.* **2005**, *311*, 45−56.
(42) Moncho, S.; Autschbach, J. Molecular Orbital Analysis of the Inverse Halogen Dependence of Nuclear Magnetic Shielding in LaX_3, X = F, Cl, Br, I. *Magn. Reson. Chem.* **2010**, *48*, S76−S85.
(43) Kaupp, M.; Malkin, O. L.; Malkin, V. G. Interpretation of ^{13}C NMR Chemical Shifts in Halomethyl Cations. On the Importance of Spin-Orbit Coupling and Electron Correlation. *Chem. Phys. Lett.* **1997**, *265*, 55−59.
(44) Kutzelnigg, W. Chemical Bonding in Higher Main Group Elements. *Angew. Chem., Int. Ed. Engl.* **1984**, *23*, 272−295.
(45) Kutzelnigg, W. Orthogonal and Non-Orthogonal Hybrids. *J. Mol. Struct.: THEOCHEM* **1988**, *169*, 403−419.
(46) Kaupp, M. The Role of Radial Nodes of Atomic Orbitals for Chemical Bonding and the Periodic Table. *J. Comput. Chem.* **2007**, *28*, 320−325.
(47) Minaev, B.; Vaara, J.; Ruud, K.; Vahtras, O.; Ågren, H. Internuclear Distance Dependence of the Spin-Orbit Coupling Contributions to Proton NMR Chemical Shifts. *Chem. Phys. Lett.* **1998**, *295*, 455−461.
(48) Cromp, B.; Carrington, T., Jr.; Salahub, D. R.; Malkina, O. L.; Malkin, V. G. Effect of Rotation and Vibration on Nuclear Magnetic Resonance Chemical Shifts: Density Functional Theory Calculations. *J. Chem. Phys.* **1999**, *110*, 7153−7159.
(49) Kaupp, M.; Malkina, O. L.; Malkin, V. G. The Role of π-Type Nonbonding Orbitals for Spin−Orbit Induced NMR Chemical Shifts: DFT Study of ^{13}C and ^{19}F Shifts in the Series CF_3IF_n (n = 0, 2, 4, 6). *J. Comput. Chem.* **1999**, *20*, 1304−1313.
(50) Gomez, S. S.; Romero, R. H.; Aucar, G. A. Fully Relativistic Calculation of Nuclear Magnetic Shieldings and Indirect Nuclear Spin-Spin Couplings in Group-15 and −16 Hydrides. *J. Chem. Phys.* **2002**, *117*, 7942−7946.
(51) Rusakov, Yu. Yu.; Rusakova, I. L.; Krivdin, L. B. On the HALA Effect in the NMR Carbon Shielding Constants of the Compounds Containing Heavy P-Elements. *Int. J. Quantum Chem.* **2016**, *116*, 1404−1412.
(52) Rusakova, I. L.; Krivdin, L. B. Relativistic Effects in the NMR Spectra of Compounds Containing Heavy Chalcogens. *Mendeleev Commun.* **2018**, *28*, 1−13.
(53) Ehlers, A. W.; RuizMorales, Y.; Baerends, E. J.; Ziegler, T. Dissociation Energies, Vibrational Frequencies, and C-13 NMR Chemical Shifts of the 18-Electron Species $M(CO)_6$ (M = Hf-Ir, Mo, Tc, Ru, Cr, Mn, Fe). A Density Functional Study. *Inorg. Chem.* **1997**, *36*, 5031−5036.
(54) Wolff, S. K.; Ziegler, T. Calculation of DFT-GIAO NMR Shifts with the Inclusion of Spin-Orbit Coupling. *J. Chem. Phys.* **1998**, *109*, 895−905.
(55) Uhl, W.; Jantschak, A.; Saak, W.; Kaupp, M.; Wartchow, R. Systematic Experimental and Quantum Chemical Investigation into the Structures, the Stability, and the Spectroscopic Properties of Alkylindium(I) Compounds: Tetrameric $In_4[C(SiMeRR')_3]_4$ versus Monomeric $InC(SiMeRR')_3$ Derivatives. *Organometallics* **1998**, *17*, 5009−5017.
(56) Manninen, P.; Lantto, P.; Vaara, J.; Ruud, K. Perturbational Ab Initio Calculations of Relativistic Contributions to Nuclear Magnetic Resonance Shielding Tensors. *J. Chem. Phys.* **2003**, *119*, 2623−2637.

https://dx.doi.org/10.1021/acs.chemrev.9b00785
Chem. Rev. 2020, 120, 7065−7103

(57) Manninen, P.; Ruud, K.; Lantto, P.; Vaara, J. Leading-Order Relativistic Effects on Nuclear Magnetic Resonance Shielding Tensors. *J. Chem. Phys.* **2005**, *122*, 114107−114108.
(58) Pyykkö, P.; Desclaux, J. P. Relativity and the Periodic System of Elements. *Acc. Chem. Res.* **1979**, *12*, 276−281.
(59) Pyykkö, P. Relativistic Effects in Structural Chemistry. *Chem. Rev.* **1988**, *88*, 563−594.
(60) Nakatsuji, H.; Hada, M.; Kaneko, H.; Ballard, C. C. Relativistic Study of Nuclear Magnetic Shielding Constants: Mercury Dihalides. *Chem. Phys. Lett.* **1996**, *255*, 195−202.
(61) Kaneko, H.; Hada, M.; Nakajima, T.; Nakatsuji, H. Spin-Orbit Effect on the Magnetic Shielding Constant Using the Ab Initio UHF Method: Tin Tetrahalides. *Chem. Phys. Lett.* **1996**, *261*, 1−6.
(62) Wan, J.; Fukuda, R.; Hada, M.; Nakatsuji, H. Quasi-Relativistic Study of ^{199}Hg Nuclear Magnetic Shielding Constants of Dimethylmercury, Disilylmercury and Digermylmercury. *J. Phys. Chem. A* **2001**, *105*, 128−133.
(63) Wolff, S. K.; Ziegler, T.; van Lenthe, E.; Baerends, E. J. Density Functional Calculations of Nuclear Magnetic Shieldings Using the Zeroth-Order Regular Approximation (ZORA) for Relativistic Effects: ZORA Nuclear Magnetic Resonance. *J. Chem. Phys.* **1999**, *110*, 7689−7698.
(64) Makulski, W.; Jackowski, K.; Antušek, A.; Jaszuński, M. Gas-Phase NMR Measurements, Absolute Shielding Scales, and Magnetic Dipole Moments of ^{29}Si and ^{73}Ge Nuclei. *J. Phys. Chem. A* **2006**, *110*, 11462−11466.
(65) Lantto, P.; Jackowski, K.; Makulski, W.; Olejniczak, M.; Jaszunski, M. NMR Shielding Constants in PH3, Absolute Shielding Scale, and the Nuclear Magnetic Moment of P-31. *J. Phys. Chem. A* **2011**, *115*, 10617−10623.
(66) Malkin, E.; Komorovsky, S.; Repisky, M.; Demissie, T. B.; Ruud, K. The Absolute Shielding Constants of Heavy Nuclei: Resolving the Enigma of The ^{119}Sn Absolute Shielding. *J. Phys. Chem. Lett.* **2013**, *4*, 459−463.
(67) Demissie, T. B.; Jaszunski, M.; Komorovsky, S.; Repisky, M.; Ruud, K. Absolute NMR Shielding Scales and Nuclear Spin-Rotation Constants in (LuX)-Lu-175 and (AuX)-Au-197 (X = F-19, Cl-35, Br-79 and I-127). *J. Chem. Phys.* **2015**, *143*, 164311.
(68) Adrjan, B.; Makulski, W.; Jackowski, K.; Demissie, T. B.; Ruud, K.; Antusek, A.; Jaszunski, M. NMR Absolute Shielding Scale and Nuclear Magnetic Dipole Moment of Pb-207. *Phys. Chem. Chem. Phys.* **2016**, *18*, 16483−16490.
(69) Aucar, G. A.; Aucar, I. A. Recent Developments in Absolute Shielding Scales for NMR Spectroscopy. In *Annu. Rep. NMR Spectrosc.*; Webb, G. A., Ed.; Academic Press: New York, 2019; Vol. *96*, pp 77−141.
(70) Pyykkö, P. The Physics behind Chemistry and the Periodic Table. *Chem. Rev.* **2012**, *112*, 371−384.
(71) Kozioł, K.; Aucar, I. A.; Aucar, G. A. Relativistic and QED Effects on NMR Magnetic Shielding Constant of Neutral and Ionized Atoms and Diatomic Molecules. *J. Chem. Phys.* **2019**, *150*, 184301−184302.
(72) Flygare, W. H.; Goodisman, J. Calculation of Diamagnetic Shielding in Molecules. *J. Chem. Phys.* **1968**, *49*, 3122−3125.
(73) Komorovsky, S.; Repisky, M.; Malkina, O. L.; Malkin, V. G. Fully Relativistic Calculations of NMR Shielding Tensors Using Restricted Magnetically Balanced Basis and Gauge Including Atomic Orbitals. *J. Chem. Phys.* **2010**, *132*, 154101−154102.
(74) London, F. Théorie quantique des courants interatomiques dans les combinaisons aromatiques. *J. Phys. Radium* **1937**, *8*, 397−409.
(75) Ditchfield, R. Theoretical Studies of Magnetic Shielding in H_2O and $(H_2O)_2$. *J. Chem. Phys.* **1976**, *65*, 3123−3133.
(76) Schreckenbach, G.; Ziegler, T. Calculation of NMR Shielding Tensors Using Gauge-Including Atomic Orbitals and Modern Density Functional Theory. *J. Phys. Chem.* **1995**, *99*, 606−611.
(77) RuizMorales, Y.; Schreckenbach, G.; Ziegler, T. Origin of the Hydridic H-1 NMR Chemical Shift in Low-Valent Transition-Metal Hydrides. *Organometallics* **1996**, *15*, 3920−3923.
(78) Ramsey, N. F. Magnetic Shielding of Nuclei in Molecules. *Phys. Rev.* **1950**, *78*, 699−703.
(79) Malkina, O. L.; Komorovský, S.; Visscher, L.; Malkin, V. G. Note: Counterintuitive Gauge-Dependence of Nuclear Magnetic Resonance Shieldings for Rare-Gas Dimers: Does a Natural Gauge-Origin for Spherical Atoms Exist? *J. Chem. Phys.* **2011**, *134*, 086101−086102.
(80) Solum, M. S.; Altmann, K. L.; Strohmeier, M.; Berges, D. A.; Zhang, Y.; Facelli, J. C.; Pugmire, R. J.; Grant, D. M. ^{15}N Chemical Shift Principal Values in Nitrogen Heterocycles. *J. Am. Chem. Soc.* **1997**, *119*, 9804−9809.
(81) *Calculation of NMR and EPR Parameters: Theory and Applications*, 1st ed.; Kaupp, M., Bühl, M., Malkin, V. G., Eds.; Wiley: Weinheim, Germany, 2004.
(82) Cramer, C. J. Introduction to Relativistic Quantum Chemistry. *Theor. Chem. Acc.* **2008**, *119*, 523−524.
(83) Reiher, M.; Wolf, A. *Relativistic Quantum Chemistry: The Fundamental Theory of Molecular Science*; Wiley-VCH Verlag GmbH: Weinheim, Germany, 2014.
(84) Repisky, M.; Komorovsky, S.; Bast, R.; Ruud, K. Relativistic Calculations of Nuclear Magnetic Resonance Parameters. In *New Developments in NMR*; Jackowski, K., Jaszunski, M., Eds.; Royal Society of Chemistry: Cambridge, U.K., 2016; pp 267−303.
(85) Autschbach, J. Relativistic Calculations of Magnetic Resonance Parameters: Background and Some Recent Developments. *Philos. Trans. R. Soc., A* **2014**, *372*, 20120489−20120490.
(86) Dyall, K. G.; Faegri, K. *Introduction to Relativistic Quantum Chemistry*; Oxford University Press: New York, 2007.
(87) Xiao, Y.; Liu, W.; Cheng, L.; Peng, D. Four-Component Relativistic Theory for Nuclear Magnetic Shielding Constants: Critical Assessments of Different Approaches. *J. Chem. Phys.* **2007**, *126*, 214101−214102.
(88) Cheng, L.; Xiao, Y.; Liu, W. Four-Component Relativistic Theory for Nuclear Magnetic Shielding: Magnetically Balanced Gauge-Including Atomic Orbitals. *J. Chem. Phys.* **2009**, *131*, 244113−244114.
(89) Olejniczak, M.; Bast, R.; Saue, T.; Pecul, M. A Simple Scheme for Magnetic Balance in Four-Component Relativistic Kohn-Sham Calculations of Nuclear Magnetic Resonance Shielding Constants in a Gaussian Basis. *J. Chem. Phys.* **2012**, *136*, 014108−014109.
(90) Gohr, S.; Hrobárik, P.; Repiský, M.; Komorovský, S.; Ruud, K.; Kaupp, M. Four-Component Relativistic Density Functional Theory Calculations of EPR g- and Hyperfine-Coupling Tensors Using Hybrid Functionals: Validation on Transition-Metal Complexes with Large Tensor Anisotropies and Higher-Order Spin−Orbit Effects. *J. Phys. Chem. A* **2015**, *119*, 12892−12905.
(91) Vícha, J.; Marek, R.; Straka, M. High-Frequency ^{1}H NMR Chemical Shifts of Sn^{II} and Pb^{II} Hydrides Induced by Relativistic Effects: Quest for Pb^{II} Hydrides. *Inorg. Chem.* **2016**, *55*, 10302−10309.
(92) Demissie, T. B. Relativistic Effects on the NMR Parameters of Si, Ge, Sn, and Pb Alkynyl Compounds: Scalar versus Spin-Orbit Effects. *J. Chem. Phys.* **2017**, *147*, 174301−174302.
(93) Repisky, M.; Komorovsky, S.; Kadek, M.; Konecny, L.; Ekstrom, U.; Malkin, E.; Kaupp, M.; Ruud, K.; Malkina, O. L.; Malkin, V. G. ReSpect: Relativistic Spectroscopy DFT Program Package. *J. Chem. Phys.* **2020**, *152*, 184101.
(94) Casella, G.; Bagno, A.; Komorovsky, S.; Repisky, M.; Saielli, G. Four-Component Relativistic DFT Calculations of ^{13}C Chemical Shifts of Halogenated Natural Substances. *Chem. - Eur. J.* **2015**, *21*, 18834−18840.
(95) Hrobárik, P.; Hrobáriková, V.; Meier, F.; Repisky, M.; Komorovsky, S.; Kaupp, M. Relativistic Four-Component DFT Calculations of H-1 NMR Chemical Shifts in Transition-Metal Hydride Complexes: Unusual High-Field Shifts Beyond the Buckingham-Stephens Model. *J. Phys. Chem. A* **2011**, *115*, 5654−5659.
(96) Vícha, J.; Novotný, J.; Straka, M.; Repisky, M.; Ruud, K.; Komorovsky, S.; Marek, R. Structure, Solvent, and Relativistic Effects on the NMR Chemical Shifts in Square-Planar Transition-Metal Complexes: Assessment of DFT Approaches. *Phys. Chem. Chem. Phys.* **2015**, *17*, 24944−24955.
(97) Greif, A. H.; Hrobárik, P.; Autschbach, J.; Kaupp, M. Giant Spin-Orbit Effects on H-1 and C-13 NMR Shifts for Uranium(VI) Complexes Revisited: Role of the Exchange-Correlation Response

https://dx.doi.org/10.1021/acs.chemrev.9b00785
Chem. Rev. 2020, 120, 7065−7103

Kernel, Bonding Analyses, and New Predictions. *Phys. Chem. Chem. Phys.* **2016**, *18*, 30462−30474.
(98) Sun, Q.; Xiao, Y.; Liu, W. Exact Two-Component Relativistic Theory for NMR Parameters: General Formulation and Pilot Application. *J. Chem. Phys.* **2012**, *137*, 174105−174106.
(99) Novotný, J.; Vícha, J.; Bora, P. L.; Repisky, M.; Straka, M.; Komorovsky, S.; Marek, R. Linking the Character of the Metal-Ligand Bond to the Ligand NMR Shielding in Transition-Metal Complexes: NMR Contributions from Spin-Orbit Coupling. *J. Chem. Theory Comput.* **2017**, *13*, 3586−3601.
(100) Vícha, J.; Komorovsky, S.; Repisky, M.; Marek, R.; Straka, M. Relativistic Spin−Orbit Heavy Atom on the Light Atom NMR Chemical Shifts: General Trends Across the Periodic Table Explained. *J. Chem. Theory Comput.* **2018**, *14*, 3025−3039.
(101) Kramers, H. A. Théorie Générale de La Rotation Paramagnétique Dans Les Cristaux. *Proc. Acad. Amsterdam* **1930**, *33*, 959−972.
(102) Pauli, W. Zur Quantenmechanik Des Magnetischen Elektrons. *Z. Phys.* **1927**, *43*, 601−608.
(103) Baerends, E. J.; Schwarz, W. H. E.; Schwerdtfeger, P.; Snijders, J. G. Relativistic Atomic Orbital Contractions and Expansions: Magnitudes and Explanations. *J. Phys. B: At., Mol. Opt. Phys.* **1990**, *23*, 3225−3240.
(104) Pawlak, T.; Munzarova, M. L.; Pazderski, L.; Marek, R. Validation of Relativistic DFT Approaches to the Calculation of NMR Chemical Shifts in Square-Planar Pt^{2+} and Au^{3+} Complexes. *J. Chem. Theory Comput.* **2011**, *7*, 3909−3923.
(105) Standara, S.; Malinakova, K.; Marek, R.; Marek, J.; Hocek, M.; Vaara, J.; Straka, M. Understanding the NMR Chemical Shifts for 6-Halopurines: Role of Structure, Solvent and Relativistic Effects. *Phys. Chem. Chem. Phys.* **2010**, *12*, 5126−5139.
(106) Vaara, J.; Ruud, K.; Vahtras, O.; Ågren, H.; Jokisaari, J. Quadratic Response Calculations of the Electronic Spin-Orbit Contribution to Nuclear Shielding Tensors. *J. Chem. Phys.* **1998**, *109*, 1212−1222.
(107) Olsen, J.; Jorgensen, P. Linear and Nonlinear Response Functions for an Exact State and for an MCSCF State. *J. Chem. Phys.* **1985**, *82*, 3235−3264.
(108) Berger, R. J. F.; Repisky, M.; Komorovsky, S. How Does Relativity Affect Magnetically Induced Currents? *Chem. Commun.* **2015**, *51*, 13961−13963.
(109) Vícha, J.; Straka, M.; Munzarova, M. L.; Marek, R. Mechanism of Spin-Orbit Effects on the Ligand NMR Chemical Shift in Transition-Metal Complexes: Linking NMR to EPR. *J. Chem. Theory Comput.* **2014**, *10*, 1489−1499.
(110) Bora, P. L.; Novotný, J.; Ruud, K.; Komorovsky, S.; Marek, R. Electron-Spin Structure and Metal−Ligand Bonding in Open-Shell Systems from Relativistic EPR and NMR: A Case Study of Square-Planar Iridium Catalysts. *J. Chem. Theory Comput.* **2019**, *15*, 201−214.
(111) Autschbach, J.; Sutter, K.; Truflandier, L. A.; Brendler, E.; Wagler, J. Atomic Contributions from Spin-Orbit Coupling to ^{29}Si NMR Chemical Shifts in Metallasilatrane Complexes. *Chem. - Eur. J.* **2012**, *18*, 12803−12813.
(112) Hierso, J.-C. Indirect Nonbonded Nuclear Spin−Spin Coupling: A Guide for the Recognition and Understanding of "Through-Space" NMR J Constants in Small Organic, Organometallic, and Coordination Compounds. *Chem. Rev.* **2014**, *114*, 4838−4867.
(113) Hyvarinen, M.; Vaara, J.; Goldammer, A.; Kutzky, B.; Hegetschweiler, K.; Kaupp, M.; Straka, M. Characteristic Spin-Orbit Induced H-1(CH_2) Chemical Shifts upon Deprotonation of Group 9 Polyamine Aqua and Alcohol Complexes. *J. Am. Chem. Soc.* **2009**, *131*, 11909−11918.
(114) Vícha, J.; Foroutan-Nejad, C.; Pawlak, T.; Munzarová, M. L.; Straka, M.; Marek, R. Understanding the Electronic Factors Responsible for Ligand Spin-Orbit NMR Shielding in Transition-Metal Complexes. *J. Chem. Theory Comput.* **2015**, *11*, 1509−1517.
(115) Greif, A. H.; Hrobárik, P.; Hrobáriková, V.; Arbuznikov, A. V.; Autschbach, J.; Kaupp, M. A Relativistic Quantum-Chemical Analysis of the Trans Influence on H-1 NMR Hydride Shifts in Square-Planar Platinum(II) Complexes. *Inorg. Chem.* **2015**, *54*, 7199−7208.
(116) Bickelhaupt, F. M.; Baerends, E. J. Kohn-Sham Density Functional Theory: Predicting and Understanding Chemistry. *Rev. Comput. Chem.* **2007**, *15*, 1−86.
(117) Mitoraj, M. P.; Michalak, A.; Ziegler, T. A Combined Charge and Energy Decomposition Scheme for Bond Analysis. *J. Chem. Theory Comput.* **2009**, *5*, 962−975.
(118) Vícha, J.; Patzschke, M.; Marek, R. A Relativistic DFT Methodology for Calculating the Structures and NMR Chemical Shifts of Octahedral Platinum and Iridium Complexes. *Phys. Chem. Chem. Phys.* **2013**, *15*, 7740−7754.
(119) Greif, A. H.; Hrobárik, P.; Kaupp, M. Insights into Trans-Ligand and Spin-Orbit Effects on Electronic Structure and Ligand NMR Shifts in Transition-Metal Complexes. *Chem. - Eur. J.* **2017**, *23*, 9790−9803.
(120) Rocchigiani, L.; Fernandez-Cestau, J.; Chambrier, I.; Hrobárik, P.; Bochmann, M. Unlocking Structural Diversity in Gold(III) Hydrides: Unexpected Interplay of Cis/ Trans-Influence on Stability, Insertion Chemistry, and NMR Chemical Shifts. *J. Am. Chem. Soc.* **2018**, *140*, 8287−8302.
(121) Denning, R. G. Electronic Structure and Bonding in Actinyl Ions. In *Complexes, Clusters and Crystal Chemistry*; Springer-Verlag: Berlin, 1992; Vol. *79*, pp 215−276.
(122) Lewis, A. J.; Carroll, P. J.; Schelter, E. J. Stable Uranium(VI) Methyl and Acetylide Complexes and the Elucidation of an Inverse Trans Influence Ligand Series. *J. Am. Chem. Soc.* **2013**, *135*, 13185−13192.
(123) O'Grady, E.; Kaltsoyannis, N. On the Inverse Trans Influence. Density Functional Studies of $[MOX_5]^{n-}$ (M = Pa, n = 2; M = U, n = 1; M = Np, n = 0; X = F, Cl or Br). *J. Chem. Soc., Dalton Trans.* **2002**, *6*, 1233−1239.
(124) La Pierre, H. S.; Rosenzweig, M.; Kosog, B.; Hauser, C.; Heinemann, F. W.; Liddle, S. T.; Meyer, K. Charge Control of the Inverse Trans-Influence. *Chem. Commun.* **2015**, *51*, 16671−16674.
(125) Cano, J.; Ruiz, E.; Alvarez, S.; Verdaguer, M. Spin Density Distribution in Transition Metal Complexes: Some Thoughts and Hints. *Comments Inorg. Chem.* **1998**, *20*, 27−56.
(126) Novotný, J.; Sojka, M.; Komorovsky, S.; Nečas, M.; Marek, R. Interpreting the Paramagnetic NMR Spectra of Potential Ru(III) Metallodrugs: Synergy between Experiment and Relativistic DFT Calculations. *J. Am. Chem. Soc.* **2016**, *138*, 8432−8445.
(127) Malkina, O. L.; Malkin, V. G. Visualization of Nuclear Spin−Spin Coupling Pathways by Real-Space Functions. *Angew. Chem., Int. Ed.* **2003**, *42*, 4335−4338.
(128) Marek, R.; Křístková, A.; Maliňáková, K.; Toušek, J.; Marek, J.; Hocek, M.; Malkina, O. L.; Malkin, V. G. Interpretation of Indirect Nuclear Spin−Spin Couplings in Isomers of Adenine: Novel Approach to Analyze Coupling Electron Deformation Density Using Localized Molecular Orbitals. *J. Phys. Chem. A* **2010**, *114*, 6689−6700.
(129) Malkin, V. G.; Malkina, O. L.; Zhidomirov, G. M. Visualization of Electron Paramagnetic Resonance Hyperfine Structure Coupling Pathways. *J. Phys. Chem. A* **2017**, *121*, 3580−3587.
(130) Wodynski, A.; Gryff-Keller, A.; Pecul, M. The Influence of a Presence of a Heavy Atom on C-13 Shielding Constants in Organomercury Compounds and Halogen Derivatives. *J. Chem. Theory Comput.* **2013**, *9*, 1909−1917.
(131) Bora, P. L.; Novák, M.; Novotný, J.; Foroutan-Nejad, C.; Marek, R. Supramolecular Covalence in Bifurcated Chalcogen Bonding. *Chem. - Eur. J.* **2017**, *23*, 7315−7323.
(132) Vícha, J.; Marek, R.; Straka, M. High-Frequency ^{13}C and ^{29}Si NMR Chemical Shifts in Diamagnetic Low-Valence Compounds of Tl^{I} and Pb^{II}: Decisive Role of Relativistic Effects. *Inorg. Chem.* **2016**, *55*, 1770−1781.
(133) van Lenthe, E.; Snijders, J. G.; Baerends, E. J. The Zero-order Regular Approximation for Relativistic Effects: The Effect of Spin−Orbit Coupling in Closed Shell Molecules. *J. Chem. Phys.* **1996**, *105*, 6505−6516.
(134) ADF 2018, SCM, *Theoretical Chemistry*; Vrije Universiteit, Amsterdam, The Netherlands; http://www.scm.com.

https://dx.doi.org/10.1021/acs.chemrev.9b00785
Chem. Rev. 2020, 120, 7065−7103

(135) Kantola, A. M.; Lantto, P.; Vaara, J.; Jokisaari, J. Carbon and Proton Shielding Tensors in Methyl Halides. *Phys. Chem. Chem. Phys.* **2010**, *12*, 2679−2692.
(136) Cukras, J.; Sadlej, J. Predicted NMR Properties of Noble Gas Hydride Cations RgH$^+$. *Chem. Phys. Lett.* **2008**, *467*, 18−22.
(137) Hrobárik, P.; Hrobáriková, V.; Greif, A. H.; Kaupp, M. Giant Spin-Orbit Effects on NMR Shifts in Diamagnetic Actinide Complexes: Guiding the Search of Uranium(VI) Hydride Complexes in the Correct Spectral Range. *Angew. Chem., Int. Ed.* **2012**, *51*, 10884−10888.
(138) Xue, Z.-L.; Cook, T. M.; Lamb, A. C. Trends in NMR Chemical Shifts of D0transition Metal Compounds. *J. Organomet. Chem.* **2017**, *852*, 74−93.
(139) Alkan, F.; Holmes, S. T.; Dybowski, C. Role of Exact Exchange and Relativistic Approximations in Calculating F-19 Magnetic Shielding in Solids Using a Cluster Ansatz. *J. Chem. Theory Comput.* **2017**, *13*, 4741−4752.
(140) Hegetschweiler, K.; Kuppert, D.; Huppert, J.; Straka, M.; Kaupp, M. Spin-Orbit-Induced Anomalous pH-Dependence in H-1 NMR Spectra of Co-III Amine Complexes: A Diagnostic Tool for Structure Elucidation. *J. Am. Chem. Soc.* **2004**, *126*, 6728−6738.
(141) Gagliardi, L.; Pyykkö, P. Cesium and Barium as Honorary d Elements: CsN_7Ba as an Example. *Theor. Chem. Acc.* **2003**, *110*, 205−210.
(142) Dye, J. L. Compounds of Alkali Metal Anions. *Angew. Chem., Int. Ed. Engl.* **1979**, *18*, 587−598.
(143) Nicol, A. T.; Vaughan, R. W. Proton Chemical Shift Tensors of Alkaline Earth Hydrides. *J. Chem. Phys.* **1978**, *69*, 5211−5213.
(144) Hayashi, K.; Sushko, P. V.; Hashimoto, Y.; Shluger, A. L.; Hosono, H. Hydride Ions in Oxide Hosts Hidden by Hydroxide Ions. *Nat. Commun.* **2014**, *5*, 3515−3523.
(145) Bagno, A.; Saielli, G. Relativistic DFT Calculations of the NMR Properties and Reactivity of Transition Metal Methane Sigma-Complexes: Insights on C-H Bond Activation. *Phys. Chem. Chem. Phys.* **2011**, *13*, 4285−4291.
(146) Demissie, T. B.; Kostenko, N.; Komorovsky, S.; Repisky, M.; Isaksson, J.; Bayer, A.; Ruud, K. Experimental and Four-Component Relativistic DFT Studies of Tungsten Carbonyl Complexes. *J. Phys. Org. Chem.* **2015**, *28*, 723−731.
(147) Pawlak, T.; Niedzielska, D.; Vícha, J.; Marek, R.; Pazderski, L. Dimeric Pd(II) and Pt(II) Chloride Organometallics with 2-Phenylpyridine and Their Solvolysis in Dimethylsulfoxide. *J. Organomet. Chem.* **2014**, *759*, 58−66.
(148) Buckingham, A. D.; Stephens, P. J. 528. Proton Chemical Shifts in the Nuclear Magnetic Resonance Spectra of Transition-Metal Hydrides: Octahedral Complexes. *J. Chem. Soc.* **1964**, 2747−2759.
(149) Buckingham, A. D.; Stephens, P. J. 874. Proton Chemical Shifts in the Nuclear Magnetic Resonance Spectra of Transition-Metal Hydrides: Square-Planar Platinum(II) Complexes. *J. Chem. Soc.* **1964**, 4583−4587.
(150) Bhagan, S.; Wayland, B. B. Formation and Reactivity of a Porphyrin Iridium Hydride in Water: Acid Dissociation Constants and Equilibrium Thermodynamics Relevant to Ir−H, Ir−OH, and Ir−CH_2− Bond Dissociation Energetics. *Inorg. Chem.* **2011**, *50*, 11011−11020.
(151) Florez, E.; Maldonado, A. F.; Aucar, G. A.; David, J.; Restrepo, A. Microsolvation of Methylmercury: Structures, Energies, Bonding and NMR Constants (Hg-199, C-13 and O-17). *Phys. Chem. Chem. Phys.* **2016**, *18*, 1537−1550.
(152) Vícha, J.; Demo, G.; Marek, R. Platinum-Modified Adenines: Unprecedented Protonation Behavior Revealed by NMR Spectroscopy and Relativistic Density-Functional Theory Calculations. *Inorg. Chem.* **2012**, *51*, 1371−1379.
(153) Autschbach, J. The Role of the Exchange-Correlation Response Kernel and Scaling Corrections in Relativistic Density Functional Nuclear Magnetic Shielding Calculations with the Zeroth-Order Regular Approximation. *Mol. Phys.* **2013**, *111*, 2544−2554.
(154) Repisky, M.; Komorovsky, S.; Malkin, V. G.; Malkina, O. L.; Kaupp, M.; Ruud, K.; Bast, R.; Ekstrom, U.; Kadek, M.; Knecht, S.; et al. *Relativistic Spectroscopy DFT Program ReSpect*, Developer Version 4.0.0; www.respectprogram.org.
(155) Gowda, V.; Sarma, B.; Öberg, S.; Telkki, V.-V.; Larsson, A.-C.; Lantto, P.; Antzutkin, O. N. Structure Elucidation of an Yttrium Diethyldithiocarbamato-Phenanthroline Complex by X-Ray Crystallography, Solid-State NMR, and Ab-Initio Quantum Chemical Calculations. *Eur. J. Inorg. Chem.* **2016**, *2016*, 3278−3291.
(156) Halbert, S.; Coperet, C.; Raynaud, C.; Eisenstein, O. Elucidating the Link between NMR Chemical Shifts and Electronic Structure in d^0 Olefin Metathesis Catalysts. *J. Am. Chem. Soc.* **2016**, *138*, 2261−2272.
(157) Haller, L. J. L.; Mas-Marza, E.; Cybulski, M. K.; Sanguramath, R. A.; Macgregor, S. A.; Mahon, M. F.; Raynaud, C.; Russell, C. A.; Whittlesey, M. K. Computation Provides Chemical Insight into the Diverse Hydride NMR Chemical Shifts of $[Ru(NHC)_4(L)H]^{0/+}$ Species (NHC = N-Heterocyclic Carbene; L = Vacant, H_2, N_2, CO, MeCN, O_2, P_4, SO_2, H^- F^- and Cl^-) and Their $[Ru(R_2PCH_2CH_2PR_2)_2(L)H]^+$ Congeners. *DALTON Trans* **2017**, *46*, 2861−2873.
(158) Poblador-Bahamonde, A. I.; Poteau, R.; Raynaud, C.; Eisenstein, O. DFT Calculations of ^{29}Si-NMR Chemical Shifts in Ru(II) Silyl Complexes: Searching for Trends and Accurate Values. *Dalton Trans* **2011**, *40*, 11321−11326.
(159) Garbacz, P.; Terskikh, V. V.; Ferguson, M. J.; Bernard, G. M.; Kedziorek, M.; Wasylishen, R. E. Experimental Characterization of the Hydride ^{1}H Shielding Tensors for $HIrX_2(PR_3)_2$ and $HRhCl_2(PR_3)_2$: Extremely Shielded Hydride Protons with Unusually Large Magnetic Shielding Anisotropies. *J. Phys. Chem. A* **2014**, *118*, 1203−1212.
(160) Metsänen, T. T.; Hrobárik, P.; Klare, H. F. T.; Kaupp, M.; Oestreich, M. Insight into the Mechanism of Carbonyl Hydrosilylation Catalyzed by Brookhart's Cationic Iridium(III) Pincer Complex. *J. Am. Chem. Soc.* **2014**, *136*, 6912−6915.
(161) Stahl, T.; Hrobárik, P.; Königs, C. D. F.; Ohki, Y.; Tatsumi, K.; Kemper, S.; Kaupp, M.; Klare, H. F. T.; Oestreich, M. Mechanism of the Cooperative Si−H Bond Activation at Ru−S Bonds. *Chem. Sci.* **2015**, *6*, 4324−4334.
(162) Chierotti, M. R.; Garlaschelli, L.; Gobetto, R.; Nervi, C.; Peli, G.; Sironi, A.; Della Pergola, R. An Unusual Carbonyl Chemical Shift in a Carbonylhexairidium Cluster: A Combined Solid-State NMR and DFT Approach. *Eur. J. Inorg. Chem.* **2007**, *2007*, 3477−3483.
(163) Maldonado, A. F.; Aucar, G. A.; Melo, J. I. Core-Dependent and Ligand-Dependent Relativistic Corrections to the Nuclear Magnetic Shieldings in MH_4-NY_n (n = 0−4; m = Si, Ge, Sn, and Y = H, F, Cl, Br, I) Model Compounds. *J. Mol. Model.* **2014**, *20*, 2417−2418.
(164) Rusakov, Y. Y.; Rusakova, I. L. Relativistic Heavy Atom Effect On ^{13}C NMR Chemical Shifts Initiated by Adjacent Multiple Chalcogens. *Magn. Reson. Chem.* **2018**, *56*, 716−726.
(165) Truflandier, L. A.; Brendler, E.; Wagler, J.; Autschbach, J. ^{29}Si DFT/NMR Observation of Spin-Orbit Effect in Metallasilatrane Sheds Some Light on the Strength of the Metal→Silicon Interaction. *Angew. Chem., Int. Ed.* **2011**, *50*, 255−259.
(166) Wiegand, T.; Eckert, H.; Grimme, S.; Malberg, J.; Wolf, R. Solid State NMR Studies and Chemical Shift Calculations of a Gold(I) Complex with a Diphosphacyclobutadiene Cobaltate Sandwich Anion. *Solid State Nucl. Magn. Reson.* **2013**, *53*, 13−19.
(167) Sutter, K.; Autschbach, J. Computational Study and Molecular Orbital Analysis of NMR Shielding, Spin-Spin Coupling, and Electric Field Gradients of Azido Platinum Complexes. *J. Am. Chem. Soc.* **2012**, *134*, 13374−13385.
(168) Le Guennic, B.; Neugebauer, J.; Reiher, M.; Autschbach, J. The "Invisible" ^{13}C NMR Chemical Shift of the Central Carbon Atom in $[(Ph_3PAu)_6C]^{2+}$: A Theoretical Investigation. *Chem. - Eur. J.* **2005**, *11*, 1677−1686.
(169) Uhl, W.; Jantschak, A.; Saak, W.; Kaupp, M.; Wartchow, R. Systematic Experimental and Quantum Chemical Investigation into the Structures, the Stability, and the Spectroscopic Properties of Alkylindium(I) Compounds: Tetrameric $In_4[C(SiMeRR')_3]_4$ versus Monomeric $InC(SiMeRR')_3$ Derivatives. *Organometallics* **1998**, *17*, 5009−5017.

https://dx.doi.org/10.1021/acs.chemrev.9b00785
Chem. Rev. 2020, 120, 7065−7103

(170) Jaszuński, M.; Ruud, K. Nuclear Magnetic Resonance Shielding Constants in XH_4 group XIV Hydrides. *Mol. Phys.* **2006**, *104*, 2139−2148.
(171) Schneider, J.; Sindlinger, C. P.; Eichele, K.; Schubert, H.; Wesemann, L. Low-Valent Lead Hydride and Its Extreme Low-Field ^{1}H NMR Chemical Shift. *J. Am. Chem. Soc.* **2017**, *139*, 6542−6545.
(172) Queen, J. D.; Fettinger, J. C.; Power, P. P. Two Quasi-Stable Lead(II) Hydrides at Ambient Temperature. *Chem. Commun.* **2019**, *55*, 10285−10287.
(173) Weiß, S.; Schubert, H.; Wesemann, L. Low Valent Lead Hydride Chemistry: Hydroplumbylation of Phenylacetylene and 1,1-Dimethylallene. *Chem. Commun.* **2019**, *55*, 10238−10240.
(174) Driess, M.; Martin, S.; Merz, K.; Pintchouk, V.; Pritzkow, H.; Grützmacher, H.; Kaupp, M. $Sn_6(PR)_6$], [$Sn_3(Pr)_2$, and [$Cu_{24}(PR)_{12}$] (R = Triorganoisilyl): New Tin and Copper Phosphanediyl Clusters. *Angew. Chem., Int. Ed. Engl.* **1997**, *36*, 1894−1896.
(175) Kawamura, T.; Abe, M.; Saito, M.; Hada, M. Quantum-Chemical Analyses of Aromaticity, UV Spectra, and NMR Chemical Shifts in Plumbacyclopentadienylidenes Stabilized by Lewis Bases. *J. Comput. Chem.* **2014**, *35*, 847−853.
(176) Guthardt, R.; Oetzel, J.; Schweizer, J. I.; Bruhn, C.; Langer, R.; Maurer, M.; Vícha, J.; Shestakova, P.; Holthausen, M. C.; Siemeling, U. Reactive Dimerization of an N-Heterocyclic Plumbylene: C−H Activation with PbII. *Angew. Chem., Int. Ed.* **2019**, *58*, 1387−1391.
(177) Field-Theodore, T. E.; Olejniczak, M.; Jaszuński, M.; Wilson, D. J. D. NMR Shielding Constants in Group 15 Trifluorides. *Phys. Chem. Chem. Phys.* **2018**, *20*, 23025−23033.
(178) Tähtinen, P.; Saielli, G.; Guella, G.; Mancini, I.; Bagno, A. Computational NMR Spectroscopy of Organoarsenicals and the Natural Polyarsenic Compound Arsenicin A. *Chem. - Eur. J.* **2008**, *14*, 10445−10452.
(179) Berger, R. J. F.; Rettenwander, D.; Spirk, S.; Wolf, C.; Patzschke, M.; Ertl, M.; Monkowius, U.; Mitzel, N. W. Relativistic Effects in Triphenylbismuth and Their Influence on Molecular Structure and Spectroscopic Properties. *Phys. Chem. Chem. Phys.* **2012**, *14*, 15520−15524.
(180) Ashe, A. J.; Ludwig, E. G.; Oleksyszyn, J. Preparation and Properties of Dibismuthines. *Organometallics* **1983**, *2*, 1859−1866.
(181) Hardman, N. J.; Twamley, B.; Power, P. P. (2,6-$Mes_2H_3C_6)_2$BiH, a Stable, Molecular Hydride of a Main Group Element of the Sixth Period, and Its Conversion to the Dibismuthene (2,6-$Mes_2H_3C_6$)BiBi(2,6-$Mes_2C_6H_3$). *Angew. Chem., Int. Ed.* **2000**, *39*, 2771−2773.
(182) Rusakov, Y. Y.; Rusakova, I. L.; Krivdin, L. B. Relativistic Heavy Atom Effect on the P-31 NMR Parameters of Phosphine Chalcogenides. Part 1. Chemical Shifts. *Magn. Reson. Chem.* **2018**, *56*, 1061−1073.
(183) Chernyshev, K. A.; Krivdin, L. B.; Fedorov, S. V.; Arbuzova, S. N.; Ivanova, N. I. Quantum Chemical Calculations of NMR Chemical Shifts of Organic Molecules: XI. Conformational and Relativistic Effects on the P-31 and Se-77 Chemical Shifts of Phosphine Selenides. *Russ. J. Org. Chem.* **2013**, *49*, 1420−1427.
(184) Mirzaeva, I. V.; Kozlova, S. G.; Anyushin, A. V. Relativistic Effects in NMR of New Prospective Water-Soluble Ligands SeP-$(CH_2OH)_3$ and H[$Se_2P(CH_2OH)_2$]. *Appl. Magn. Reson.* **2015**, *46*, 1147−1157.
(185) Lantto, P.; Vaara, J.; Kantola, A. M.; Telkki, V.-V.; Schimmelpfennig, B.; Ruud, K.; Jokisaari, J. Relativistic Spin-Orbit Coupling Effects on Secondary Isotope Shifts Of ^{13}C Nuclear Shielding in CX_2 (X = O, S, Se, Te). *J. Am. Chem. Soc.* **2002**, *124*, 2762−2771.
(186) Lantto, P.; Kangasvieri, S.; Vaara, J. Electron Correlation and Relativistic Effects in the Secondary NMR Isotope Shifts of CSe_2. *Phys. Chem. Chem. Phys.* **2013**, *15*, 17468−17478.
(187) Rusakov, Y. Y.; Rusakova, I. L.; Krivdin, L. B. On the Significant Relativistic Heavy Atom Effect on C-13 NMR Chemical Shifts of Beta- and Gamma-Carbons in Seleno- and Telluroketones. *Mol. Phys.* **2017**, *115*, 3117−3127.
(188) Rusakov, Y. Y.; Rusakova, I. L. Long-Range Relativistic Heavy Atom Effect on ^{1}H NMR Chemical Shifts of Selenium- and Tellurium-Containing Compounds. *Int. J. Quantum Chem.* **2019**, *119*, e25809−e25810.
(189) Melo, J. I.; Ruiz de Azua, M. C.; Giribet, C. G.; Aucar, G. A.; Provasi, P. F. Relativistic Effects on Nuclear Magnetic Shielding Constants in HX and CH_3X (X = Br, I) Based on the Linear Response within the Elimination of Small Component Approach. *J. Chem. Phys.* **2004**, *121*, 6798−6808.
(190) Reis, A. K. C. A.; Rittner, R. Substituent Effects in the C-13 NMR Chemical Shifts of Alpha-Mono-Substituted Acetonitriles. *Spectrochim. Acta, Part A* **2007**, *66*, 681−685.
(191) Neto, A. C.; Ducati, L. C.; Rittner, R.; Tormena, C. F.; Contreras, R. H.; Frenking, G. Heavy Halogen Atom Effect on C-13 NMR Chemical Shifts in Monohalo Derivatives of Cyclohexane and Pyran. Experimental and Theoretical Study. *J. Chem. Theory Comput.* **2009**, *5*, 2222−2228.
(192) Radula-Janik, K.; Kupka, T.; Ejsmont, K.; Daszkiewicz, Z.; Sauer, S. P. A. Halogen Effect on Structure and C-13 NMR Chemical Shift of 3,6-Disubstituted-N-Alkyl Carbazoles. *Magn. Reson. Chem.* **2013**, *51*, 630−635.
(193) Macháček, J.; Bühl, M.; Fanfrlík, J.; Hnyk, D. Nuclear Magnetic Shielding of Monoboranes: Calculation and Assessment of ^{11}B NMR Chemical Shifts in Planar BX_3 and in Tetrahedral $[BX_4]^-$Systems. *J. Phys. Chem. A* **2017**, *121*, 9631−9637.
(194) Gomez, S. S.; Aucar, G. A. Relativistic Effects on the Nuclear Magnetic Resonance Shielding of FX (X = F, Cl, Br, I, and At) Molecular Systems. *J. Chem. Phys.* **2011**, *134*, 204314.
(195) Fedorov, S. V.; Rusakov, Y. Y.; Krivdin, L. B. Relativistic Environmental Effects in Si-29 NMR Chemical Shifts of Halosilanes: Light Nucleus, Heavy Environment. *J. Phys. Chem. A* **2015**, *119*, 5778−5789.
(196) Viesser, R. V.; Ducati, L. C.; Autschbach, J.; Tormena, C. F. Effects of Stereoelectronic Interactions on the Relativistic Spin-Orbit and Paramagnetic Components of the C-13 NMR Shielding Tensors of Dihaloethenes. *Phys. Chem. Chem. Phys.* **2015**, *17*, 19315−19324.
(197) Straka, M.; Lantto, P.; Rasanen, M.; Vaara, J. Theoretical Predictions of Nuclear Magnetic Resonance Parameters in a Novel Organo-Xenon Species: Chemical Shifts and Nuclear Quadrupole Couplings in HXeCCH. *J. Chem. Phys.* **2007**, *127*, 234314−234315.
(198) Lantto, P.; Standara, S.; Riedel, S.; Vaara, J.; Straka, M. Exploring New^{129}Xe Chemical Shift Ranges in HXeY Compounds: Hydrogen More Relativistic than Xenon. *Phys. Chem. Chem. Phys.* **2012**, *14*, 10944−10952.
(199) Gowda, V.; Laitinen, R. S.; Telkki, V.-V.; Larsson, A.-C.; Antzutkin, O. N.; Lantto, P. DFT Calculations in the Assignment of Solid-State NMR and Crystal Structure Elucidation of a Lanthanum-(III) Complex with Dithiocarbamate and Phenanthroline. *Dalton Trans* **2016**, *45*, 19473−19484.
(200) Kaminský, J.; Vícha, J.; Bouř, P.; Straka, M. Properties of the Only Thorium Fullerene, Th@C_{84}, Uncovered. *J. Phys. Chem. A* **2017**, *121*, 3128−3135.
(201) Seaman, L. A.; Hrobárik, P.; Schettini, M. F.; Fortier, S.; Kaupp, M.; Hayton, T. W. A Rare Uranyl(VI)-Alkyl Ate Complex [Li-$(DME)_{1.5}]_2$[$UO_2(CH_2SiMe_3)_4$] and Its Comparison with a Homoleptic Uranium(VI)-Hexaalkyl. *Angew. Chem., Int. Ed.* **2013**, *52*, 3259−3263.
(202) Schreckenbach, G. Density Functional Calculations of ^{19}F and ^{235}U NMR Chemical Shifts in Uranium (VI) Chloride Fluorides $UF_{6-n}Cl_n$: Influence of the Relativistic Approximation and Role of the Exchange-Correlation Functional. *Int. J. Quantum Chem.* **2005**, *101*, 372−380.
(203) Saielli, G.; Bini, R.; Bagno, A. Computational ^{19}F NMR. 1. General Features. *Theor. Chem. Acc.* **2012**, *131*, 1140−1151.
(204) Liang, B.; Hunt, R. D.; Kushto, G. P.; Andrews, L.; Li, J.; Bursten, B. E. Reactions of Laser-Ablated Uranium Atoms with H_2O in Excess Argon: A Matrix Infrared and Relativistic DFT Investigation of Uranium Oxyhydrides. *Inorg. Chem.* **2005**, *44*, 2159−2168.
(205) Fortier, S.; Walensky, J. R.; Wu, G.; Hayton, T. W. High-Valent Uranium Alkyls: Evidence for the Formation of $U^{VI}(CH_2SiMe_3)_6$. *J. Am. Chem. Soc.* **2011**, *133*, 11732−11743.

https://dx.doi.org/10.1021/acs.chemrev.9b00785
Chem. Rev. 2020, 120, 7065−7103

(206) Smiles, D. E.; Wu, G.; Hrobárik, P.; Hayton, T. W. Use of ^{77}Se and ^{125}Te NMR Spectroscopy to Probe Covalency of the Actinide-Chalcogen Bonding in $[Th(E_n)\{N(SiMe_3)_2\}_3]^-$ (E = Se, Te; n = 1, 2) and Their Oxo-Uranium(VI) Congeners. *J. Am. Chem. Soc.* **2016**, *138*, 814−825.
(207) Cho, H.; De Jong, W. A.; Soderquist, C. Z. Probing the Oxygen Environment in UO_2^{2+} by Solid-State O-17 Nuclear Magnetic Resonance Spectroscopy and Relativistic Density Functional Calculations. *J. Chem. Phys.* **2010**, *132*, 084501−084502.
(208) Reta, D.; Ortu, F.; Randall, S.; Mills, D. P.; Chilton, N. F.; Winpenny, R. E. P.; Natrajan, L.; Edwards, B.; Kaltsoyannis, N. The Performance of Density Functional Theory for the Description of Ground and Excited State Properties of Inorganic and Organometallic Uranium Compounds. *J. Organomet. Chem.* **2018**, *857*, 58−74.
(209) Greif, A. H. Quantenchemische Untersuchungen Der NMR-Verschiebungen Für Komplexe Schwerer Und Superschwerer Elemente. Bachelor Thesis, Technische Universität Berlin, Germany, 2011.
(210) Hilton, J.; Sutcliffe, L. H. The "Through-space" Mechanism in Spin-Spin Coupling. *Prog. Nucl. Magn. Reson. Spectrosc.* **1975**, *10*, 27−39.
(211) Ariai, J.; Saielli, G. Through-space" Relativistic Effects on NMR Chemical Shifts of Pyridinium Halide Ionic Liquids. *ChemPhysChem* **2019**, *20*, 108−115.
(212) Straka, M.; Andris, E.; Vícha, J.; Růžička, A.; Roithová, J.; Rulíšek, L. Spectroscopic and Computational Evidence of Intramolecular $Au^{I}\cdots H^{+}$−N Hydrogen Bonding. *Angew. Chem.* **2019**, *131*, 2033−2038.
(213) Vícha, J.; Švec, P.; Růžičková, Z.; Samsonov, M.; Bártová, K.; Růžička, A.; Straka, M.; Dračínský, M. Experimental and Theoretical Evidence of Spin-Orbit Heavy Atom on the Light Atom ^{1}H NMR Chemical Shifts Induced through H•••I$^-$ Hydrogen Bond. *Chem. - Eur. J.* **2020**, accepted, DOI: 10.1002/chem.202001532.
(214) Viger-Gravel, J.; Leclerc, S.; Korobkov, I.; Bryce, D. L. Correlation between ^{13}C Chemical Shifts and the Halogen Bonding Environment in a Series of Solid Para-Diiodotetrafluorobenzene Complexes. *CrystEngComm* **2013**, *15*, 3168−3177.
(215) Glaser, R.; Chen, N.; Wu, H.; Knotts, N.; Kaupp, M. ^{13}C NMR Study of Halogen Bonding of Haloarenes: Measurements of Solvent Effects and Theoretical Analysis. *J. Am. Chem. Soc.* **2004**, *126*, 4412−4419.
(216) Rege, P. D.; Malkina, O. L.; Goroff, N. S. The Effect of Lewis Bases on the ^{13}C NMR of Iodoalkynes. *J. Am. Chem. Soc.* **2002**, *124*, 370−371.
(217) Aubauer, C.; Kaupp, M.; Klapötke, T. M.; Nöth, H.; Piotrowski, H.; Schnick, W.; Senker, J.; Suter, M. Characterisation of the Tetrahalophosphonium Cations $PBrnI_4N^+$ ($0 \le n \le 4$) by ^{31}P MAS NMR, IR and Raman Spectroscopy and the Crystal Structures of $PI_4^+AlCl_4^-$, $PI_4^+AlBr_4^-$ and $PI_4^+GaI_4^-$. *J. Chem. Soc., Dalton Trans.* **2001**, 1880−1889.
(218) Widdifield, C. M.; Cavallo, G.; Facey, G. A.; Pilati, T.; Lin, J.; Metrangolo, P.; Resnati, G.; Bryce, D. L. Multinuclear Solid-State Magnetic Resonance as a Sensitive Probe of Structural Changes upon the Occurrence of Halogen Bonding in Co-Crystals. *Chem. - Eur. J.* **2013**, *19*, 11949−11962.
(219) Viger-Gravel, J.; Leclerc, S.; Korobkov, I.; Bryce, D. L. Direct Investigation of Halogen Bonds by Solid-State Multinuclear Magnetic Resonance Spectroscopy and Molecular Orbital Analysis. *J. Am. Chem. Soc.* **2014**, *136*, 6929−6942.
(220) Balasubramani, S. G.; Chen, G. P.; Coriani, S.; Diedenhofen, M.; Frank, M. S.; Franzke, Y. J.; Furche, F.; Grotjahn, R.; Harding, M. E.; Hättig, C.; Hellweg, A.; Helmich-Paris, B.; Holzer, C.; Huniar, U.; Kaupp, M.; Marefat Khah, A.; Karbalaei Khani, S.; Müller, T.; Mack, F.; Nguyen, B. D.; Parker, S. M.; Perlt, E.; Rappoport, D.; Reiter, K.; Roy, S.; Rückert, M.; Schmitz, G.; Sierka, M.; Tapavicza, E.; Tew, D. P.; van Wüllen, C.; Voora, V. K.; Weigend, F.; Wodyński, A.; Yu, J. M. TURBOMOLE: Modular Program Suite for Ab Initio Quantum-Chemical and Condensed-Matter Simulations. *J. Chem. Phys.* **2020**, *152* (18), 184107.
(221) Perdew, J. P.; Burke, K.; Ernzerhof, M. Generalized Gradient Approximation Made Simple. *Phys. Rev. Lett.* **1996**, *77*, 3865−3868.
(222) Neese, F. The ORCA Program System. *Wiley Interdiscip. Rev.: Comput. Mol. Sci.* **2012**, *2*, 73−78.
(223) Glendening, E. D.; Reed, A. E.; Carpenter, J. E.; Weinhold, F. *NBO*.
(224) Frisch, M. J.; et al. *Gaussian 16*; Gaussian, Inc.: Wallingford CT, 2016.
(225) Mitoraj, M.; Michalak, A. Natural Orbitals for Chemical Valence as Descriptors of Chemical Bonding in Transition Metal Complexes. *J. Mol. Model.* **2007**, *13*, 347−355.
(226) te Velde, G.; Bickelhaupt, F. M.; Baerends, E. J.; Fonseca Guerra, C.; van Gisbergen, S. J. A.; Snijders, J. G.; Ziegler, T. Chemistry with ADF. *J. Comput. Chem.* **2001**, *22*, 931−967.
(227) Perdew, J. P.; Burke, K.; Ernzerhof, M. Generalized Gradient Approximation Made Simple [Phys. Rev. Lett. 77, 3865 (1996)]. *Phys. Rev. Lett.* **1997**, *78*, 1396−1396.
(228) Dyall, K. G. Relativistic Double-Zeta, Triple-Zeta, and Quadruple-Zeta Basis Sets for the 6d Elements Rf−Cn. *Theor. Chem. Acc.* **2011**, *129*, 603−613.
(229) Dyall, K. G. Relativistic and Nonrelativistic Finite Nucleus Optimized Double Zeta Basis Sets for the 4p, 5p and 6p Elements (Theor Chem Acc (1998) 99:366−371): Addendum. *Theor. Chem. Acc.* **2002**, *108*, 365−365.
(230) Dyall, K. G. Relativistic Quadruple-Zeta and Revised Triple-Zeta and Double-Zeta Basis Sets for the 4p, 5p, and 6p Elements. *Theor. Chem. Acc.* **2006**, *115*, 441−447.
(231) Jensen, F. Polarization Consistent Basis Sets: Principles. *J. Chem. Phys.* **2001**, *115*, 9113−9125.
(232) Jensen, F. Erratum: "Polarization Consistent Basis Sets: Principles" [J. Chem. Phys. 115, 9113 (2001)]. *J. Chem. Phys.* **2002**, *116*, 3502−3502.

https://dx.doi.org/10.1021/acs.chemrev.9b00785
Chem. Rev. 2020, 120, 7065−7103